NKK TECHNICAL REVIEW

No. 76
JULY 1997

NKK

ISSN 0915-0544

NKK TECHNICAL REVIEW

No.76 July 1997

CONTENTS

Articles

New Achievements

Published by
Intellectual Property Dept., NKK CORPORATION
Edited by
NK Techno Service Co., Ltd.
1-1, Minamiwatarida, Kawasaki-ku,
Kawasaki, 210 JAPAN

DISCLAIMER

This document contains

tone-on-tone or color

graphs, charts and/or pictures

which have been reproduced in

black and white.

Electrical Instrumentation Computer (EIC) Integrated System for Labor Saving in the Basic Oxygen Furnace Operation

Hiroaki Miyahara*, Toshio Hatanaka**,
Yukio Arai***, Masafumi Ikeda****,
Shinichi Okimoto***** and Noriyasu Kato******

An EIC integrated BOF system was developed for the basic oxygen furnace (BOF) plant at the Keihin Works to save labor and rationalize furnace operation. This system uses comprehensive blowing process control technology that NKK has developed over the past several decades. The characteristics of this system consist of (1) automatic process control for one man operation, (2) enhanced centralization of operating and monitoring functions, (3) improvement of blowing control models, (4) introduction of microwave hot metal level meter, and (5) low-cost system configuration with the possibility of future expansion. The BOF operation has been greatly improved with this new EIC integrated system.

1. Introduction

The economic condition of the steel industry in Japan is worsening, and further reductions in labor and manufacturing costs are now necessary to compete in the international market. However, although the BOFs at NKK's Keihin Works have been in operation since 1976, most of the BOF operation desks and control devices have never been replaced or improved. As a result, they have hindered the progress of labor saving and plant rationalization.

On the other hand, EIC integrated controlling systems have been developed and introduced in many fields, due to the advancement of electronic technology and semiconductors. These systems consist of three basic elements: electrical (E), instrumentation (I) and computers (C). Furthermore, the rapid progress of high performance CRTs has changed the man-machine interface for operation and monitoring from conventional operation control panels to CRT screens.

An EIC integrated system was introduced into the BOF process to save labor and rationalize plant operations. Drastic replacement and modifications of the existing computers and control devices were implemented. Each BOF equipped with this new system started up successively after the EIC integrated system was first introduced in November 1995. Since then, the operations have been satisfactory. This paper re-

* Deputy General Manager, Planning Section, Information Innovating Dept.
** Assistant Manager, Technology Section, Process Control Dept., Keihin Works
*** Technology Section, Process Control Dept., Keihin Works
**** Manager, Steel Making Shop, Iron & Steel Making Dept., Keihin Works
***** Assistant Superintendent, Steel Making Shop, Iron & Steel Making Dept., Keihin Works
****** Assistant Manager, Steel Making Shop, Iron & Steel Making Dept., Keihin Works

ports the characteristics and implementation of the EIC integrated system and presents an outline of the blowing control technology.

2. Outline of EIC integrated system

2.1 BOF specifications

The steelmaking plant at the Keihin Works has two top and bottom combined blowing furnaces (NK-CB) and is currently running a single furnace operation at all times except during the changing phase period with the two furnaces. **Table 1** gives the main specifications of the BOF facility. Various types of steel products are produced at the Works. A single BOF performs refining operations for not only ordinary hot metal, but also dephosphorized hot metal (approximately 40% of the operation). Even the types of processes after BOF refining are diverse. Therefore, the range of carbon content at turndown in the furnace is as wide as 0.04 to 0.90%, and the refining techniques are quite diverse and complicated.

2.2 Prerequisite for system design

The purpose of EIC integrated system development is to cut the BOF labor cost by accomplishing a one man blowing operation while accommodating the diverse and complicated refining methods mentioned above. High performance, automatic blowing that can cope with any type of refining, and centralization of the operational and monitoring functions are needed to achieve this goal.

For that reason, the following two points were considered in configuring the system.

Table 1 Main specification of BOF

Item	Specification
Type	Symmetric trunion type (NK-CB)
Capacity	Nominal;250t/heat,Max;340t/heat
Top blowing	Gas species:O_2 Gas flow rate:Max 70000Nm^3/h
Bottom blowing	Gas species:N_2,Ar Gas flow rate:45Nm^3/min
Waste gas treatment	OG type

(1) Automatic blowing

The overall functions of the conventional computer system were reviewed, and the assignment of the electrical, instrumentation and computer functions as well as the system configuration were optimized. This lowered the cost of the system while enhancing the possibility of future expansion.

(2) Centralization of operational and monitoring functions

To save space, all operations except for emergency control switches can be performed from the CRT, and the number of CRT units were reduced to the absolute minimum.

As a result, an EIC integrated system was introduced that shares individual items of information from the electrical, instrumentation and computer components, and integrates the man-machine interface.

2.3 Characteristics of the system

2.3.1 System configuration

Fig. 1 shows the overall configuration of the EIC integrated BOF system. Although independent of each other, each of the new electrical, instrumentation and computer components are connected by a network that includes the CRT controller as well as the tapping side operation panel. As process data and internal information are rapidly transmitted via the network into the corresponding common memory in each unit, the independent electrical, instrumentation and computer units can closely exchange information, resulting in drastic savings in the construction cost due to the reduction of equipment required.

Furthermore, each furnace has three CRT units and one emergency operation board for one man operation and monitoring. As a result, the length of the operation panel was reduced by more than half, and the operation and monitoring space was reduced to approximately one third of that for the conventional system.

2.3.2 Optimizing the functional assignment of EIC integrated system

Fig. 2 shows the functional assignment of each electrical, instrumentation and computer unit. The main functions of the process computer are: calculation using blowing models, blowing pattern design, heat scheduling and actual results management, hot metal management, and communications with other systems.

Furnace sequence management and automatic blowing control, which were previously performed by the process computer, are now assigned to electrical or instrumentation control station. Automatic blowing control functions such as lance, sublance, submaterial and ferroalloy require a control response speed of several tens of milliseconds and are assigned to the elec-

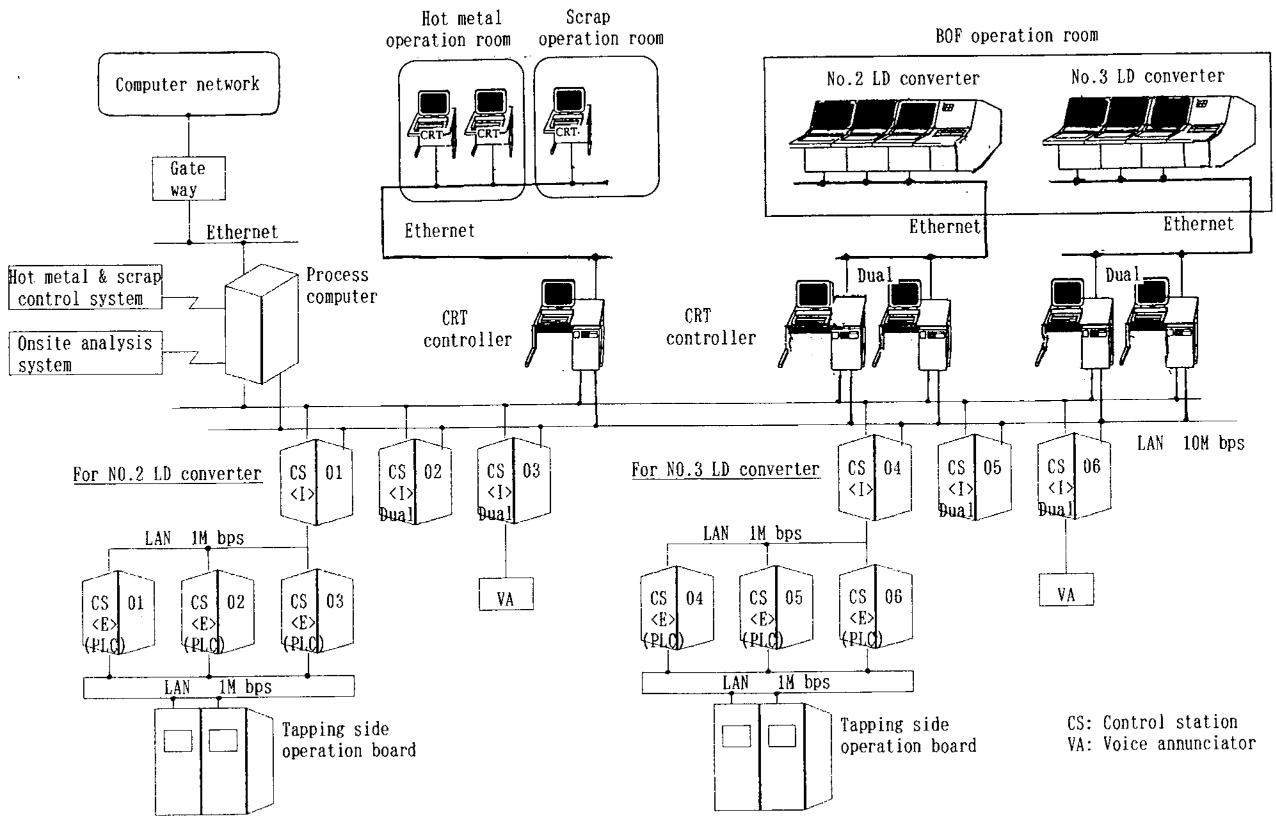

Fig. 1 EIC integrated BOF system

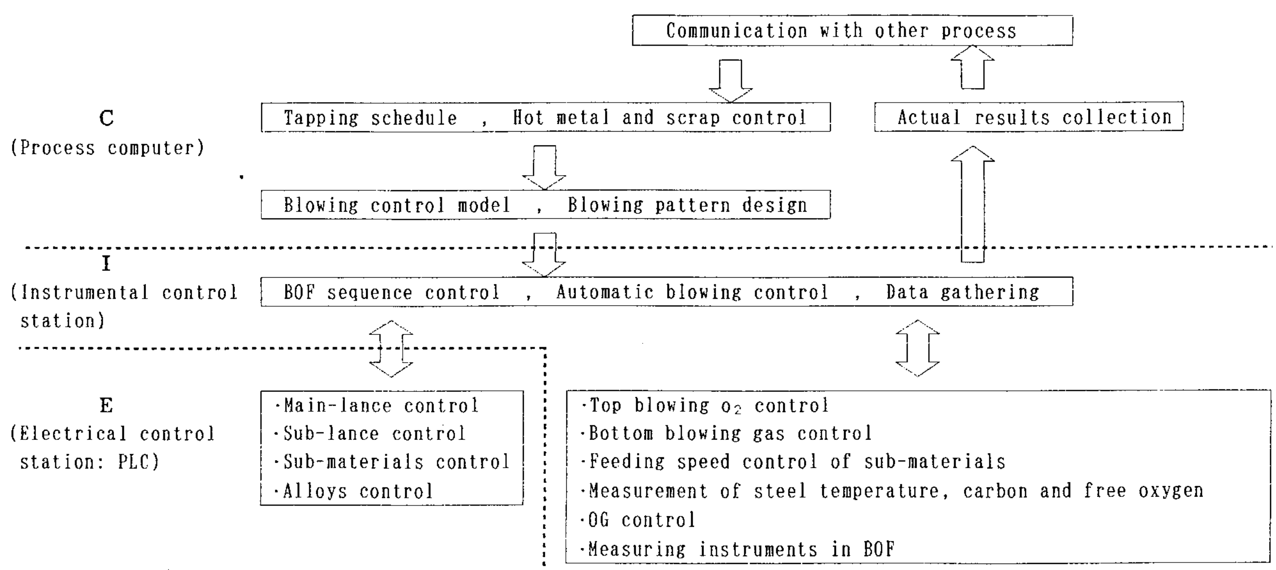

Fig. 2 Functional assignment of EIC integrated system

trical control station. Functions that require response speeds of over 100 ms, such as top and bottom blowing, are assigned to the instrumentation control station.

As a result, even load distribution was accomplished over the entire system, and an optimum functional assignment was achieved that is expandable and prospective of keeping a low operating cost.

2.3.3 Man-machine interface

(1) CRT operation

In this system, the monitoring information was thoroughly centralized, and the operation was simplified to suit the one man blowing operation. Furthermore, with the introduction of a multi-window function, other information windows can be displayed while keeping a data display window on the screen.

Fig. 3 is an example of a CRT data display. The operator can freely use the windowing function on the current data display and show the necessary information on the screen sequentially just by touching the corresponding area on the primary data display without being conscious of classification of the process computer or control station. Furthermore, a display window can be automatically overlaid on the current display window, when necessary, to show temperature measurement results or a task completion, or to show instructions from the process computer.

As a result, the number of primary data display windows used for normal operation is limited to about four for blowing preparation, and six for the process from the start of blowing to the end of tapping. This screen layout is optimum for one operator to operate and monitor three CRTs.

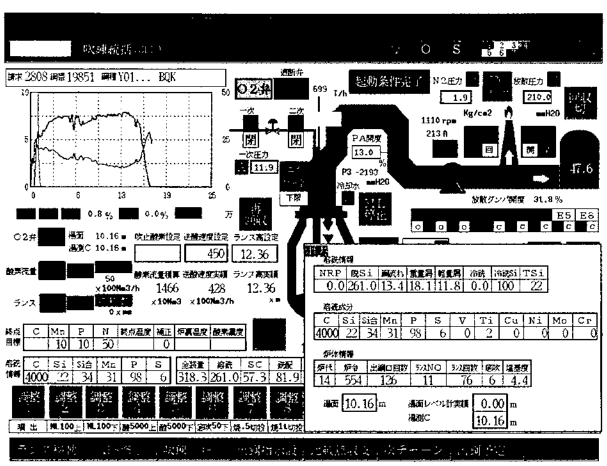

Fig. 3 An example of CRT display

(2) Voice annunciator

The voice annunciator is used to reduce the effort to monitor the CRT by conveying guidance to the operator that is necessary for monitoring automatic blowing and by sending messages that the display information on the screen can not fully convey.

(3) Elimination of chart making and output labor

The instantaneous molten steel temperature, which was previously documented by a pen recorder and filed, is now sampled at 100 ms intervals, and displayed on the CRT in 500 ms intervals. Furthermore, the actual waveforms for the past 2000 heats are now kept in the process computer and can be read from the CRT display at any time. As a result, chartmaking was completely eliminated in the new system.

2.3.4 Reliability of system

A malfunction of the system affects the operation and facilities. On the other hand, duplication of the whole system would more than double the construction cost. Considering the cost effectiveness, only the core of the main equipment that is vital in running the system is now duplicated. Examples of duplicated equipment include control stations for top blowing, bottom blowing and OG (oxygen gas recovery or purge), CRT controller and control LAN.

Furthermore, the process computer consists of an operation system and a development system. Actual, on-line tests of blowing control models of the development system can be easily made by running both systems in parallel.

3. BOF process control by EIC integrated system

3.1 Automatic process control functions[1)]

Only partial automatic control was possible in the previous system due to the limited performance and capacity of the process computer. The new system has improved the overall automatic control for the following.

(1) lance height
(2) oxygen gas flow rate for top blowing
(3) gas flow rate for bottom blowing

(4) type of bottom blowing gas
(5) weighing and charging of submaterial
(6) charging speed of submaterial
(7) weighing of ferroalloy

For other functions, such as OG control, sublance control and turndown control, the existing automatic functions were used on the new system without modification.

The extent and timing of each operation for items (1) through (6) listed above are determined by the process computer. The process computer develops a suitable control pattern based on the blowing conditions for every heat before blowing starts. Blowing is executed according to the control pattern. As the blowing reaction spontaneously fluctuates, however, the initial pattern may need to be adjusted for a short period of time in actual operation. The new system provides a function that can take necessary actions immediately, without changing the operation mode to the manual mode, to rectify the fluctuation. A one touch operation can then return the system to the initial control pattern.

Fig. 4 shows an example of adjustments during blowing. For the submaterials such as for the slag coating material, weighing and feeding patterns are grouped into several model patterns, and the weighing and charging can be performed by simply pressing the corresponding button.

For weighing the ferroalloy as mentioned above in (7), the weighing commences when the operator confirms the charging weight and press the button. For weighing a specific type with other types, weighing is performed automatically in accordance with a predetermined order to avoid the simultaneous charging of different types. As a result, weighing of the ferroalloys, which used to be done manually at the tapping side of the furnace, can now be performed automatically from the operation room.

Almost 100% of the automatic process control functions for (1) through (7) listed above have been implemented since the system started operation. As a result, one man blowing operation was realized, and the reduction in BOF operators was achieved. **Fig. 5** shows the improvement in the operator assignment for the BOF.

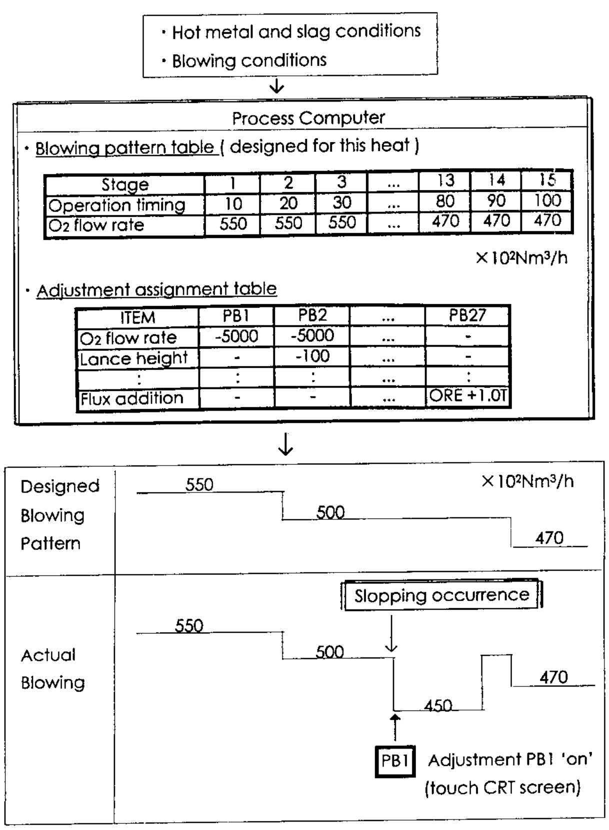

Fig. 4 **An example of adjustment practiced during blowing**

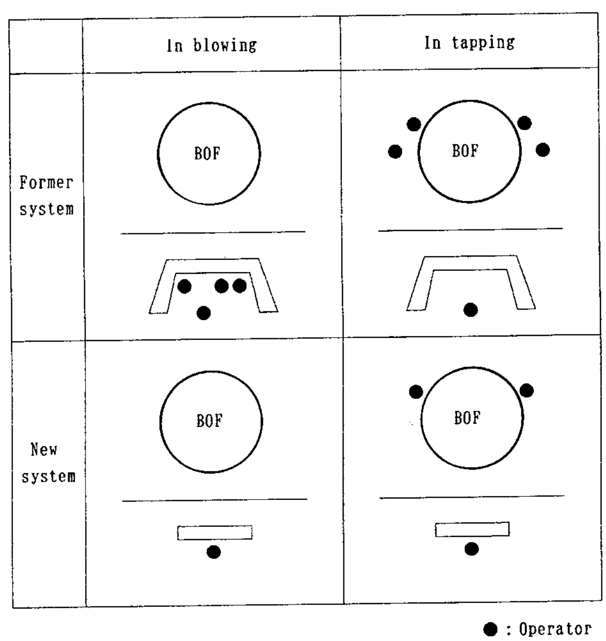

Fig. 5 **Operator assignment of automatic refining system**

3.2 Introduction of microwave hot metal level meter

Placing the lance at the proper height is very important for stabilizing the blowing operation as well as for protecting the refractories used in the furnace. Thus, determining the optimum model pattern for the lance height is needed, as previously mentioned in **Section 3.1**. However, the lance height is a relative height determined from the hot metal level, so precise measurement of the hot metal level is a prerequisite to determine the model pattern.

In the previous system, the hot metal level was determined by taking physical measurements by a probe attached to the sublance. If this was not possible, the height was calculated from the charging weight of hot metal and scrap considering the number of heats after the furnace started operation. For this system, the M-sequence signal modulated microwave level meter[2], which was developed by NKK, was installed and used. As a result, the hot metal level after charging hot metal can automatically be determined for every heat.

Table 2 lists the specifications of the M-sequence signal modulated microwave level meter, while **Fig. 6** shows a schematic diagram for the hot metal level measurement. A pair of transmitting and receiving microwave antennas are mounted on a mobile car. The car is moved horizontally to a point above the sublance hole for the measurement and then retracted automatically to the standby position upon task completion.

Table 2 Specifications of M-seq. signal modulated microwave level meter

Item	Specification
Carrier frequency	16.0 GHz
Output power	100 mW
Clock frequencies	430.000 MHz 430.005 MHz
Code length of M-seq.	1023 bit
Response	200 ms
Measuring time	20 s
Antennas	Horn antennas Rec./Trans. separate type Size: w 100 × d 80 × h 75mm

When a large amount of scrap is charged, the level meter is affected by reflections from the scrap floating on the hot metal. For that reason, signal processing is performed to remove the incorrect reflections from the scrap and record only those from the hot metal. **Fig. 7** shows a comparison between microwave and conventional hot metal level measurements. The measurement results show the conformity between the two.

3.3 Process control models[3]

With the new process computer, the calculation speed was increased, and the memory capacity was expanded. The blowing process control models, which were developed by NKK, were partially improved at this occasion and integrated into the new system. **Fig. 8** shows the overall functional configuration of the BOF process control models. Furthermore, three new kinds of models were added into the EIC integrated system. These improvements, altogether, contribute to the rationalization of the operation, as well as to the reduction of the work load of the operators.

(1) Heat balance model based on the past records[4]

Previous heat data taken from actual operations

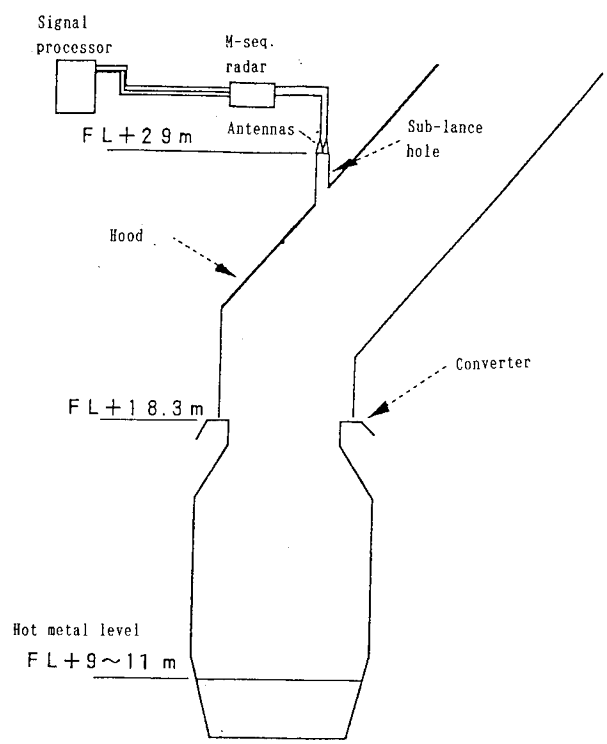

Fig. 6 Schematic diagram of hot metal level measurement

are accumulated, and before blowing starts, heat data that is similar to the starting heat is extracted. The data is used to calculate the necessary amount of coolant and other materials by comparing the heat balance of the selected data and that of the current heat. The database is classified into ordinary operation heats, special operation heats and special steel operation heats, and can hold up to 9000 heats of data.

(2) Ferroalloy calculation model

The necessary amount of ferroalloy is calculated from the target chemical composition, the end point chemical composition and the alloy yield for each component. The calculation is performed so that the most inexpensive adjustment of chemical composition is made by using inexpensive ferroalloys as much as possible. When the calculation result is confirmed by the operator, automatic weighing is started by one touch operation.

(3) Slopping prediction model[5]

The time and the scale of slopping are forecast from the wave shapes of the waste gas flow rate, decarbonizing oxygen efficiency, furnace top pressure, etc., as well as from information on the hot metal, simultaneously while blowing is performed. When the occurrence of slopping is forecasted, the voice annunciator is activated to notify the operator of the fact. Appropriate actions can be taken automatically to cope with the expected results.

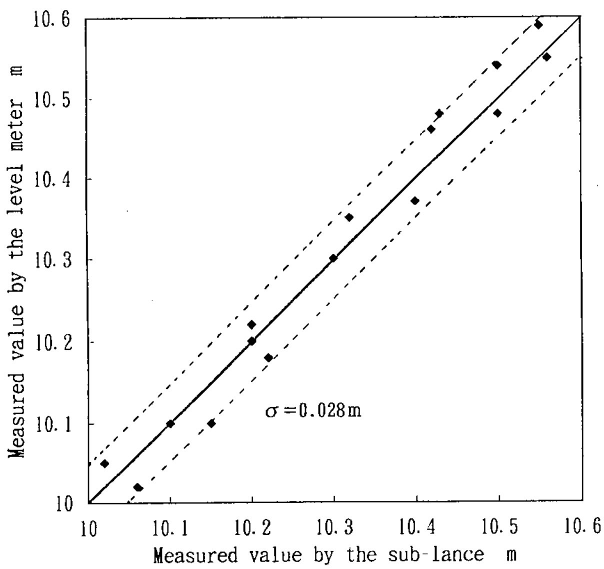

Fig. 7 Results of hot metal level measurements

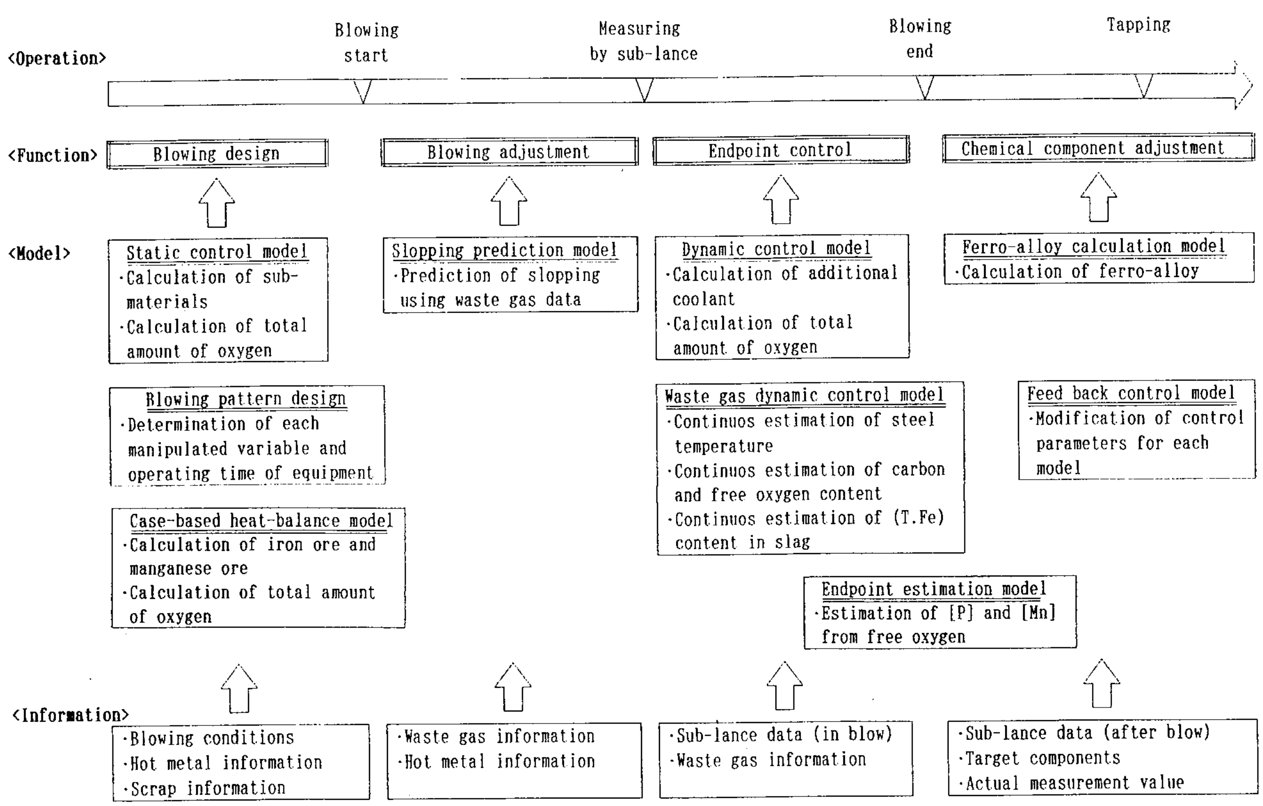

Fig. 8 Outline of BOF blowing control models

4. Conclusion

The EIC integrated BOF system, which includes the accumulated blowing process control technology developed by NKK, was installed for the BOF operations at the NKK Keihin works. Each furnace was equipped with the system during a single maintenance shutdown and restarted without any significant problem. The system has been making great contributions to the reduction of labor and the rationalization of manufacturing cost.

For further development of the EIC integrated system, new kinds of sensors along with process control model improvements are inevitable. Furthermore, in order to cope with the aging of workers and the decreasing number of skilled operators, tapping, repairing and other related works need to be automated as well as the main process. From this viewpoint, we will make continuous efforts to develop a system with increased automation for even better BOF operation.

References

1) Hatanaka, T et al. "Development of Blowing Control System in BOF Applying AI". NKK Technical Report. No.134, p.23 - 28 (1991).
2) Tezuka, K et al. "Development of M-sequence Signal Modulated Microwave Level Meter". NKK Technical Report. No.137, p.71 - 76 (1991).
3) Miyahara, H et al. "Total Factory Automation System of Steel MakingWorks". NKK Technical Report. No.125, p.10 - 21 (1989).
4) Wakamatsu, S et al. "Development of Heat-balance Comparing Model". CAMP - ISIJ. Vol.5, No.1, P. 216(1992).
5) Tachikawa, Y et al. "Development of Slopping Prediction in BOF". CAMP - ISIJ. Vol.5, No.1, p.214 (1992).

Operation and Reaction Analyses of New Stainless Steel Refining Process

Chihiro Taki*, Atsushi Watanabe**,
Akihito Inoue***, Manabu Tano****,
Toshio Takaoka***** and Yasuhito Miyata******

A new refining process for stainless steel was developed at NKK Fukuyama Works to meet the increasing demands for stainless steel production. Features of the new process include:A top and bottom blowing converter is used. Chromium ore, nickel ore and scrap are used for chromium and nickel raw materials. Coke and oxygen are added as energy sources. Conventional existing secondary refining facilities and a continuous casting machine are used after the new refining process. The process flow and advantages of the new process are described in this paper.

1. Introduction

A new stainless steel refining facility was placed into operation at the Fukuyama Iron and Steel Works in September 1990 to improve the stainless steel production process. The new Stainless Steel Refining Furnace (SRF) uses a single converter system, in which inexpensive raw materials that are selected from various Ni and Cr sources, such as nickel ore, chromium ore and scrap, are added to the pre-treated molten iron. Oxygen and coke are used as a heat source to directly refine the molten stainless steel. Furthermore, after the molten steel is tapped from the SRF, existing secondary refining and casting facilities are used to produce inexpensive stainless steel slabs[1)-3)].

This report presents an outline of the SRF facility and process, and describes operational conditions that include the reduction rate of Ni and Cr ore and yield improvements by decreasing the dust loss during blowing. The influence of operating conditions on the furnace are also discussed.

2. Process flow

Fig. 1 shows a conceptual flow diagram for the new process of making austenitic stainless steel. Ni-containing molten iron is produced by charging Ni oxide ore into the pretreated, molten iron in the SRF (Ni ore reduction). The molten iron is dephosphorized in the existing molten iron pretreatment facility after

* Manager, Planning & Coordination, Fukuyama Works
** Assistant Superintendent, No. 2 Steel Making Shop, Fukuyama Works
*** Assistant Manager, No. 2 Steel Making Shop, Fukuyama Works
**** No. 2 Steel Making Shop, Fukuyama Works
***** Senior Research Engineer, Steelmaking Lab, Materials and Processing Research Center
****** Research Engineer, Steelmaking Lab, Materials and Processing Research Center

tapping the SRF. The dephosphorized molten iron is charged into the SRF for the second time to produce Cr- and Ni-containing molten iron by adding Cr ore (Cr ore reduction). The molten iron is then tapped from the SRF into the ladle, while residual slag inside the SRF is completely removed. The molten iron is then returned into the SRF for the third time.

Oxygen blowing is initiated for decarbonization after additional materials such as scrap are added. After the decarbonization process is completed, final refining is carried out at existing secondary refining facilities (NK-AP, RH). The steel is then cast either at the conventional No. 2 SLCC or ingot making facility.

One characteristic of this process is that it provides wide flexibility in the selection of raw materials. **Fig. 2** shows examples of the range of Ni source charging ratios. The ratio between the ore and scrap can be broadly altered, and the optimum composition can be determined by considering productivity and the prices of raw materials.

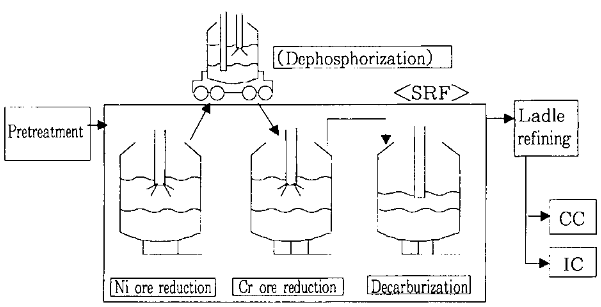

Fig. 1 Process flow of new stainless steel refining process

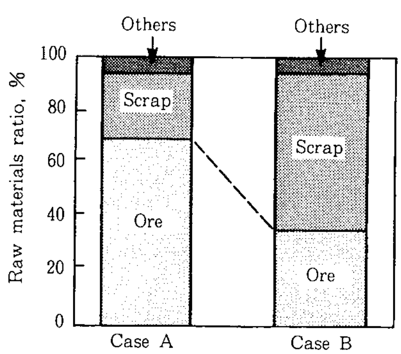

Fig. 2 Flexibility of raw material ratio in new process

3. Facility outline

A converter in No. 2 steel making shop that had been not in operation since 1986 was modified for use as the SRF. **Table 1** and **Fig. 3** provide specifications of the SRF facility and a schematic outline of the facility, respectively.

The main improvements are as follows:

(1) Continual charging of the raw materials from the furnace top hoppers is possible, which permits the extensive usage of ore.

(2) A horizontal hot cyclone, which is easy to handle and operate, was installed to selectively recover the generated dust and recycle it as a Ni and Cr source, etc. Furthermore, a wet type, dust collector is also used for selective dust recovery.

(3) A furnace top pressure control system and IDF inlet dumper were installed to accommodate fluctuations in the post combustion ratio inside the furnace and enhance the recovery gas heat, even at the low exhaust

Table 1 Main specifications of SRF

Capacity	120 t/ch
Productivity	max 10000 t/M
Furnace	BOF type
Vessel shell	ϕ 6600 × h 10080 mm
Lining	MgO-C
Process gas	
Top blown O_2	max 48000 Nm^3/h (16 kgf/cm^2)
Bottom blown N_2/Ar	max 12000 Nm^3/h (30 kgf/cm^2)
Off gas system	OG system
Dust collector	Hot cyclon + Satulater

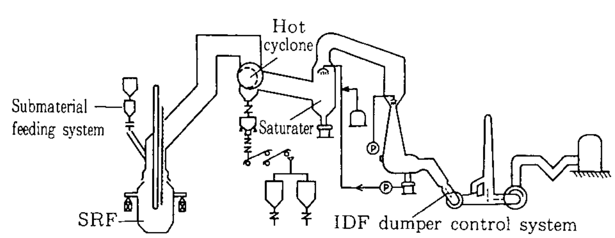

Fig. 3 Schematic view of SRF equipment (Exhaust gas treatment system)

gas flow rate. The use of a hood boiler together with these, improves energy recovery efficiency.

4. Operation outline

4.1 Reduction of Ni ore

Table 2 shows a typical example of the Ni ore composition used at the Fukuyama Works. This is garnierite ore, which contains approximately 30% moisture in the untreated ore. For that reason, the ore is dried by a rotary drier to a water content of approximately 7% before being added into the SRF. Part of the ore is used after briquetting.

Fig. 4 shows a typical example of the operation of the Ni ore reduction process. The pretreated molten iron is first charged into the SRF. Oxygen blowing is then started, and coke and flux are added for heating-up and slag making. Ni ore is added when the metal bath temperature reaches approximately 1500 °C.

The oxygen blowing rate, as well as the ore and coke charging rate, are controlled to maintain the metal bath temperature at the required level during the addition of ore. As a large amount of slag is generated during blowing, the process is interrupted to discharge slag after a specified amount of ore is added. Ni ore can be easily reduced with a sufficient heat supply[4]. Therefore, ore is reduced efficiently by optimizing the combination of the oxygen blowing rate and the post combustion ratio.

4.2 Cr ore reduction

Table 3 and **Fig. 5** show typical examples of the Cr ore composition and the Cr reduction process operation pattern, respectively.

The dephosphorized, Ni-containing, molten iron, as well as cool iron sources such as scrap, are first charged into the SRF. Oxygen blowing is then started, and coke and flux are added for heating-up and slag-making. Cr ore is added after the molten metal temperature reaches approximately 1600 °C. The oxygen

Table 2 Typical composition of Ni ore used in SRF

%

T.Ni	T.Fe	T.Cr	SiO_2	MgO	Al_2O_3	Adhesion moisture
2.5	13.2	0.6	35.2	25.9	1.1	7

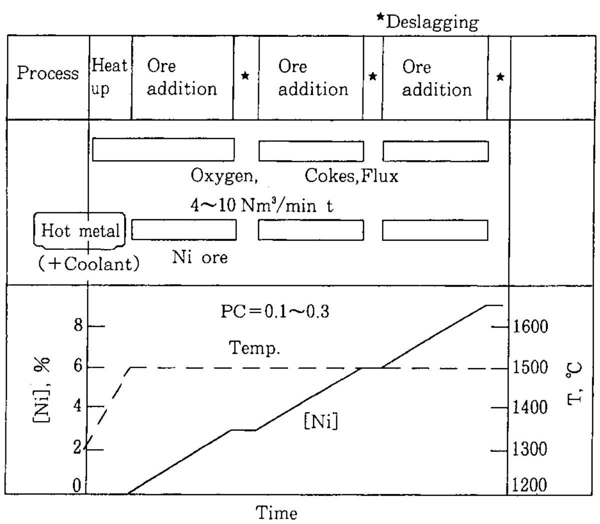

Fig. 4 Typical operational conditions in Ni ore reduction process

Table 3 Typical composition of Cr ore used in SRF

%

T.Cr	T.Fe	MgO	SiO_2	Al_2O_3	CaO
30.9	19.3	11.1	2.6	14.5	0.3

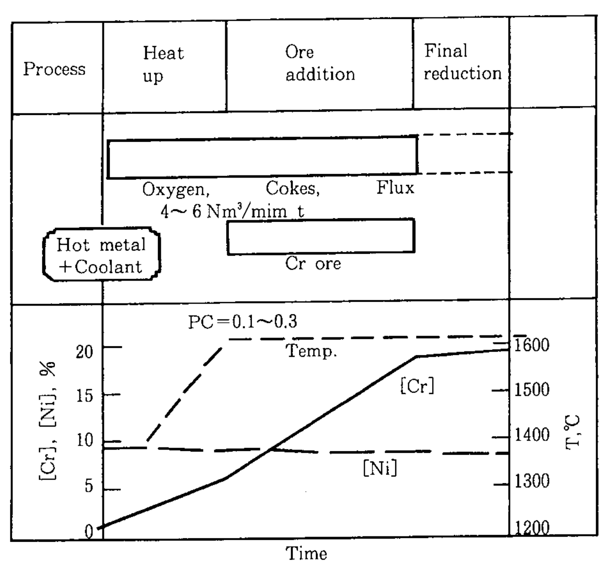

Fig. 5 Typical operational conditions in Cr ore reduction process

blowing rate, as well as the ore and coke charging rates, are controlled to maintain the metal bath temperature at the required level while adding ore. After the specified amount of ore is added, the oxygen blowing rate is gradually decreased to carry out the final reduction of ore. FeSi is added at the end to make the total Cr (T.Cr) less than 1%.

5. Ni ore reduction rate

Fig. 6 shows the relationship between the charging rate of Ni ore and the rate of Ni ore reduction, with both expressed using kg/min. The NiO in the Ni ore is very easily reduced. The results of operating both an experimental small furnace (100 kg - 5 ton) and the actual commercial SRF demonstrated that the reduction rate is not dependent on conditions such as stirring, but it is entirely dependent on the charging rate of Ni ore. The NiO content in the slag during and after blowing is less than 0.05%, indicating that reduction progresses at a steady rate without delays.

The rate of Cr ore reduction is determined by the combination of the Cr ore melting rate and the Cr transfer rate within the slag layer (from the slag to the metal). Thus, the reduction rate can be expressed as shown in Equation (1)[5)6)]:

$$d[Cr]/dt = \alpha(Cr) + \beta \exp(-\Delta H/T) \quad .....(1)$$

where,

α , β : constant of apparent reaction rate

ΔH : constant of temperature dependence

As shown in **Fig. 7**, the reduction rate for the actual commercial SRF was calculated from the Equation (1) model that was empirically made using the results of the 5 ton furnace experiments and the calculated values showed good agreement with the observed values.

By increasing the stirring intensity and controlling the temperature, a high reduction rate of 0.3%/minute was achieved with the commercial SRF.

6. Improvement of yield by minimizing the dust loss

The dust loss was relatively large compared to a typical converter because the blowing time needed for Ni ore and Cr ore reduction is longer.

Although most of the generated dust is recovered and recycled, over-generation of dust decreases the energy efficiency and increases the operation cost undesirably. For that reason, dry and wet dusts were collected during and after the blowing process of Ni ore

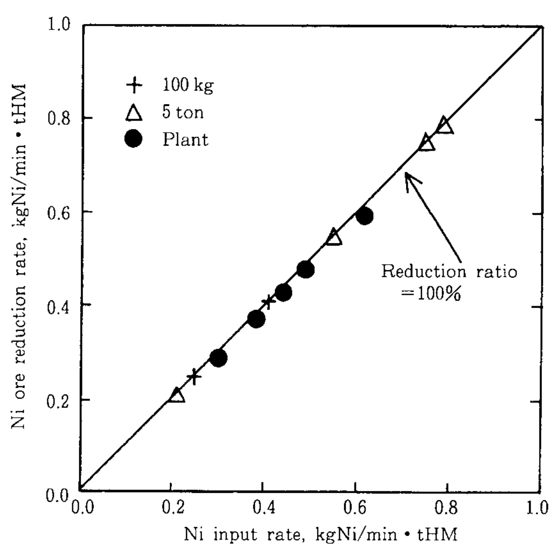

Fig. 6 Reduction rate of Ni ore

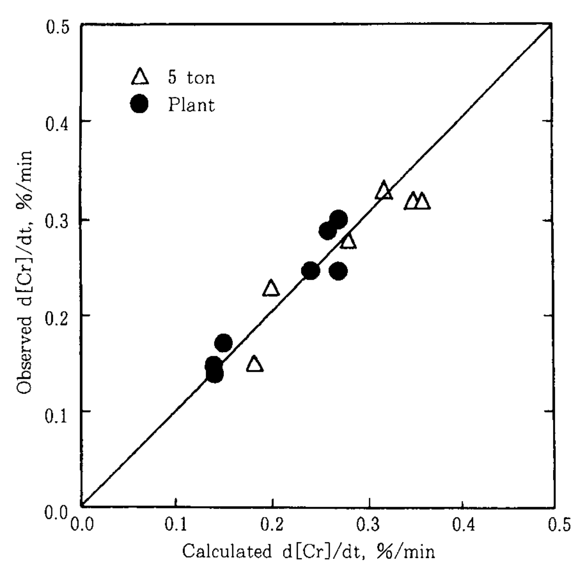

Fig. 7 Comparison of observed and calculated Cr ore reduction rate

and Cr ore reduction to examine the characteristics of the dusts and identify the dust generating mechanism. Countermeasures were then carried out to decrease the amount of dust generation.

Photo 1 shows SEM images of dry dust collected during the Ni and Cr ore reduction processes. **Fig. 8** shows examples of the particle size distribution collected in the Ni and Cr ore reduction processes. **Table 4** shows the estimation of dry dust levels by percentage at three origins, based on an incoming and outgoing material balance. The ore and coke contents are high in the dry dust generated during the Ni ore reduction process, and the dry dust often maintains its original shape from the reduction operation. This suggests that most of the dust generated is Ni ore that was carried over during the charging process. The following countermeasures are required to decrease the carry-over of raw materials;

(1) Adjust the raw material grain size, while giving consideration to the apparent linear velocity and the carry-over limit[7] inside the SRF (**Fig. 9**).

(2) Ensure the thermal strength of raw materials to prevent pulverization and fining during the charging process.

On the other hand, the dry dust generated during Cr ore reduction mainly consists of metals. The generating mechanism is considered to be the same as that of metallic wet dust, as described below.

Photo 2 shows SEM images of wet dust generated from the Ni and Cr ore reduction processes. **Fig. 10** shows an example of the particle size distribution generated from the Ni and Cr ore reduction processes. The estimation of the composition of wet dust **(Table 5)** was based on an incoming and outgoing material balance that was collected in the same manner as that for

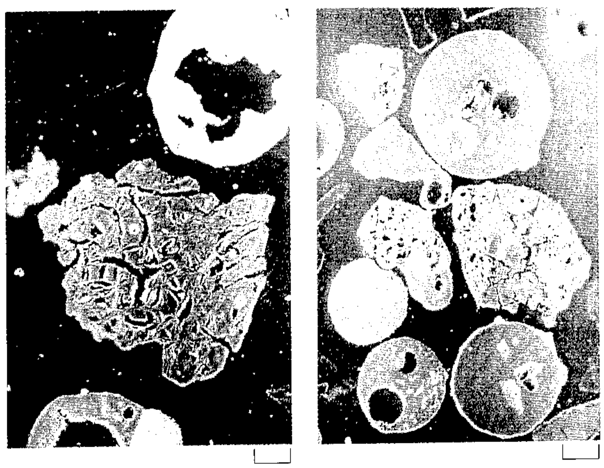

Ni ore reduction 100 μm Cr ore reduction 100 μm

Photo 1 SEM images of dry dust collected in Ni ore and Cr ore reduction process

Table 4 Estimated composition of dry dust collected in Ni ore and Cr ore reduction process

%

	Ore	Cokes	Metal
Ni ore reduction	70~80	10~20	10~20
Cr ore reduction	<15	<15	70~80

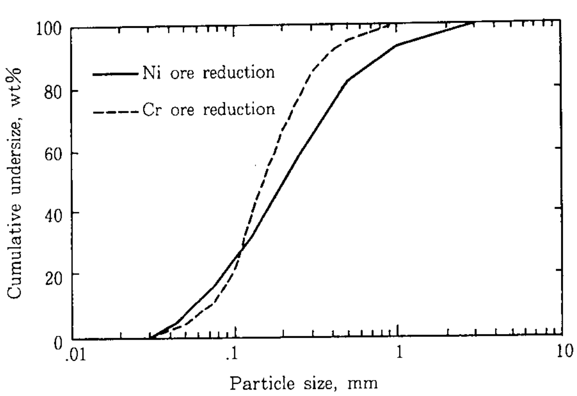

Fig. 8 Particle size distribution of dry dust collected in Ni ore and Cr ore reduction process

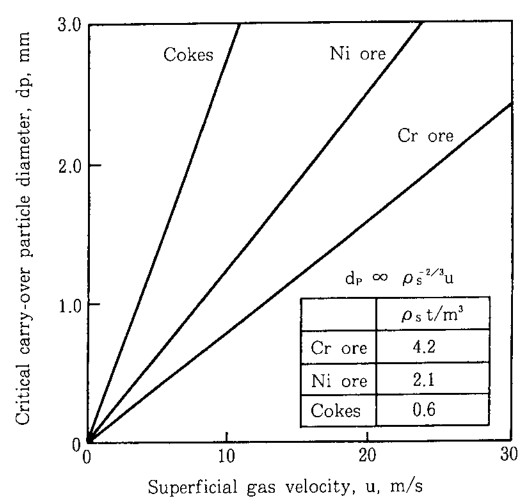

Fig. 9 Effect of superficial gas velocity on critical carry-over particle size for various raw materials

the dry dust. The results show that the dust mainly consists of metallic origins.

Furthermore, the results of an EPMA analysis of the metals in the dust show that the composition of the metals in the dust is close to that of the bulk metal during the blowing process.

Therefore, the wet dust (and the dry dust in Cr ore reduction) are not from fume generated at the fire spot of the metal bath surface, but are generated when the metallic droplets suspended in the slag contact the oxygen gas.

Figs. 11 and **12** show how the gas flow rate in bottom blowing and the oxygen blowing conditions in top blowing affect the rate of wet dust generation. Less dust is generated when the gas flow rate is reduced in bottom blowing and when top blowing is weakened.

Fig. 13 shows the distribution of metallic droplets in the slag layer. The amount of metallic droplets in the slag layer decreases in proportion to the distance from the metal bath surface. Therefore, control of the penetration of the oxygen jet into the slag layer is important for decreasing dust generation. For that purpose, the following two methods were considered:

(1) Decrease the penetration depth[8] of the oxygen jet into the slag layer to minimize the chances for metal-

Table 5 Estimated composition of wet dust collected in Ni ore and Cr ore reduction process

%

	Ore	Cokes	Metal
Ni ore reduction	10~20	<10	70~80
Cr ore reduction	<15	<15	70~80

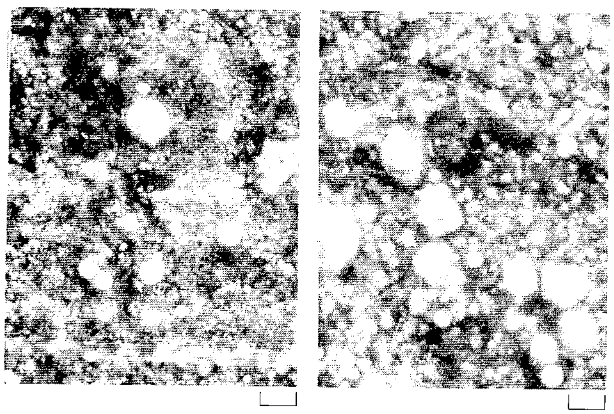

Photo 2 SEM images of wet dust collected in Ni ore and Cr ore reduction process

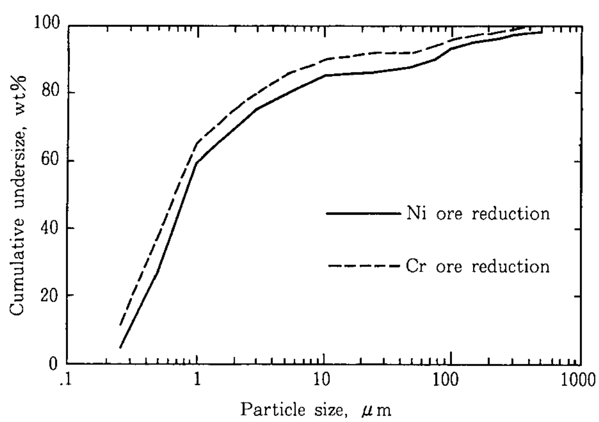

Fig. 10 Particle size distribution of wet dust collected in Ni ore and Cr ore reduction process

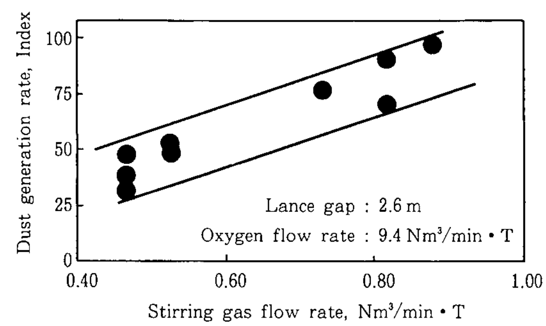

Fig. 11 Effect of gas flow rate on wet dust generation rate in Ni ore reduction process

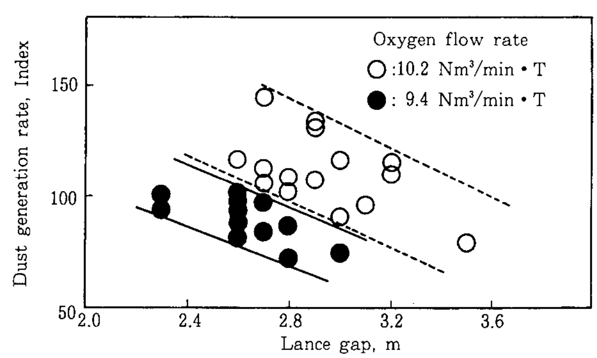

Fig. 12 Relation between top blowing condition and wet dust generation rate in Ni ore reduction process

lic droplets in the slag to contact the oxygen gas.
(2) Decrease the bottom gas blowing rate to minimize the content of metallic droplets in the slag.

These countermeasures may have an adverse effect on heating-up and on Cr mass transfer. For that reason, variations of the heating-up efficiency and the rate of Ni and Cr ore reduction were carefully observed to determine the most suitable gas flow rate in bottom blowing and top oxygen blowing under actual operation. Fig. 13 shows the reaching area of the oxygen jet for actual operations as calculated from the Engh et al formula[8].

Fig. 14 shows the effects obtained using the countermeasures described above. Approximately 70% of dry dust and 40% of wet dust were eliminated. As a result, the overall yield of both Ni and Cr in the total SRF process reached over 97%.

7. Improvement of furnace life

Fig. 15 shows the change in SRF furnace life.

Wear of side wall refractories was minimized by the following countermeasures;

- The quality of MgO-C brick for the side wall was upgraded.
- The slag composition during blowing was optimized and controlled by calculating the amount and kinds of charging materials.
- The method of slag making at the initial stage was improved.

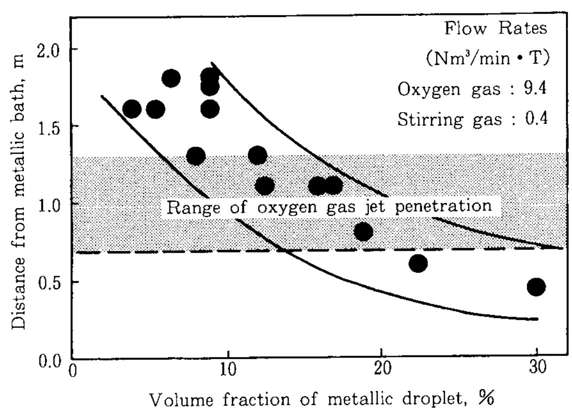

Fig. 13 Distribution of metallic droplets in slag for Ni ore reduction process

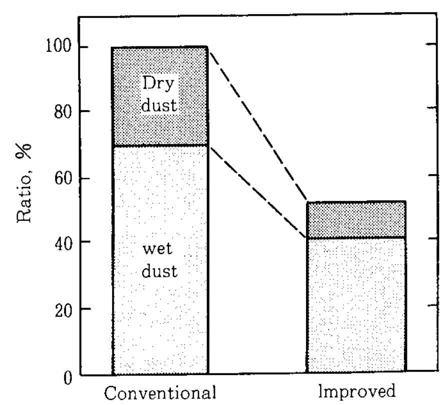

Fig. 14 Decrease in the amount of dust generation in Cr ore reduction process

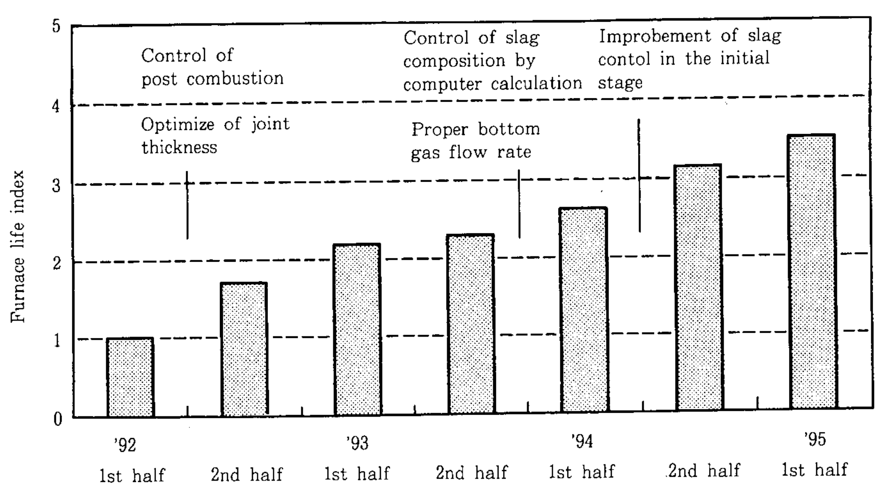

Fig. 15 Change in furnace life

In addition, the resistance to spalling of the tuyere bricks at the furnace bottom was improved by increasing the C content in the brick. Further, the tightness between refractory bricks was optimized to prevent spalling due to thermal expansion.

Prolongation of the furnace life was achieved as shown in **Fig. 15** after these countermeasures were introduced.

8. Conclusions

A new technology to produce inexpensive, high quality, stainless steel slabs was established by utilizing the superior refining capability of a converter and by using existing facilities for molten iron pretreatment, secondary refining and casting. This technology makes it possible not only to select a wide range of inexpensive raw materials such as Ni ore, Cr ore and scrap, but also to assure stable production yields.

References

1) Watanabe et al. CAMP-ISIJ. 7(1994), p. 254.
2) Inoue et al. CAMP-ISIJ. 7(1994), p. 255.
3) Uchino et al. CAMP-ISIJ. 7(1994), p. 256.
4) Takaoka et al. CAMP-ISIJ. 2(1989), p. 1083.
5) Takaoka et al. Tetsu-to Hagane. 76 (1990), p. 1839.
6) T. Takaoka et al. "Proc. Intl. Symp. on Ferrous and Non-Ferrous Alloy Processes". CIM 29th Annual Conference of Metallurgists. Hamilton, Ontario (1990-08), p. 164.
7) Association of Chemical Engineering, Chemical Engineering Manual, 3rd Edition, p.141.
8) T. A. Engh et al. Scan. J. Met. 4 (1975), p 241.

Horizontal Directional Drilling Method for Pipeline Crossing (NK-RAPID)

Tsunao Hirata*, Toru Ogawara*,
Takashi Nakajima*, Yasuhiro Matsuo**,
Kazuhiko Koike** and Tsukasa Ishikawa***

Horizontal directional drilling (HDD) of a pipeline crossing is done by drilling an arched hole from the ground surface along a specified path beneath obstructions, followed by pulling the pipeline through the hole. The HDD method was introduced to NKK from the Cherrington Corporation in the USA under a technical transfer agreement. NKK named this method "NK-RAPID" and used it for a pipeline crossing in Hong Kong. This paper presents an outline of NK-RAPID and the Hong Kong project undertaken by NKK.

1. Introduction

The horizontal directional drilling (HDD) method was developed in the USA in early 1970s. In this method, a hole is drilled obliquely from the ground surface along a smoothly curved path beneath obstructions such as rivers. A steel pipe is then pulled into the hole. Pits do not need to be dug on the entry and exit sides as they are with conventional drilling methods. The method uses directional drilling technology as applied in oil fields, in which the direction can be controlled flexibly while drilling an inclined hole. Last year, NKK entered into an agreement with the Cherrington Corporation, which has used this method in more than 350 locations, to introduce this advanced technology. We named this method "NK-RAPID" because of its very high drilling speed.

This paper presents an outline of NK-RAPID and describes the crossing at Lantau Island in Hong Kong, the site where this method was first used by NKK.

2. NK-RAPID method

2.1 Features of the method

The features of this method are:
(1) Pits on the entry and exit sides are not needed, leading to increased economy.
(2) Long-distance drilling is possible.
(3) No environmental pollution is created, such as contamination of river or sea water.
(4) Work can be performed in a short period of time.

2.2 Work procedure

This method is broadly divided into three steps, as shown in **Fig. 1.**
(1) First, a pilot hole is drilled using a 5-in. drill pipe.
(2) Next, the hole is reamed to expand the pilot hole to a diameter larger than that of the pipe to be pulled.
(3) The final stage is product pipe pullback, in which

* Manager, Pipeline Technology Sec., Pipeline System Technology Dept.
** Manager, Engineering Dept., Technical Development Center, Nippon Kokan Koji K.K.
*** Research & Development Dept., Nippon Kokan Koji K.K.

the product pipe to be laid is pulled in.

(1) Pilot hole drilling

Drilling is performed using a drill head attached to the tip of a 5-in. drill pipe. Two types of drill heads are available: the "spud jet" type, which discharges a mud slurry, and the "mud motor" type, which uses a rotating tip. The spud jet type is used for drilling through sand or silt, while the mud motor type is used for drilling through gravel, cobble, limestone and granite. With the mud motor type, the flow of mud slurry in the drill pipe is converted into a rotational force in a Moineau pump, rotating the tip, which crushes the rock and performs drilling. The same drill pipe is used, so there is no need to change the drill pipe.

Directional control is carried out based on measurements taken by an accelerometer and a magnetic sensor housed in a vessel behind the drill head. The surveyor determines the drilling direction by monitoring this data and gives instructions to the rig operator. The tip of the drill head is slightly curved and receives a reaction force when it is pushed into the ground, causing the drilling direction to change. The direction of the tip is adjusted by the drilling rig, permitting directional control.

To increase the accuracy of measurement near the entry and exit sides, an electric current is run through a cable laid on the ground to develop a magnetic field. This field is measured by a magnetic sensor installed behind the drill head to determine the position.

(2) Reaming (hole expansion)

Upon the completion of pilot hole drilling, a reamer is used to expand the hole. There are two reaming (hole expansion) methods. In the "forward ream" method, the reamer is pushed in from the entry side, while in the "back ream' method, it is pulled in from the exit toward the entry side. **Fig. 1** shows the "back ream" method. The method used is determined according to the soil type and other local conditions. In general, the "forward ream" method is preferred because it does not require relocation of the mud slurry facility and the slurry itself. A large amount of bentonite mud slurry is injected while reaming, which fills up the expanded hole and maintains the wall of the hole.

(3) Product pipe pullback

After the hole is expanded by reaming, a swivel is used to pull the product pipe in. A feature of this method is that reaming and pipe pullback are two separate steps (i.e., the product pipe is not pulled in while reaming). In methods that combine these steps, a large pulling force is required when encountering gravel or driftwood, which are often buried in a river bed. Separating these processes has the advantage of needing a smaller rig capacity and size.

Product pipe pullback is performed while the bentonite mud slurry is injected, as it is during the reaming operation. The mud slurry holds the wall of the hole and carries the cuttings out of the hole. It also functions as a lubricant between the hole wall and the

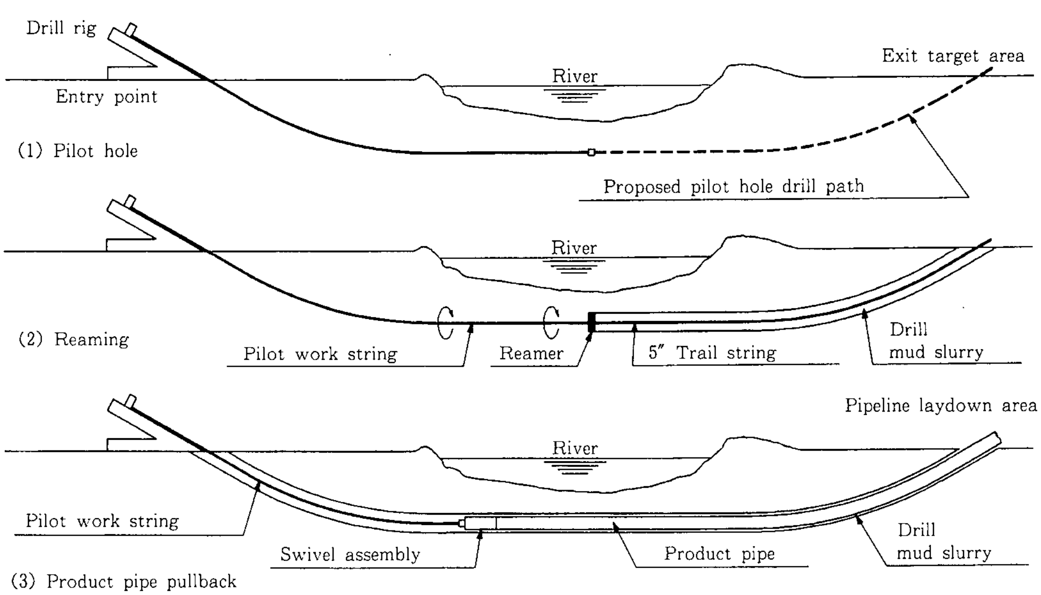

Fig. 1 Procedure for NK-RAPID

pipe being pulled. If the mud slurry hardens, the pipe pulling operation must stop. Therefore, the mud slurry is continuously circulated from the start to the completion of pipe pullback, during which time the work cannot be stopped.

2.3 Dedicated drilling rig for NK-RAPID

To comply with Japan's transportation regulations, the drilling rig was divided into two units: the operation room plus power source, and rig body. This division makes each unit light and compact. **Photo 1** shows the drilling rig specially designed for NK-RAPID.

The specifications of the new rig are as follows:

(1) 2.45 m wide, 13.11 m long, and 2.16 m high
(2) Empty weight 25.9 tf
(3) Pulling force 136 tf

2.4 Scope of application

This method can be used for drilling holes as long as 1800 m. The diameter of the pipe that can be laid by this method depends on the distance. Cherrington Corp. has laid a 1050 mm pipe for a distance of 1200 m.

3. Application example in Hong Kong

3.1 Outline of the work

The shore approach at Ta Pang Po on Lantau Island was carried out by the HDD method for a submarine pipeline about 4.2 km long. The HDD method was specified by the consultant of the user because of environmental concerns. The product pipe was epoxy-coated, API 5L X-52 with an outside diameter of 323.85 mm. The span was 400 m, but to facilitate the connection to the submarine pipe, the 400 m epoxy-coated and 200m concrete-coated pipe was pulled. Two such gas pipelines, the East and West Lines, were laid in parallel. The distance between the twin pipelines was 5 m. Details of this work using NK-RAPID are as follows:

(1) Owner: The Hong Kong and China Gas Co., Ltd.
(2) Work site: Lantau Island, Hong Kong
(3) Work period: June to August 1995
(4) Crossing: Rock sea wall
(5) Work content:
 Length 400 m,Two lines in parallel
 Minimum radius of curvature 300 m R
 Soil condition Silt
(6) Specifications of product pipe:
 API 5L X-52
 Outside diameter 323.85 mm, thickness 12.7 mm
 Inside and outside coating Epoxy coating
(7) Pipe content: Town gas

3.2 Work site

The work site is shown in **Fig. 2**. A summer resort called Gold Coast is located one hour from downtown Hong Kong. The site at Ta Pang Po on Lantau Island is 25 minutes from Gold Coast using a high-speed crew boat. A new airport is being constructed 5 km from the site. Lantau Island has an area that is twice that of Hong Kong Island, but only the east side has been developed. There is no road from the east

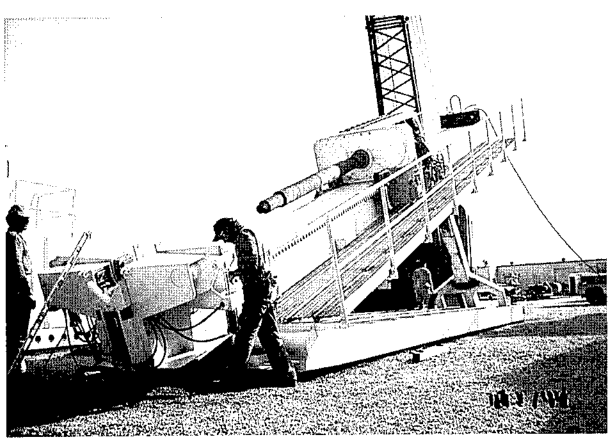

Photo 1 Drilling rig for NK-RAPID

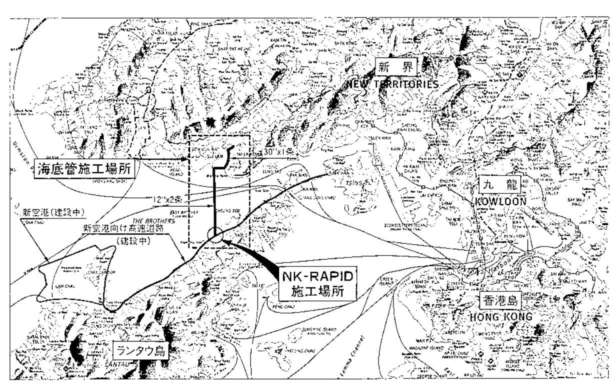

Fig. 2 Site location

side to the west side, and Ta Pang Po is a closed district controlled by the Lantau Expressway Joint Venture of Hong Kong's new Chek Lap Kok International Airport. An access road is being constructed in parallel with the construction of the new airport. As such, the site was inconveniently located, making it difficult to transport workers, rig equipment and materials.

The site is between the sea and a rocky hill, which is covered by grass and has a crystalline deposit underground. It is extremely hot when the weather is fine, but when the rains start, it rains torrentially, and the ground immediately turns into a bog. There are no inhabitants in the vicinity. **Photo 2** shows an general view of the site.

3.3 Work procedure

The basic work procedure was as follows.

(1) Mobilization of rig and plants
(2) Setting up of rig and plants
(3) Pilot hole
(4) Tripping of pilot hole
(5) Reaming (hole expansion)
(6) Tie-in of pilot pipe to product pipe
(7) Product pipe pullback
(8) Cleanup
(9) Demobilization of rig and plants

It was necessary to excavate a pipe trench on the sea bottom and to temporarily lay the product pipe in the trench before starting step (6). **Fig. 3** is a cross sectional view of the work.

3.4 Laying of product pipe in pipe trench on sea bottom

If the sea wall crossing was first completed by the HDD method, and the trench for the submarine pipeline was then excavated starting from the tip of the crossing, the accuracy of the HDD would not be of much concern. However, this procedure could not be used because of the work schedule. First, a 15 m wide pipe trench was excavated, and twin product pipes were temporarily laid at the center of the trench with a clearance of 5 m between them. Then, a pilot hole was drilled aiming at these pipes. **Photo 3** shows a submarine pipeline being laid.

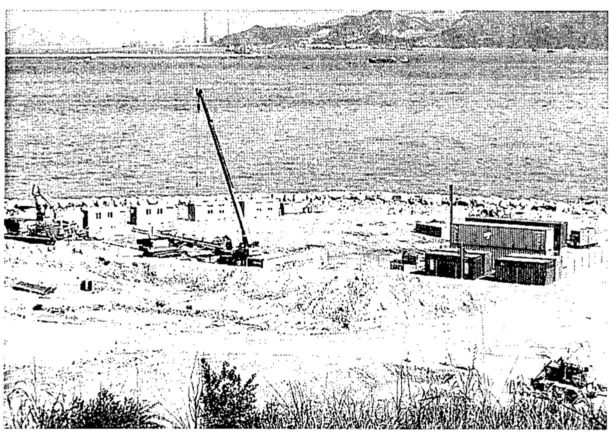

Photo 2 Site at Ta Pang Po

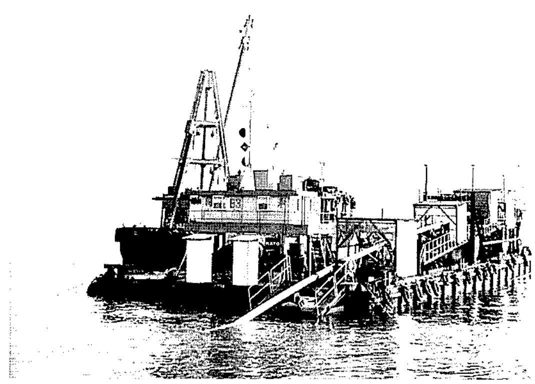

Photo 3 Pipe laying at sea

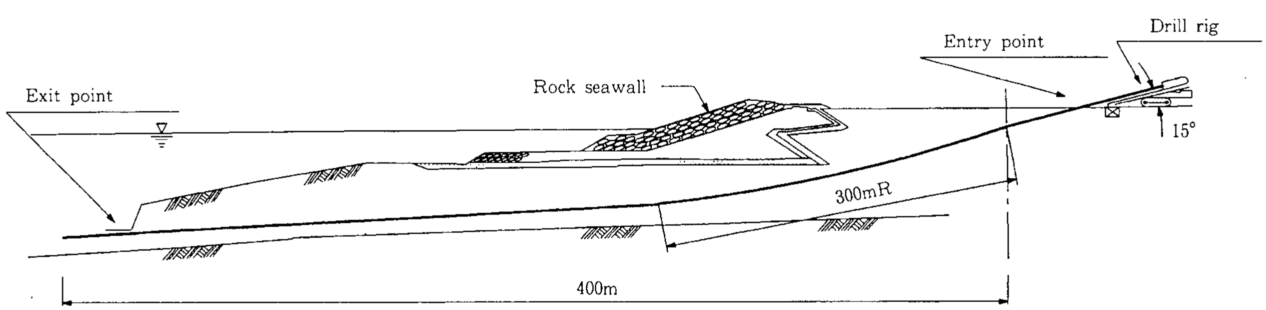

Fig. 3 Shore approach details

3.5 Mobilization of rig and plants

The rig and plants used for drilling were transported from the United States. They were transferred to a derrick lighter off Hong Kong Island. Boom trucks and trailers were loaded at the Port of Kowloon. The derrick lighter came alongside the pier at a port called Sham Shui Kok, on Lantau Island. The port has no unloading facilities. From there, the rig and equipment were carried on land about 2 km to the site.

3.6 Site area

Initially, a work area of about 1500 m^2 was planned to be used. However, after the work began, the area expanded to 2944 m^2 (46 m x 64 m), or twice the planned area, since additional area was available adjacent to the site. The site was expanded to include a storage area for containers for materials and equipment and for a temporary storage area for cuttings, which became necessary. In addition, moving the heavy machinery used for the work (boom crane, backhoe, forklift) requires a large area. **Fig. 4** shows the arrangement of the main equipment.

3.7 Rig equipment and mud slurry plant

The rig used for this project was equipped with a crawler for mobility and weighed 33 tf. Since this type of rig can move freely by itself, it is very convenient for cases where the rig must be moved during the work to lay twin pipelines, as in this project. Fine adjustment does not require additional heavy machines, such as a boom truck. A mud slurry plant was needed in addition to the rig. The mud slurry plant for this project had a device for mixing the bentonite mud slurry, a device for separating sand and silt, water and mud slurry tanks, a generator, and other equipment. It is a very compact rig that can be towed by a wheeled trailer truck.

3.8 Setting up of rig

The planned entry angle was 12 degrees. However, it became apparent from drawings obtained later that there was a possibility of penetrating the foundation of the sea wall located in front. Even if the hole did not penetrate, there was a risk of losing the mud slurry circulation if the pipe came too close to the foundation. Increasing the angle to 18 degrees would produce an excessive load to the box culvert under the rig. The loads on the box culvert were calculated, and an angle of 15 degrees was determined as a compromise.

3.9 Water

Initially, water was planned to be transported by barge. However, this method was found too costly, and water from a mountain stream near the site was used. The water was transported by a hose laid through the box culvert under the site, and a submersible pump was installed deep in the water at the mouth of the valley. Because of the abundant rainfall, no suspension of work was caused by water shortage.

3.10 Pilot hole

Pilot hole drilling proceeded very smoothly, probably because the soil was soft silt. If the pilot hole

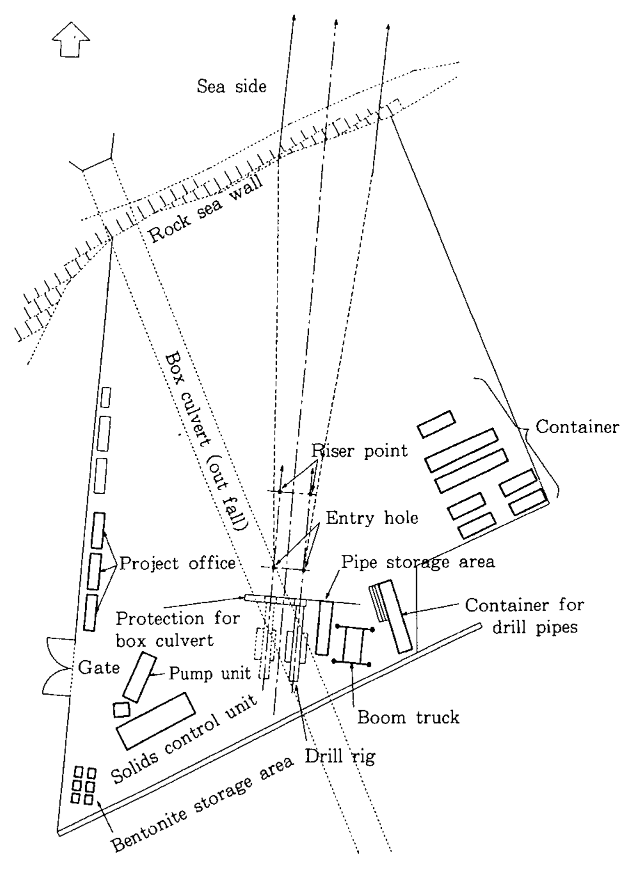

Fig. 4 General arrangement of yard at Ta Pang Po

was directed down too steeply, it might not meet with the pipe trench. Therefore, drilling was performed slightly upward, and a downward correction was needed at the final stage. Correction of the position is very difficult using the pipe jacking or shield tunneling methods. In the HDD method, however, correction of the position is very easy. For correction work in this project, there was one case where three pipes were pulled back and four pipes were pushed, and another case where seven pipes were pulled back and eight pipes were pushed. In either case, the work took less than half a day. This is one of the advantages of the HDD method. Pilot hole drilling work is shown in **Photo 4**.

On the other hand, checking the position of the exit of the pilot pipe on the sea bottom took more time than expected. Delays were caused by poor visibility in the muddy sea, suspension of work because of tides, diving time limited by the 20 m water depth, and other problems.

3.11 Reaming (hole expansion)

Reaming was performed from the rig side on the shore toward the sea. This was because of the difficulty in installing a reamer on the exit side on the sea bottom. Also, the favorable hardness of the soil made this method possible.

3.12 Tie-in of pilot pipe to product pipe

The visibility in the sea was only 1 m or less, and the sea bottom was soft. The divers worked by groping in silt. The sea bottom was first checked by a probe bar to find the tip of the pilot pipe. After the pilot pipe was found, the tip was removed and a swivel lowered by the derrick lighter was installed. The swivel was turned with a rod-shaped tool and screwed into position. The entire pilot pipe was then pushed out toward the product pipe using the rig, and the swivel and the product pipe were brought together and connected with a shackle. The connection between the swivel and the pilot pipe was further tightened by the rig. Tightening was performed by holding the pilot pipe in position, moving the tool with the derrick lighter, and rotating the swivel. Finally, the jigs and tools were removed. This procedure took a considerable number of days as did the pilot pipe position check.

3.13 Product pipe pullback

The product pipes were temporarily laid in the sea bottom trench for 26 days for the West Line and 44 days for East Line. The product pipes might be covered with silt due to tidal movement, or they could stick to the sea bottom, requiring additional pulling force. Although the rig had sufficient pulling force, the pilot pipe could cut into the soft ground when pulled. The West Line, which had been in place for a shorter period of time, was pulled first, followed by the East Line. Both lines were pulled without problem using a maximum pulling force of about 34 tf. For the East Line, however, it was necessary to pull little by little, increasing and decreasing the load with each step, and a longer time was spent. The epoxy coating of the product pipes was examined after they had been pulled back, and no damage, such as caused by gravel, was found. The product pipe after pulling is shown in **Photo 5**.

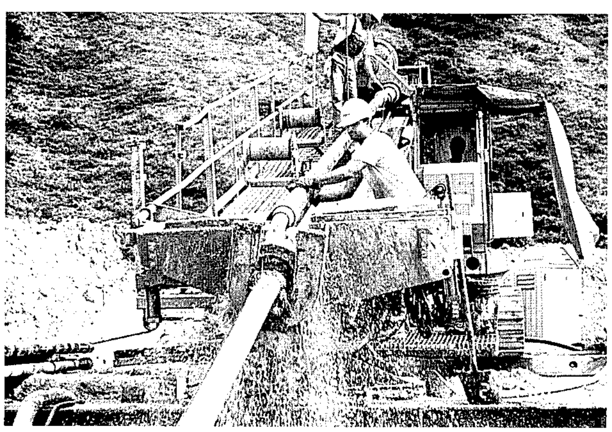

Photo 4 Work for pilot hole

Photo 5 Pull back line

3.14 Term of work

The work was started in July, 1995. It took about a month for the two product pipes (600 m each) to be temporarily laid on the sea bottom. Although preparation for drilling took much time, only about three weeks was required from the start of pilot hole drilling to the completion of pullback of the twin product pipes. All the work including demobilization was completed on schedule by the middle of August.

4. Concluding remarks

In the open-cut method, various kinds of work can be done in parallel. In the HDD method, however, they need to be carried out in series. Therefore, if part of the equipment or system fails, all the work must be suspended. If the pilot pipe merely collides with an obstruction in the ground, all of the work is interrupted. If the diver cannot find the pilot pipe on the sea bottom, or if the diver cannot connect the pilot pipe to the product pipe, the work cannot continue. Each time a problem occurs, a quick decision is required. However, advantages of the HDD method include its short term of work and the cost savings over conventional methods such as shield tunnelling and bridge crossing.

NKK introduced the advanced HDD technology, named it the NK-RAPID method, and applied it to the rock sea wall crossing at Lantau Island in Hong Kong. In this project, we satisfactorily completed the laying of twin 323.85 mm x 400 m gas pipelines in two and a half months without damaging the sea wall. We hope this project report is helpful for pipeline construction in the future.

Magnetizing Eddy Current Tool

Munetaka Kondo*, Kikuji Murashita*,
Hiroshi Honma*, Mineo Kurashima*,
Michiharu Toge** and Sueyoshi Nishino**

Conventional eddy current tools can only detect internal corrosion. However, NKK's new pipeline inspection tool uses magnetizing eddy current (MEC) to detect both internal and external corrosion and to differentiate between them. The new tools were evaluated in test loops and demonstrated good performance. This paper summarizes the new MEC Tools and presents the results from the test loops.

1. Introduction

Pipelines are widely used as an economic means for transporting oil and gas, and their maintenance and safety are important. Therefore, the early detection of corrosion occurring on the internal and external pipe surfaces is indispensable for preventing accidents.

Various types of pipeline inspection tools have been used to meet these needs. NKK developed an inspection tool that uses ultrasonic techniques and has used it in actual inspections in operating pipelines. However, there is a strong demand for the development of a tool that can meet more diversified inspection requirements.

To meet this need, NKK developed a magnetizing eddy current inspection tool that can simultaneously inspect corrosion on the internal and external pipe surfaces, which is difficult using conventional eddy current methods.

2. Principle of detection

2.1 Sensor

As is well known, the principle for detecting metal loss using the eddy current method is as follows: The sensor has a primary and secondary coil. When an AC signal is applied to the primary coil, a magnetic field is produced, and concentric eddy currents are generated in the metal to be inspected. If the metal has corrosion or metal loss, the magnitude of the eddy current changes. The state of metal loss can be detected by sensing this change with the secondary coil. The absolute value types of eddy current sensors that are used conventionally are unsuitable for inspections made while the inspection tool is moving. However, the new inspection tool uses a sensor that detects the differential signal between two secondary coils, as shown in **Fig. 1**.

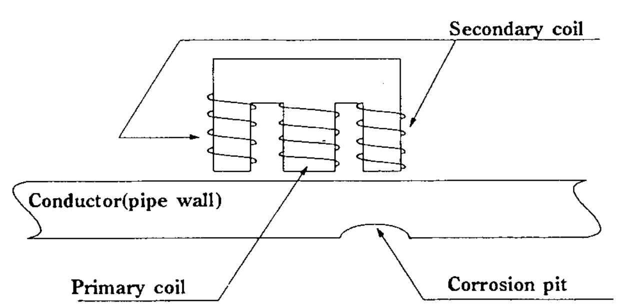

Fig. 1 E-shaped core sensor

* Manager, Pipeline System Engineering Dept.
** Manager, Nippon Kokan KOji k.k, Engineering Dept.

2.2 Effect of DC magnetization

When a steel pipeline is inspected by an eddy current sensor, a strong eddy current is generated on the internal pipe surface adjacent to the primary coil of the eddy current sensor. The eddy current does not normally penetrate to the external surface of the pipe, making it difficult to detect external metal loss by this method. With the magnetizing eddy current method, an eddy current can be generated that reaches the external pipe surface by locally magnetizing the pipe, as shown in **Fig. 2**. With this method, both the internal and external pipe surfaces can be simultaneously inspected.

3. Configuration of inspection tool

As shown in **Fig. 3**, the magnetizing eddy current inspection tool has a pressure-resistant vessel that houses a variety of measurement devices and that has seal cups for moving the tool by using the fluid in the pipeline. The devices are powered by a battery mounted in the tool. Signals from the eddy current sensors arranged around the circumference are converted into digital signals and recorded in memory after being processed. The relationship between the recorded signal and the location in the pipeline are determined by simultaneously recording a position signal from the odometer mounted at the rear of the tool. An oscillator can also be installed to detect the position of the tool from outside of the pipeline.

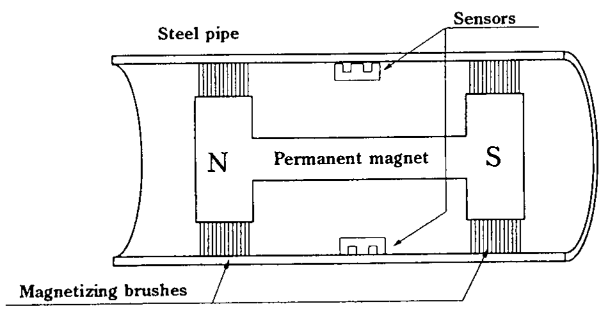

Fig. 2 Sensor arrangement

4. Features

The magnetizing eddy current inspection tool has the following features:

(1) Corrosion (depth and extent) on both internal and external pipe surfaces can be inspected simultaneously.
(2) Internal and external corrosion can be classified.
(3) Detection can be done at bends.
(4) Inspection results can be displayed graphically.
(5) The transport fluid may be either gas or liquid.
(6) Long-distance inspection is possible because the system is cable-less.
(7) Inspection can be made using the transported fluid pressure without stopping operation of the pipeline.

5. Design specifications

(1) Applicable pipeline
(a) Diameter: 8 in. to 12 in. (200 to 300 A)
(b) Bend radius: 1.5 DR (possible to pass elbow)
(c) Dent and deformation: 5% D or less
(d) Inspection distance: about 2 km
(2) Fluid specifications
(a) Kind: liquids such as crude oil, product oil and water

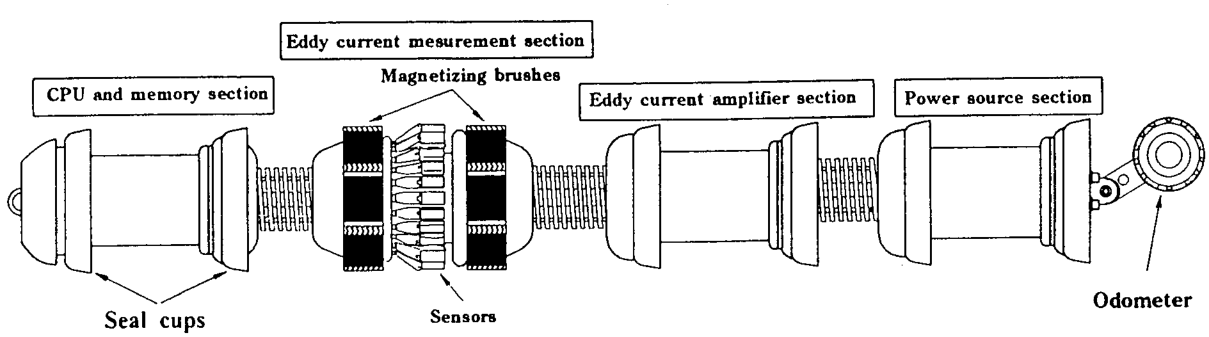

Fig. 3 Configuration of magnetizing eddy current inspection tool

gases depending on piping conditions
(b) Temperature: 50°C and lower
(c) Pressure: 40 bar and lower
(d) Flow velocity: 2 m/s and lower
(3) Inspection performance
(a) Detection performance: corrosion of 30% t (t: nominal pipe thickness) and more
(b) Measurement accuracy: ±10% t

6. Performance verification test

6.1 Testing equipment

Performance verification tests using test loops were carried out to verify the ability of the magnetizing eddy current inspection tool to negotiate pipeline geometries and to detect corrosion. The shape of the

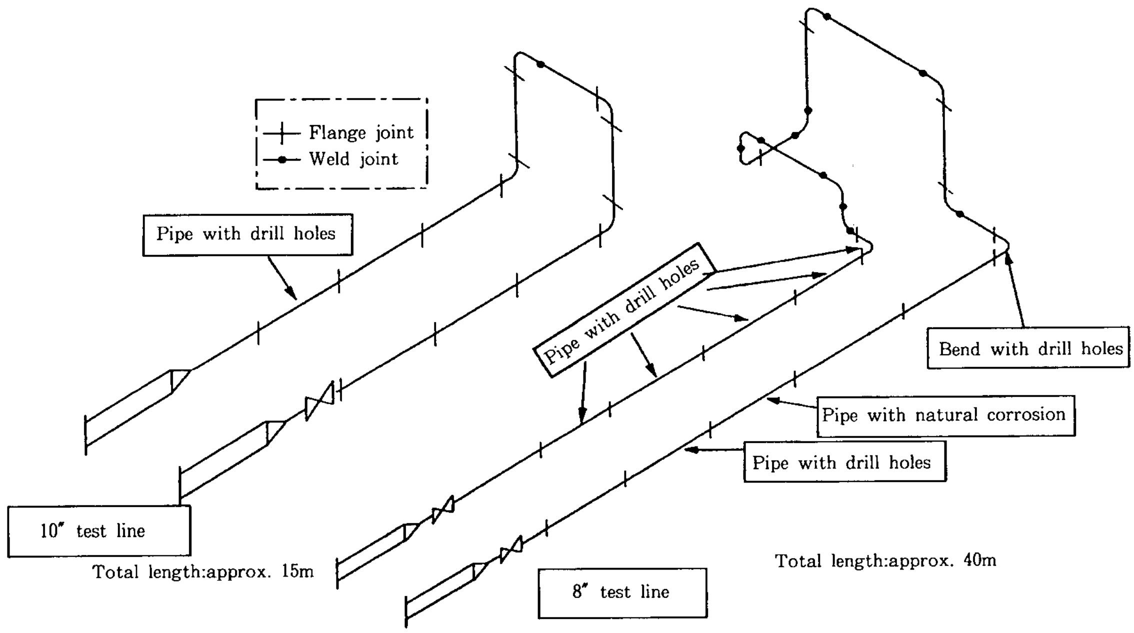

Fig. 4 Test facility

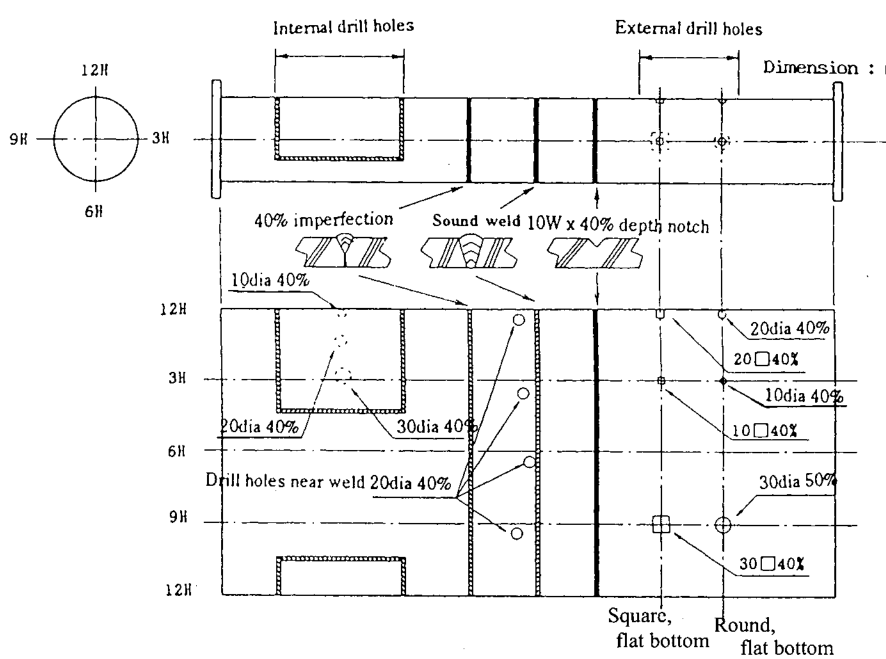

Fig. 5 Examples of artificial drill holes

test loop included bends to verify the negotiability of the inspection tool, as shown in **Fig. 4**. Also, test loop pipes had artificial drill holes, as shown in **Fig. 5**, to verify the detection ability. The total length of the test loop was 40 m for the 8-in. line and 15 m for the 10-in. line. A bend radius of 1.5 DR was used, and the pipe specifications were STPY 400 x sch 40 for both lines. **Photos 1** and **2** show a general view of the test loops and a performance verification test in progress, respectively.

6.2 Negotiability test result

In the performance verification test, industrial water fed by a pump was used as the pressure fluid for the inspection tool. The running speed was about 1.0 m/s. The differential pressure produced before and behind the tool while running was about 2.5 bar maximum for both the 8-in. and 10-in. tools. The maximum differential pressure occurred when the tool passed through a bend. The tool moved through the pipeline smoothly, and no problems were encountered negotiating the inspection tool during the test.

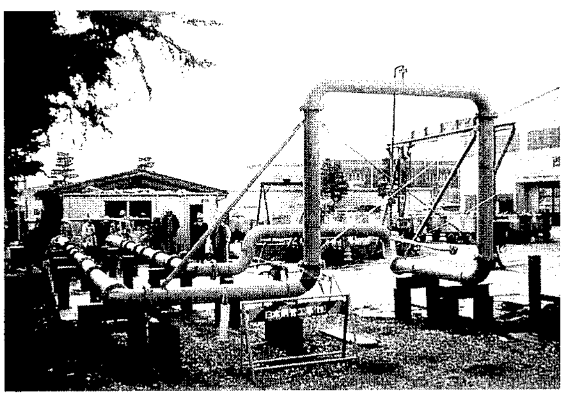

Photo 1 Overall test loop arrangement

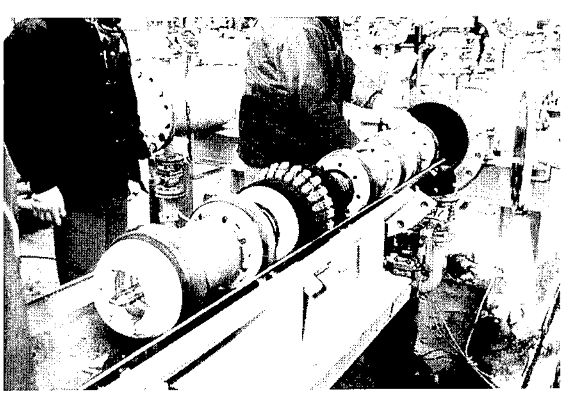

Photo 2 Testing in progress

6.3 Detection ability test result

Fig. 6 shows the results of detecting artificial drill holes made in the 8-in. pipeline by the inspection tool. In **Fig. 6**, the abscissae represent the travel distance in the pipe axial direction, while the ordinate represents the output voltage of each sensor around the circumference. This figure shows that the artificial drill holes were detected satisfactorily. **Figs. 7** and **8** show examples of the inspection of natural corrosion in the test loop. These results confirmed that natural corrosion

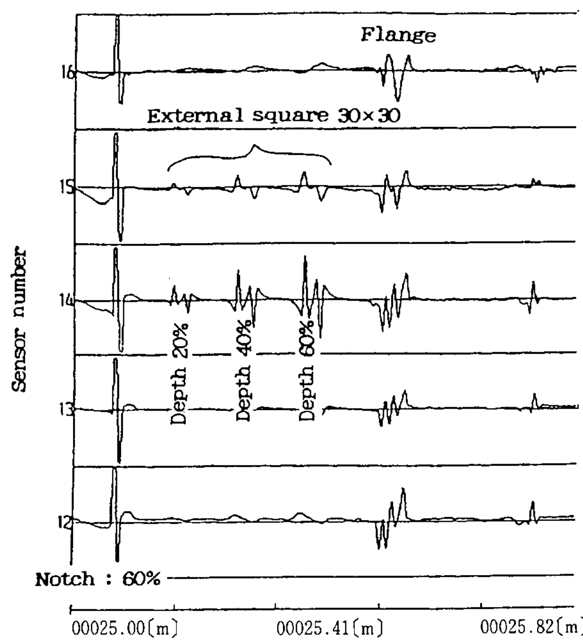

Fig. 6 Artificial drill holes analog output

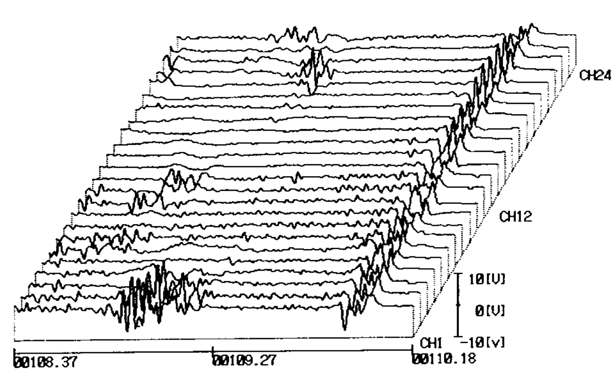

Fig. 7 Natural corrosion analog output (3D plot)

can also be positively detected, and that a good linear correlation can be obtained with respect to the corrosion depth. The corrosion location could be determined easily from the odometer data and the event characteristics (circumferential weld, elbow, nozzle, etc.).

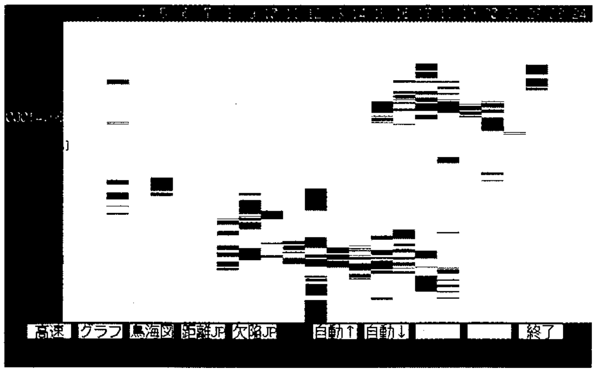

Fig. 8 Color plane view of pipe with natural corrosion

7. Concluding remarks

A magnetizing eddy current inspection tool was developed for small-diameter (8 in. to 12 in.) pipelines. Performance verification tests were carried out on test loops to verify the ability of the unit to negotiate pipeline bends and to detect significant corrosion. As a result, our purpose was accomplished.

In the future, we will try to improve the detection ability and the level of analysis to meet pipeline inspection requirements that will become increasingly severe.

Increasing Throughput of the New Tokyo International Airport Pipeline

Hiroshi Matsumoto*, Takaomi Naganuma*,
Tomoo Nezu** and Jiro Nakamura**

The aviation fuel pipeline for the New Tokyo International Airport (NTIA) has operated smoothly since it was put into service. As the fuel demand for the NTIA increased, it was feared that the pipeline throughput might not be adequate, and that the stable fuel supply might be interrupted by earthquakes or large, neighboring construction projects. The NTIA Authority planned to increase the throughput by adding a booster pump station. NKK was responsible for establishing a new control system in addition to the mechanical and piping work. Commissioning was completed in March 1996. An outline of the new control system is reported in this paper.

1. Introduction

Aviation fuel is supplied to the New Tokyo International Airport through a pipeline that was completed in 1983 between the airport and the Chiba Port. The pipeline extends over a distance of 47km, and consists of a pair of 14B pipelines. Previously, fuel was pumped with a maximum normal pressure of 29.5 kg/cm^2 at 500 kl/hour by pumps at the Chiba port. The booster pump station was planned to repressurize the pipeline and increase the throughput by approximately 50% in response to increased demand.

The use of serial pumping in this pipeline significantly changed the pipeline operation and control method, and a major expansion of the instrumentation and control system over the entire length of the pipeline was required. NKK was assigned the overall construction of the system. The new system needed to be constructed while the aviation fuel supply was continued. The system was completed without incident in March 1996 and put into service in April. This paper outlines the pipeline enhancement project, centering on the instrumentation and control system.

2. Facilities for increasing the throughput

The throughput of the pipeline was increased by constructing a booster pump station at Yotsukaidou. The throughput increase could have been achieved by adding an extra pipeline or by replacing existing pumps with higher capacity pumps, but the New Tokyo International Airport Authority adopted the booster pumping method for reasons of safety, economy, effect on existing facilities, and realistic construction planning constraints. The following is an outline of the facilities constructed to increase the throughput of the pipeline.

The overall layout is shown in **Fig.1**, and an out-

* Managing Staff, Control Technology Dept.
** Instrumentation system Div., Control Technology Dept.

line of the pipeline facility is shown in **Fig.2**. Fuel is pumped from tanks at the Chiba Port Oil Terminal, which is the pipeline takeoff terminal, to the pipeline using the increased capacity facility. The pressure is increased at the booster pump station located at Yotsukaidou, midway along the pipeline, and then fed to tanks at the New Tokyo International Airport. The pumps at Yotsukaidou raise the pressure and increase the flow rate by about 50%.

The new oil terminal at Yotsukaidou (**Photo 1**) has a pumping capacity equal to that at the Chiba Port. An associated electrical power facility and control equipment were also installed.

3. Instrumentation and control system

3.1 System configuration

The configuration of the new instrumentation and control system that was needed for the increased throughput is shown in **Fig.3**. As a comparison, the configuration of the old system is shown in **Fig.4**. In the new control system, monitoring and control functions were added to the Yotsukaidou terminal, operation of the overall fuel supply facility was integrated, and pipeline monitoring and control functions were improved.

The primary components of the system are the distributed control system (DCS) for monitoring and control of the pipeline, a computer for leak detection and transportation management, the telemeter and telecontrol system for monitoring and control of the pipeline, and another telemeter and telecontrol system for remote monitoring and control of the Yotsukaidou Oil Terminal.

The major components of primary facilities are duplicated and provided with backup functions to ensure reliability because the international airport is a facility of considerable public importance.

3.2 Functional changes in the new control system

The primary functional changes implemented in the new control system are as follows.

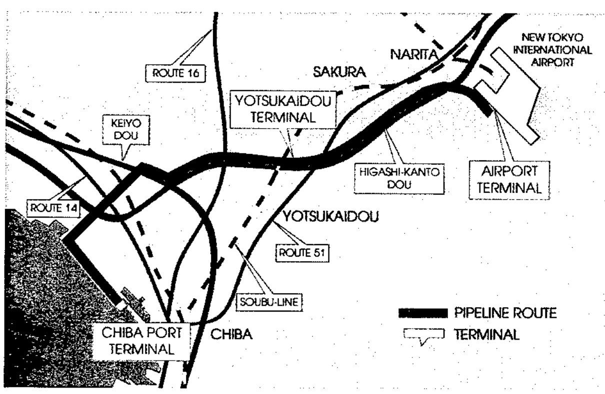

Fig. 1 Layout of pipeline

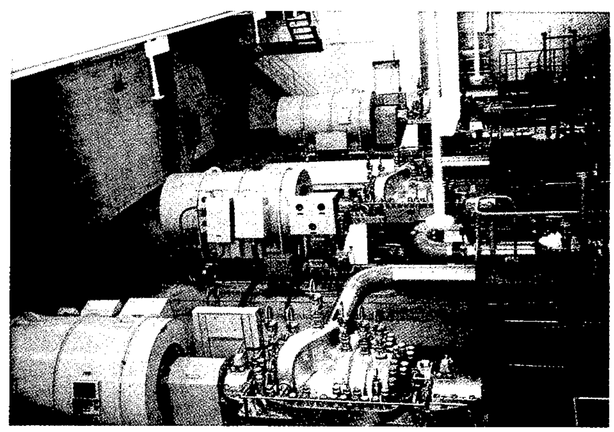

Photo 1 Yotsukaidou terminal

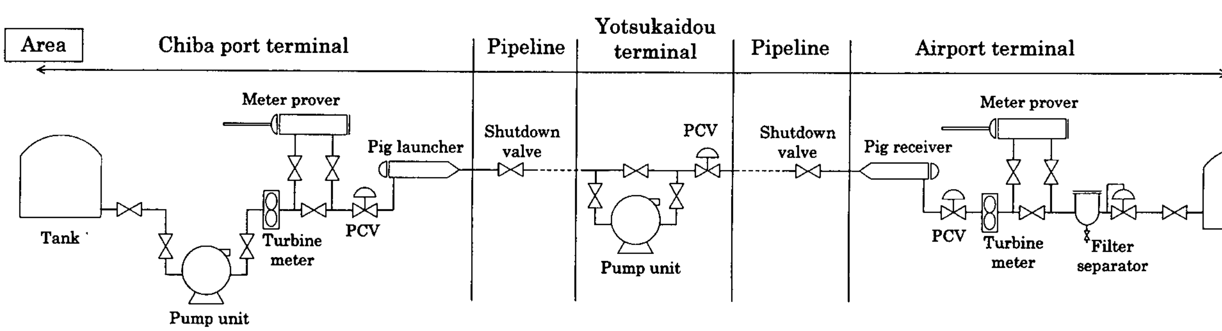

Fig. 2 Pipeline facilities

3.2.1 Functional improvements provided by the new control system

The operation and control functions were enhanced to accommodate upgrades to the basic system done to increase the throughput of the pipeline.

In addition to the monitoring and control functions added to the Yotsukaidou Terminal, optimal operation of the system requires the monitoring of large amounts of information to permit a high degree of operational freedom and accommodate varying line configurations. The classification of information according to the phase of operation and the development of a man-machine interface that permits timely access to that information was needed to reduce the load for monitoring and operating under these conditions and make the system fail-safe.

Therefore, a distributed control system operated mainly by the use of display screens and keyboards was employed to improve the man-machine interface. Further, large screens were installed for use by many people during an emergency. **Fig.5** shows the DCS operation monitoring screen, and **Photo 2** shows the large screen in the control room at the Chiba Port.

The old control system had some automated functions such as automatic shutdown by a warning signal. To reduce operators' workload, new automated functions were added for pipeline configuration control and for starting the Yotsukaidou pumps.

3.2.2 Operation and control method

A pressure control method was adopted for the new control system. Given the purpose of maximizing pipeline throughput, the control method was designed to utilize the maximum pipeline pressure allowable under the regulations and to maximize the pressure difference within this limit to obtain maximum flow.

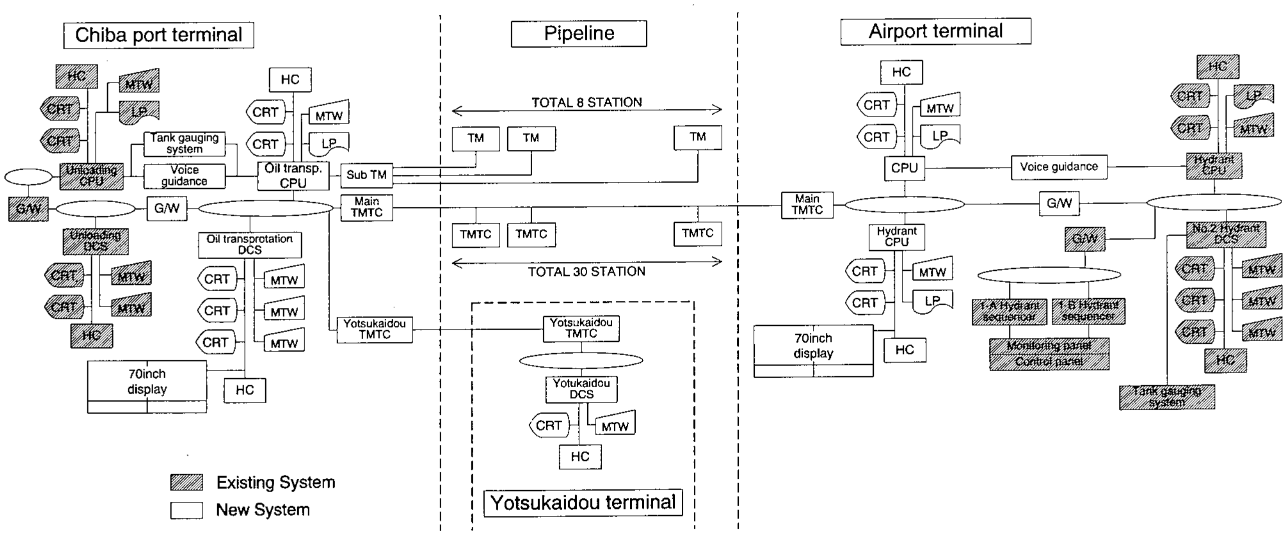

Fig. 3 New control system

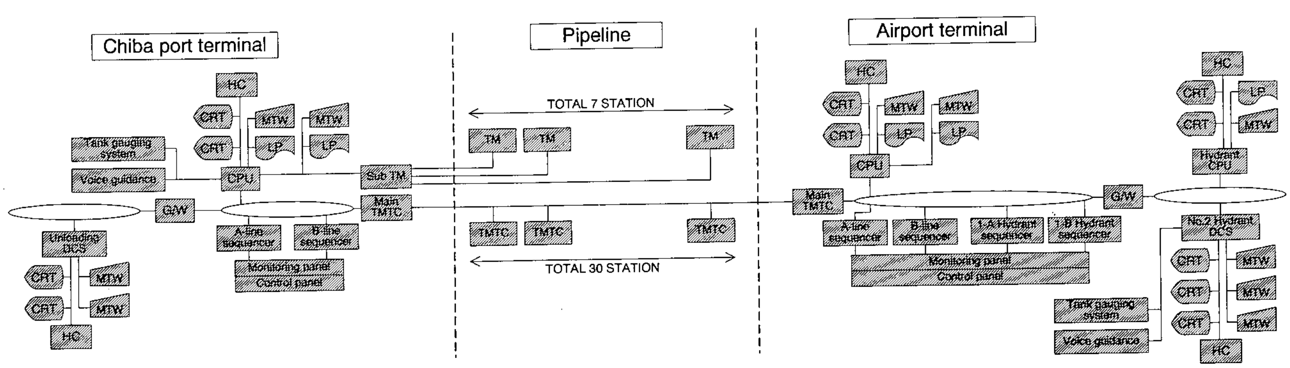

Fig. 4 Existing control system

3.3 System switching

The most important requirement for this work was the need to maintain the supply of aviation fuel while work was underway. To fulfill this requirement, the following points were considered when designing the system, scheduling, and implementing the work.

(1) Equipment dedicated to system switching was installed to reduce the time required to switch to the new system.

(2) Tests and adjustments of the new system were performed in a manner which minimizes the effect on existing facilities.

(3) A smooth startup was ensured by switching the control system one pipeline at a time.

Details of these points are given below.

3.3.1 Switching equipment

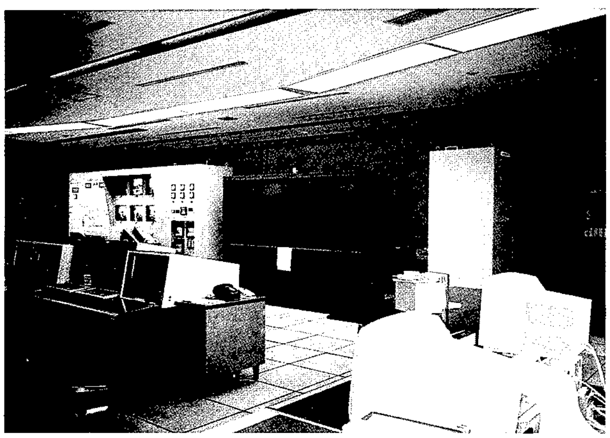

Photo 2 Chiba port terminal control room

To switch to the new system in as short a time as possible, a signal switching function was added to the marshaling panel. This function allows input and output signals to be directed to either the new or old system. Each control system could be switched independently to permit the startup of one pipeline system at a time, as described later.

Signal switching was required not only at the Chiba Port and Airport Oil Terminals, but also at approximately 30 satellite stations along the pipeline. The signal switching function allowed switching between the old and new systems within a few hours.

3.3.2 Tests and adjustments of the system

As shown in **Fig.3**, the instrumentation and control system for the increased throughput pipeline is almost entirely new. In the new system, the new and old control systems were designed to be independent and complete, which allowed tests and adjustments of the new system while operating the pipeline with the old system.

The adoption of this method limited the number of cases that required stopping the existing equipment to those tests performed to check the operation of the on-site equipment or the effect of modifications made to the software of the old system. This allowed the uninterrupted supply of aviation fuel while completing the tests and adjustments for the new control system.

Tests were also conducted for starting one system at a time, as described below, to ensure a smooth startup of the enhanced pipeline.

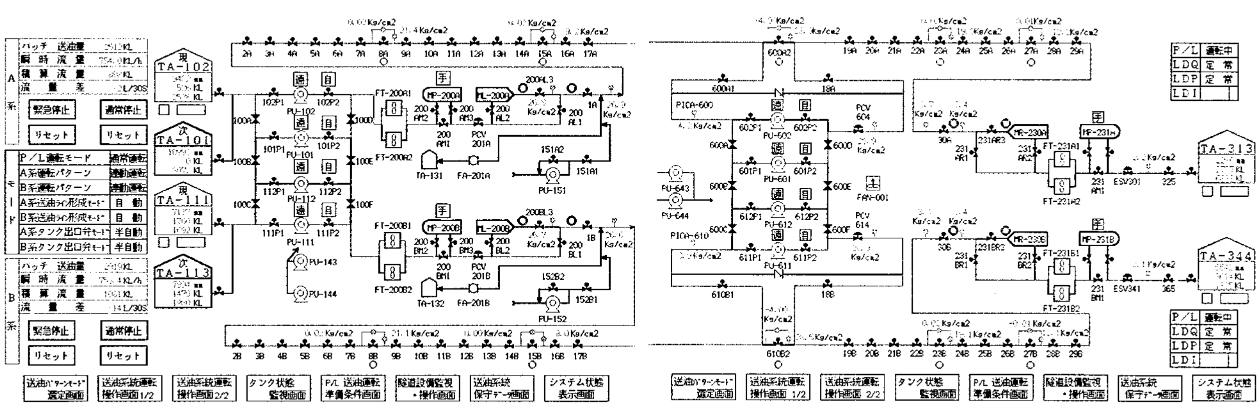

Fig. 5 DCS graphic panel

3.3.3 System startup procedure

When starting up the enhanced pipeline, the control system was switched one pipeline system at a time. This method was employed to ensure continuation of the aviation fuel supply even if a problem occurred during trial operation and the new pipeline could not be used. However, because the old system was maintained along with the new system during the transition period, it was feared that problems in one system might induce problems in the other. To eliminate this possibility, software dedicated to the transition period was used, and the signals were switched individually for each pipeline system. These measures were tested and adjusted to ensure that the old and new signals were fully isolated to prevent interference between the two.

This method allows the characteristics of the enhanced pipeline to be identified by operating one pipeline system for which switching and tuning is complete. The results for the first system can be used in the second system, providing a smoother transition to full operation with the new system.

4. Results of commissioning

4.1 Commissioning procedures

Commissioning was first carried out for one system. When commissioning was completed, the first system was handed over to the customer, and commissioning of the second system was started.

4.2 Normal starting and stopping of Yotsukaidou pumps

The timing for starting and stopping the pumps, and opening and closing the discharge valves and pressure control valves (PCV) at the Port and Yotsukaidou terminals was determined in advance by detailed dynamic simulations. These analyses allowed trial operation under conditions as close to the optimum as possible. The pressure and flow characteristics at starting and stopping are shown in **Fig.6** and **Fig.7**, respectively. These diagrams clearly show that stable flow was obtained. Also for batch counts, a batch could be stopped within an allowable lag for a set batch quantity.

4.3 Flow rate after throughput increase

As described in **3.2**, the pressure control method was employed for the new system, which is expected to have some flow rate variations. The flow rate predicted during design was a maximum of 750 and a minimum of 697 kl/hour. As expected, changes in the specific gravity, height of the receiving tanks, and condition of filter separators, etc., resulted in flow rate variations during trial operation. On the basis of data obtained during trial operations, the range of flow rate variation was calculated considering the maximum changes in operating conditions. These calculations revealed a range of 785 to 702 kl/hour, which is very close to the designed range.

4.4 Detecting flow rate differences

Due to the increased throughput of the new pipe-

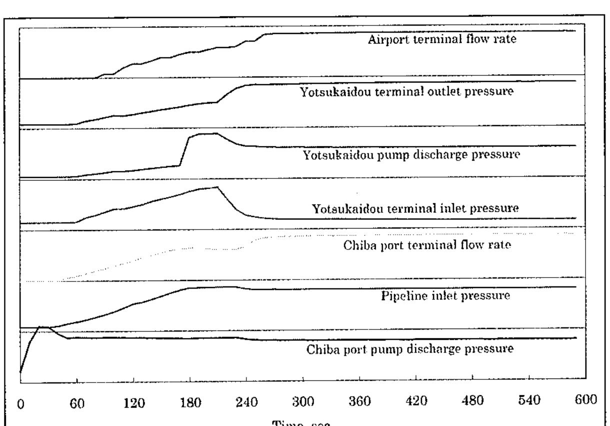

Fig. 6 Process values at start up

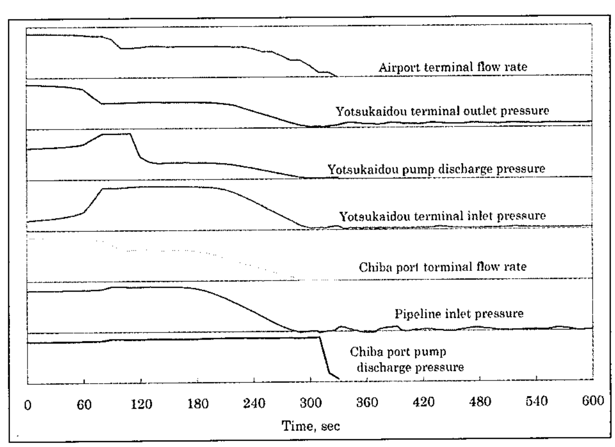

Fig. 7 Process values at stopping (T3=150sec)

line system and the use of the pressure control method instead of constant flow rate control, it was feared that the ability to detect the same level of flow rate differences as the old system might not be obtainable. An oil leak test was therefore implemented during trial operation in order to check this performance. The results are shown in **Fig.8**, and confirm that the new system can detect the flow rate difference of 80 liters/30 sec required by the Petroleum Pipeline Law. This confirmed that the performance is equal to that of the old system.

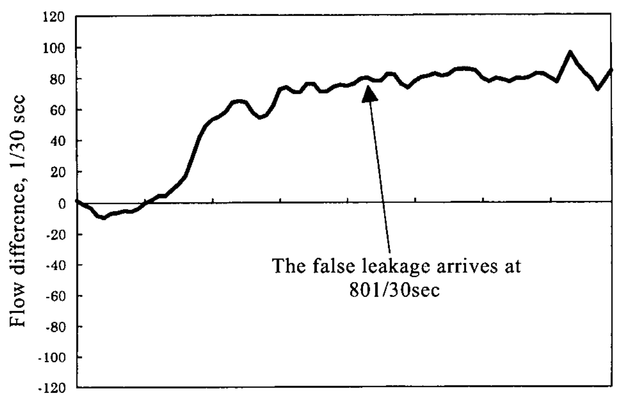

Fig. 8 Performance in detecting flow rate differences

5. Conclusion

The enhanced pipeline for the New Tokyo International Airport Authority has operated without problems since it was put into service. This is the first use of repressurizing by booster pumps in a large-scale petroleum pipeline in Japan. Maximum automation was implemented in the instrumentation and control system to reduce the necessary manpower, and an easily operated system was achieved. We believe this will become a model for future pipeline operation and control systems. Furthermore, the techniques developed in upgrading the existing system without long suspension of the operation will be applicable to other types of facilities.

We wish to express our sincere appreciation to the staff of the New Tokyo International Airport Authority for their guidance and cooperation during the construction of this instrumentation and control system.

Instrumentation and Control System for Yufutsu Gas Processing Plant

Jiichiro kakeya*

NKK has succeeded in the Yufutsu Natural Gas Project in Hokkaido in January 1996 for Japan Petroleum Exploration Co., Ltd. Natural gas is now supplied as city gas to Sapporo City via the pipeline from the gas processing plant. The overall instrumentation and control system has been designed, constructed, and commissioned for gas well facilities, a central gas processing plant, gathering and distribution pipelines, and pipeline block valve stations. In particular, advanced technology has been developed and applied to a gas calorific value adjustment and control system, and its performance has been proven effective.

1. Introduction

NKK constructed the Yufutsu Central Gas Processing Plant (GPP) of Japan Petroleum Exploration Co., Ltd., at Tomakomai, Hokkaido, in January 1996. Immediately after construction, Yufutsu GPP began gas transportation via a pipeline to a transfer station of Hokkaido Gas Co., Ltd., in the suburbs of Sapporo City. Yufutsu GPP receives natural gas from gas well facilities (Numanohata and Minami Yufutsu), conducts condensate/water separation, dew point control, and gas calorific value adjustment and control, and supplies the processed gas as city gas to the pipeline.

Yufutsu Natural Gas Project aimed to establish integrated control of functions ranging from production to supply where the instrumentation and control system is currently operating effectively.

This paper outlines the Yufutsu GPP configuration and the instrumentation and control system, with emphasis on the effectiveness of the gas calorific value adjustment and control system, which is a key technology for Yufutsu GPP performance.

2. Overview of Yufutsu GPP

2.1 Location

Yufutsu GPP is located east of the Tomakomai Port of Hokkaido, halfway between an industrial zone and a residential area. **Fig. 1** shows a bird's eye view of Yufutsu GPP. Yufutsu GPP, consisting mainly of gas processing facilities, is compactly located in a site of 188 m in the E-W direction and 675 m in the N-S direction. The site comprises the Numanohata well fa-

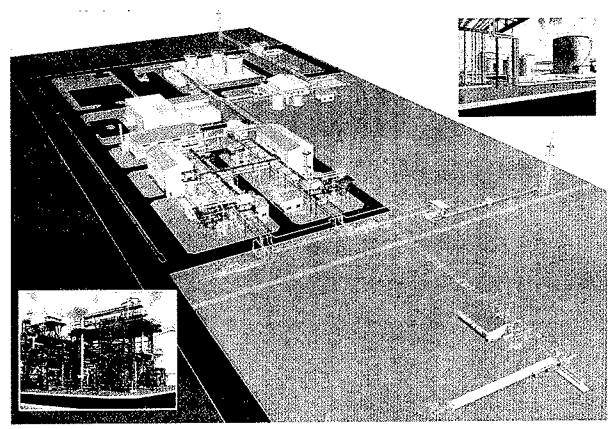

Fig. 1 Bird's eye view of Yufutsu Gas Processing Plant

* Manager, Instrumentation System Engineering Section, Electrical and Engineering Control Dept.

cilities, two trains of gas processing facilities, concerned utility and storage facilities, and gas calorific value adjustment and control units. From Minami Yufutsu well facilities 5.5 km distant from Yufutsu GPP, production gas is transported through a pipeline to Yufutsu GPP.

2.2 Process configuration

Fig. 2 shows the process block flow of Yufutsu GPP. Gas tapped from 4,500 m underground at a pressure of 35 MPa, is depressurized to 7.2 MPa, heated to 50°C in an indirect heating unit with a choke valve, and brought to the gas processing facilities. The natural gas (NG) is treated under high pressure to separate the liquid from a liquid/gas mixture, and water saturated gas is counter-currently contacted with recycle aqueous methanol solution in a contactor. The methanol solution is stripped into the water saturated gas. The gas is then brought to a LPG refrigerated chiller to separate the water content as aqueous methanol solution at a low temperature. These steps are a process licensed by Institut Francais Du Petrole (IFP) of France. Yufutsu GPP is the first plant to introduce the process in Japan. The gas is supplied to the pipeline as city gas after its dew point is controlled, and the calorie adjustment and control is made to 46.05 ± 0.42 MJ/Nm^3.

2.3 Plant operating condition

Gas demand steadily increases year after year, and it significantly varies seasonally and with the time of day. Yufutsu GPP is normally operated at constant production rate during one operating period. The pipeline is used as a buffer, as its large capacity absorbs the demand fluctuation of city gas by accommodating changes in the pressure (2.5 to 6.3 MPa) in the pipeline.

Yufutsu GPP has two trains of gas processing facilities, each having a capacity of 1.2 million Sm^3/day; a single train is under operation and the other train serves as a standby. Future expansion of the GPP to satisfy increasing demand will include an additional train, resulting in operation of two trains with one train as standby, and accounting for 2.4 million Sm^3/day of operating capacity. Existing facilities are, however, capable of two-train operation.

3. Instrumentation and control system

This section describes the plant control, focusing on a distributed control system(DCS).

3.1 System configuration

A distributed control system (DCS) directly monitors and controls both Yufutsu GPP and the adjacent Numanohata gas well facilities. A DCS at Yufutsu GPP also monitors and controls Minami Yufutsu gas well and all pipeline block valve stations via telemetry and tele-control (TM/TC) units. Some of the process data of Yufutsu GPP is also transmitted to the head office of Hokkaido Gas Co., Ltd., via the TM/TC unit.

Since Yufutsu GPP are directly connected to gas suppliers (consumers at the final stage) via pipelines, the plant needs to continuously maintain their operating capability. In this respect, the instrumentation and control system for Yufutsu GPP aims to assure good reliability, operability, and ready expandability, by configuring DCS as kernel of Yufutsu Natural Gas Project. **Fig. 3** shows the system configuration.

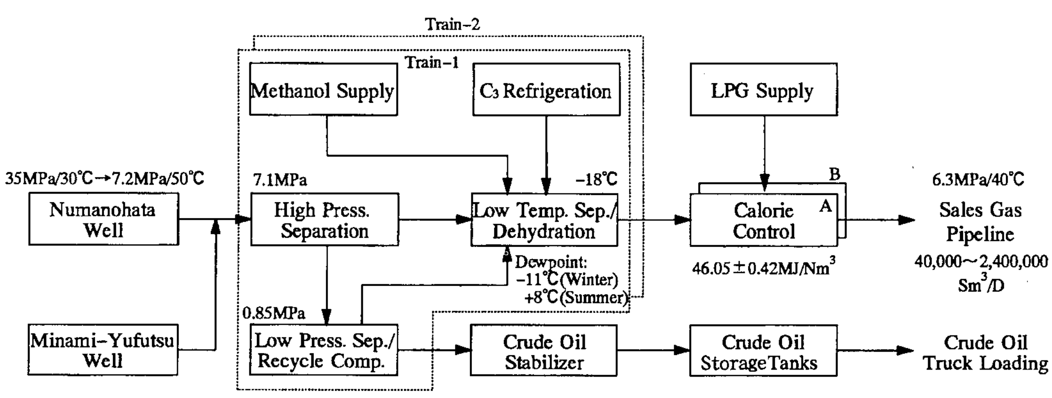

Fig. 2 Process block flow of Yufutsu Gas Processing Plant

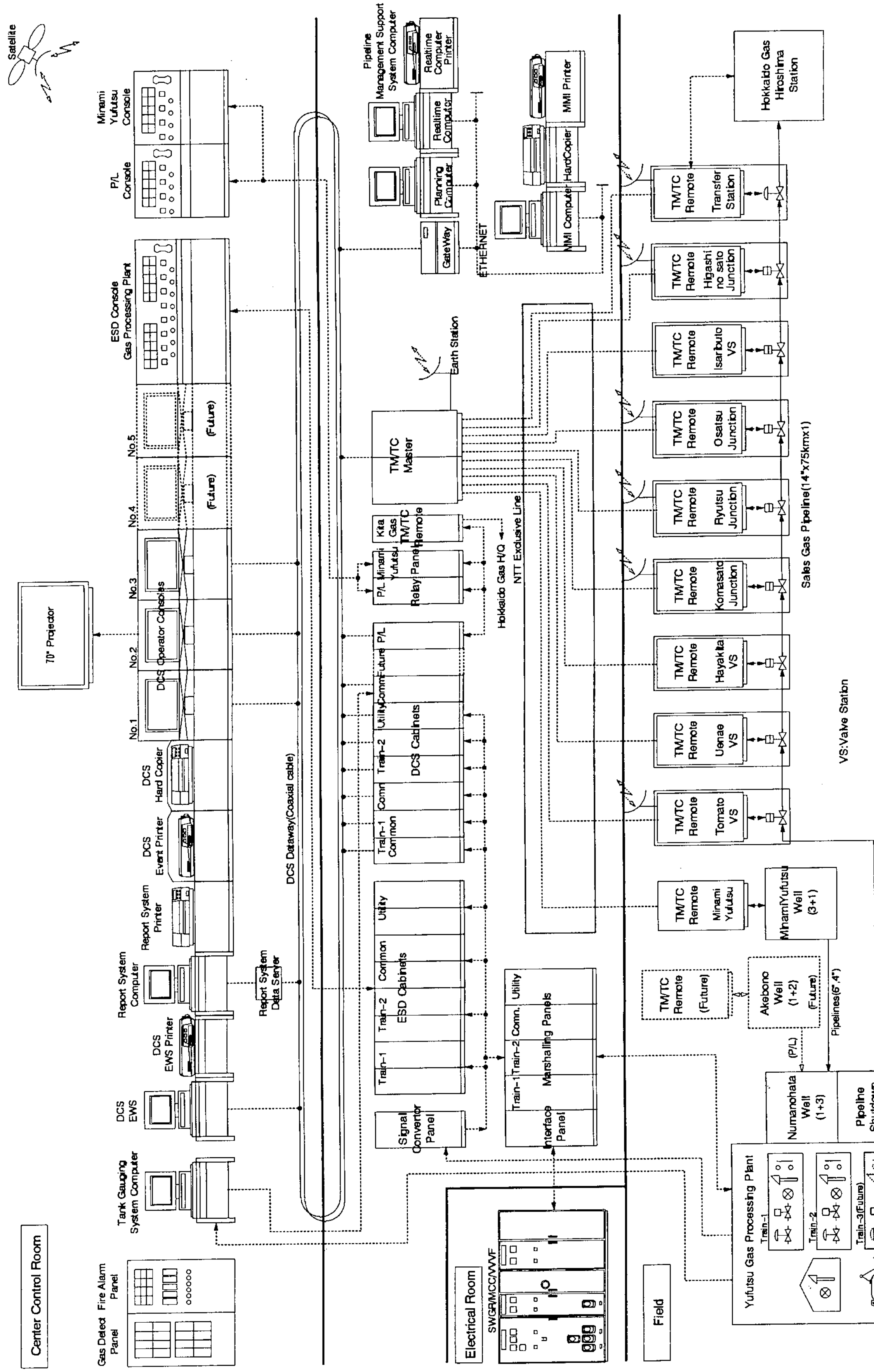

Fig.3 Control system for Yufutsu Natural Gas Project

Normally, Yufutsu GPP, gas well facilities, pipelines, and a transfer station are continuously operated by two operators in the Yufutsu GPP control room. Operators' work load was saved by the integrated control and monitoring through the DCS screens, Yufutsu GPP process and utility facilities, mainly, each gas well facilities and all pipeline block valve stations.

In addition to the DCS for plant control, the instrumentation and control system comprises subsystems such as the emergency shutdown system, the reporting system, the tank gauging system, the condensate (crude oil) truck loading and metering system, the combustible gas leak detection and alarm system, and the fire and smoke detection system.

3.2 DCS

Yufutsu GPP is largely divided into four groups, i.e. gas processing train-1, train-2, common facilities and utility facilities. In addition to pipeline facility monitoring, each of the facility control functions is allocated to an individual control station (CPU module), ensuring functional distribution. Furthermore, a redundant system is provided through a CPU module, power supply unit, data highway, and database station, to minimize the effect from trouble of a part of DCS devices on the total supervision and control function. The resulting configuration is highly reliable.

The reporting system connects with the DCS. It stores operating data for a two-month period in an exclusive data server. After the operator sets necessary items, the reporting system performs rate calculations based on independent well production data and automatically prepares daily, monthly, and operation reports.

Table 1 shows the quantity of DCS input/output signals. The Yufutsu GPP facilities alone have over 2000 such signals.

Table 1 DCS I/O

	Train-1	Train-2	Common	Utility	Total
AI	77	76	94	66	313
AO	32	34	34	35	135
DI	295	300	417	334	1,346
DO	34	36	87	52	209
PI	8	8	12	2	30
PO	0	0	4	0	4
Total	446	454	648	489	2,037

3.3 Emergency shutdown (ESD) system

Based on the principle of whole-plant block and bleed, the ESD system for Yufutsu GPP is divided into three types of functions: process shutdown, emergency depressurizing, and equipment stop/shutdown. The ESD system, including alarm generation, comprises the following five levels to ensure safe plant operation and shutdown.

(1) Total shutdown (emergency stop of whole facilities)
(2) Pressure relief device to protect vessels/equipment
(3) Unit shutdown (entailing process shutdown and equipment stop)
(4) Early warning of shutdown or stop (to prevent accidental shutdown and stop)
(5) Operation attention alarm (notification)

The ESD system uses a hard-wired relay logic independent of the DCS to attain process control, increasing the reliability of the total control system.

4. Gas calorific value adjustment and control system

This section describes the calorific value adjustment and control system, which is the key technology for the Yufutsu GPP.

4.1 Flow scheme of calorific value adjustment and control unit

The dehydrated gas from the gas processing facilities is mixed with LPG to adjust the calorific value to 46.05 ± 0.42 MJ/Nm^3 for city gas. The calorific value adjustment and control system is established by DCS software.

There are two installed calorific value adjustment and control units. Each unit treats 40000 to 1.2 million Sm^3/day of throughput NG. A single unit is operated, while the other serves as a standby unit. The system has a capacity of 2.4 million Sm^3/day given the parallel operation of the two units in future. Since Yufutsu GPP production has not only a large yearly increase and fluctuation, but also a large turn-down ratio requirement within a year, calorific value adjustment and control are provided by two lines supplying LPG addition to NG/LPG direct vaporizers and mixers: one for flow at a large rate and the other for flow at a low rate. The configuration of the scheme is shown in **Fig. 4**. During plant operation, the direct vaporizer and mixer and the LPG additive line are automatically switched to an adequate line in response to the change in flow rate to sustain calorific value adjustment and control.

4.2 Logic of calorific value adjustment and control

Determination of the amount of LPG addition is a key aspect of calorific value adjustment and control. Based on the equation of heat balance, we adopted a calorific value adjustment and control logic (shown in **Fig. 5**) that determines the amount of LPG addition in a hierarchical state in three modes: constant LPG flow rate control, flow ratio control of NG/LPG , and feedback control of unit outlet calorific value. A conventional calorific value adjustment and control system is governed by the combination of flow ratio control of NG/LPG, including the constant LPG addition flow rate control, and calorific value compensation/feed-forward control of the unit inlet calorific value. Using an opposite approach, the adopted system achieved stable control of calorific value adjustment by integrating the calorific value feedback control by PID controller in an automatic mode.

4.3 Distinctive features of the calorific value adjustment and control logic

The calorific value adjustment and control system of Yufutsu GPP has the advantages described below.

(1) Allowable calorific value fluctuation is 46.05 MJ/

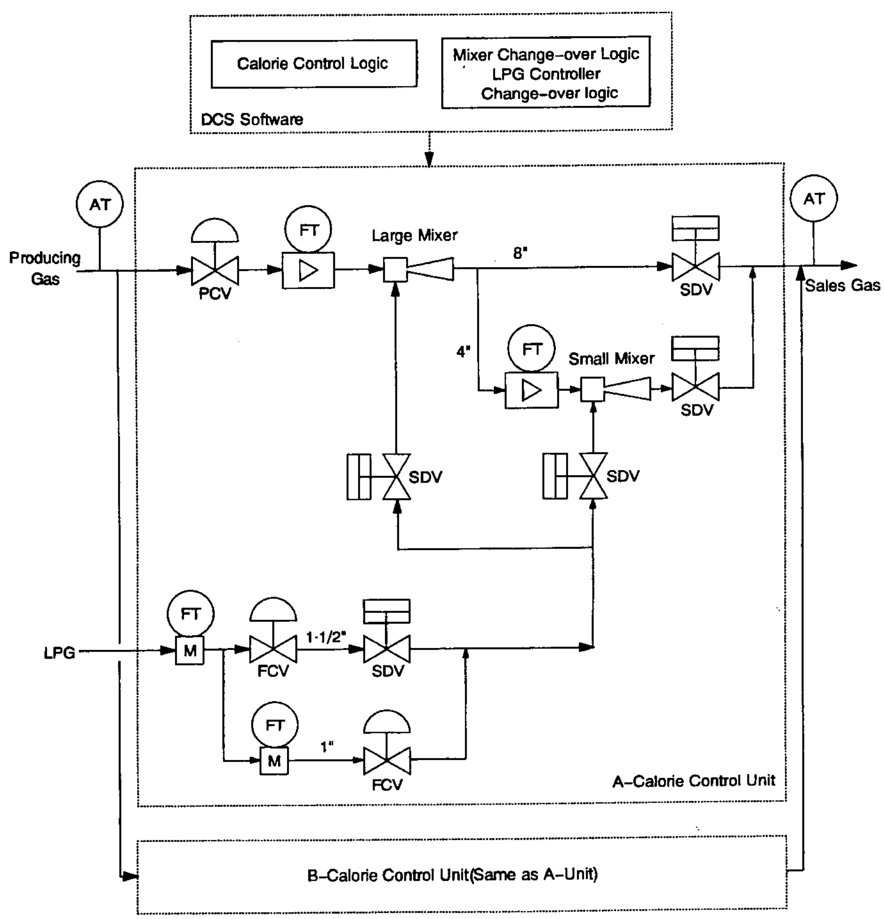

Fig. 4 Flow of calorie control unit

Nm³ within ± 1%.

The allowable limit is more severe than that of ordinary gas suppliers (whose typical fluctuation is ± 2% to 3%). We prepared a simulation model of the calorific value adjustment and control system and conducted a verification study of the system. Furthermore, we configured the calorific value adjustment and control system to include three modes for control of the amount of LPG addition. In addition, we integrated the pulse signals of the vortex flow meter for NG using a moving average process to produce a stable calculation of NG/LPG flow ratio.

(2) The system responds to a 30:1 turndown ratio (40,000 to 1.2 million Sm^3/day).

To cope with the 30:1 turndown ratio, we installed instrumentation devices for large and small flow rates, and let the DCS automatically switch these devices in response to the measurement range. When there are indicators of switching, a ramp processing function is added between the indication values of these two meters to prevent step change in the indicated values.

(3) Countermeasure for high reliability.

The DCS has a calorimeter backup function to continuously adjust and control the unit outlet calorific value by using the unit inlet calorimeter instead of the unit outlet one when an accidental failure occurs on the unit outlet calorimeter. In addition, limiting functions are placed before and after each computation to prevent irregular operation in the DCS. Furthermore, to sustain gas supply even under electrical power failure and its recovery accident, the DCS has functional logics to resume the operating condition before power failure not only for the calorific value adjustment and control units but also for gas processing and utility facilities.

4.4 Effective performance of the calorific value adjustment and control system

The major disturbances of the calorific value adjustment and control system are the fluctuations in the calorific value and the flow rate of the unit inlet NG. Since Yufutsu GPP is a gas processing facility directly connected to gas wells, the calorific value fluctuation of well production gas is expected to be small over the short term. Accordingly, the PID tuning of controllers was implemented to respond to flow rate fluctuation in a highly sensitive mode and to calorific value fluctuation in a non-sensitive mode.

The verification data for the calorific value adjustment and control system are shown in **Figs. 6** and 7. **Fig. 6** shows that calorific value is continuously adjusted and controlled within ± 0.4% of the unit outlet calorific value fluctuation, against a significant fluctuation of the unit inlet calorific value. The unit inlet calorific value fluctuation was induced both by the increase of inlet NG calorific value (due to upset condition of LPG refrigerated chiller, an upstream unit) and by the decrease of inlet NG calorific value (due to the resumed operation of LPG refrigerated chiller). **Fig. 7(a)** indicates that control was attained in a range of ± 0.5% of calorific value fluctuation against the inlet NG

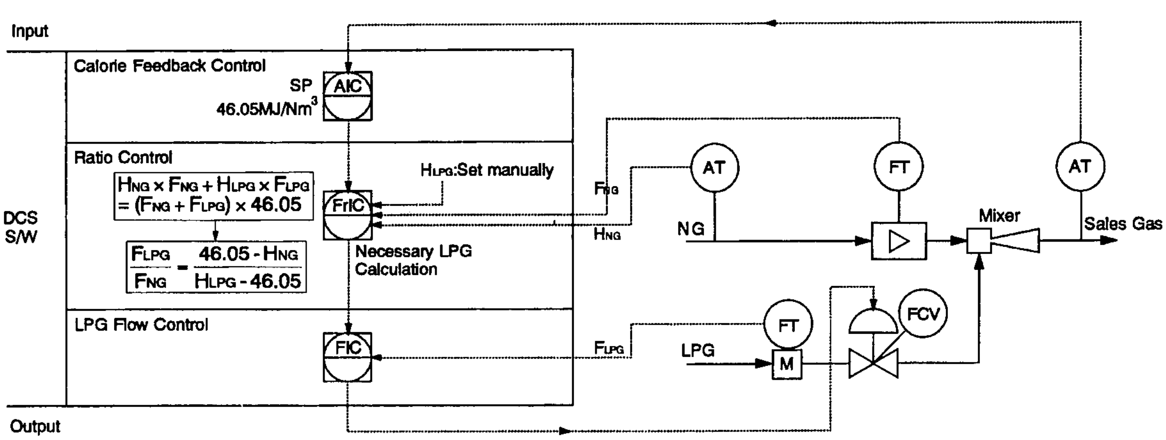

Fig. 5 Block logic for calorie control sub-system

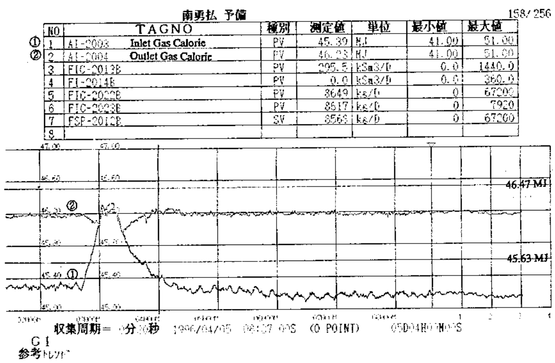

Fig. 6 Gas calorie against inlet calorie fluctuation

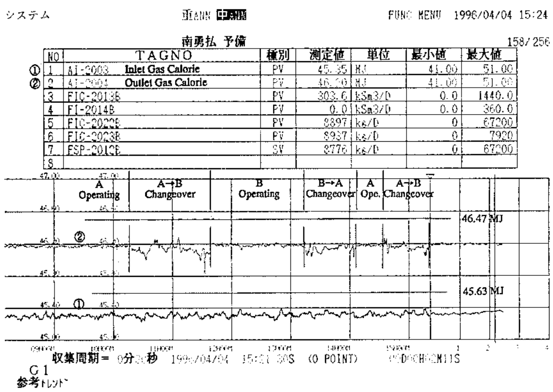

Fig. 7(a) Inlet flow fluctuation

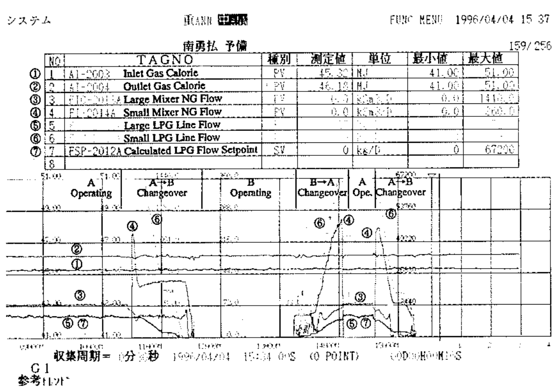

Fig. 7(b) A-unit NG flow fluctuation

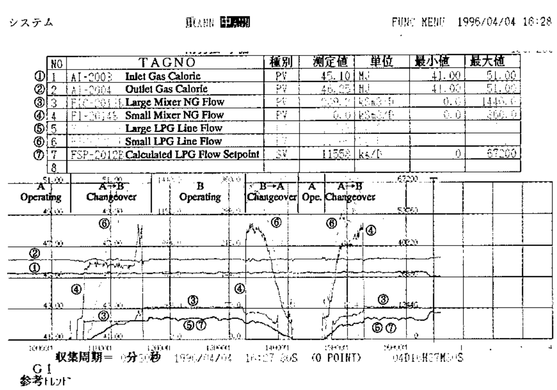

Fig. 7(c) B-unit NG flow fluctuation

flow rate fluctuation shown in **Fig. 7(b)** and **(c)**, which was triggered by changeover the A/B of the calorific value adjustment and control units. Both cases proved that the calorific value adjustment and control system of Yufutsu GPP are effective to the required specification.

5. Conclusions

The DCS of Yufutsu GPP was configured as a kernel of overall instrumentation and control system for Yufutsu Natural Gas Project, also designed and commissioned for gas utilities complex ranging from production to supply of city gas, including monitoring and control units both in Minami Yufutsu gas well facilities and all pipeline block valve stations.

The calorific value adjustment and control system is an improved and advanced version of a conventional one. It was demonstrated to be effective to the required specification. NKK is confident that the developed system is applicable to city gas production process and similar types of calorific value adjustment and control systems.

NKK would like to express its special appreciation to Japan Petroleum Exploration Co., Ltd., and related organizations for their kind support.

Automatic Combustion Control System for Refuse Incineration Plant

Masaaki Shirai*, Satoshi Fujii**,
Shinji Tomiyama***, Yuuichi Nogami****,
Hajime Ase***** and Takashi Yokoyama******

NKK developed a new combustion control system that increases the stability of steam flow from the boiler, while simultaneously reducing CO and NOx concentrations in the exhaust gas discharged from a municipal refuse incinerator. This control system consists of a simulation model based controller, which stabilizes the steam flow rate and inner temperature, and a fuzzy based controller, which adjusts the cooling air and water spray to reduce CO and NOx concentrations. We applied this system to an incinerator in service and obtained good results.

1. Introduction

Municipal refuse incinerators play an important role in processing a wide variety of municipal refuse. Recently, increasing concerns have arisen over reducing toxic substances emitted from the refuse incinerators and over recovering the vast amount of heat generated.

Statutory requirements for control of the pollution originating from municipal refuse incinerators have also become stricter each year. For example, in addition to the existing regulations on NOx, HCl, and SOx, the "Guidelines for Controlling Dioxins Emissions from Municipal Solid Waste Incineration Plants" were issued to regulate dioxins generated in the flue gas at incineration plants.

However, there are conflicts between suppressing the generation of NOx and CO, both of which affect the generation of dioxins. Accordingly, local municipal authorities and incinerator manufacturers have made great efforts to find measures for reducing the emission of these toxic substances simultaneously.

In parallel with these efforts, more refuse incineration plants are being built with a turbine and power generation boilers to utilize the heat generated from refuse incinerators. Accordingly, stabilization of the rate of steam generation from the incinerator has also become an important issue.

NKK's stoker furnace is a two-way, gas flow type incinerator with an intermediate ceiling to ensure optimum incineration. Further, its automatic combustion control system[1)] stabilizes incineration control. As a result, the amounts of toxic gases generated from the furnace are far below the limits specified by regulations. Nevertheless, the need for finer and more precise combustion control will increase to meet the re-

* Manager, Dr. Control Engineering Research Dept., Applied Technology Research Center
** Senior Research Engineer, Control Engineering Research Dept., Applied Technology Research Center
*** Research Engineer, Control Engineering Research Dept., Applied Technology Research Center
**** Manager, Electrical Control Engineering Dept.
***** Manager, Dr. Electrical Control Engineering Dept.
****** Manager, Environmental Plant Engineering Dept.

cent social requirements mentioned above.

To respond to these future requirements, NKK developed a hybrid automatic combustion control system (or "Hybrid ACC") to achieve the simultaneous reduction of CO and NOx emissions in flue gas and to stabilize the rate of steam generation. These effects of the Hybrid ACC were confirmed by a verification test using a commercial plant. The development of the Hybrid ACC and the results of verification tests are described below.

2. Outline of refuse incineration plant

Fig. 1 shows a schematic outline of the refuse incineration plant. The various kinds of refuse are mixed together by a refuse crane and charged into the refuse hopper. The refuse is then sent inside of the incineration furnace after passing over reciprocating grates. The refuse is dried and combusted with preheated air coming through the grates from below. Finally, the refuse is sent to the after-burning stoker, where it is completely converted into ash. The ash is then discharged from the furnace.

The combusted flue gas flows in two ways: through the main flue and through the bypass flue. The gases are mixed and the unburned gas is re-combusted within the gas-mixing chamber. The mixed and re-combusted flue gas enters the boiler, which recovers the heat. After passing through the flue gas treatment facility, the waste flue gas is vented through the stack to the atmosphere. The steam generated from the boilers is sent to a gas turbine to generate electric power.

3. Causes of CO and NOx generation

The relation between the actual operating conditions of the refuse incinerator and the generation of CO and NOx must be quantitatively measured to develop a method to suppress CO and NOx in the flue gas.

For this purpose, we gathered a large volume of data through systematic measurements of combustion states for a large number of the boiler-mounted, multistage, stoker incinerators that NKK constructed in recent years. Extensive findings were derived from the analysis of this data, part of which are described below.

(1) Characteristics of CO generation

Fig. 2 shows the relation between the concentration of CO and O_2 and the temperature of gas in the mixing chamber. The CO concentration is kept at a low level of around several ppm when in a stable combustion state, and when the combustion state becomes unstable, it is increased. There are two cases for the increase of CO generation.

Case 1: Increased CO generation resulting from a shortage of oxygen caused by active combustion.

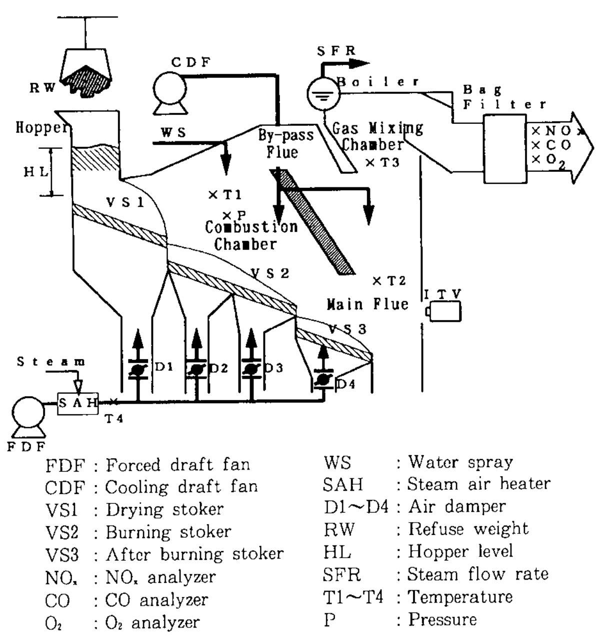

Fig. 1 Refuse incineration plant

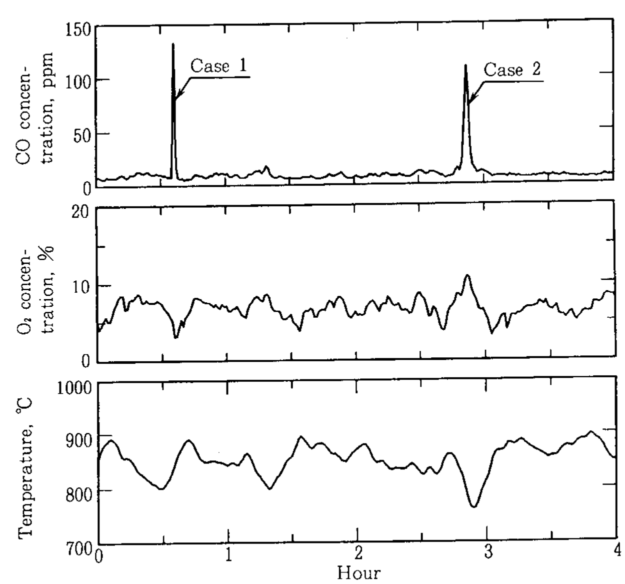

Fig. 2 Relation between CO, O_2 and temperature

Case 2: Increased CO generation resulting from O_2 failing to contribute to CO re-combustion due to insufficiently high temperature in the gas mixing chamber, even when enough oxygen is present.

(2) Characteristics of NOx generation

Concentration of NOx varies with the cooling air flow rate, as shown in **Fig. 3**.

(3) Relation between temperature and concentration of CO and NOx

The phenomena observed in cases (1) and (2) are expressed by a steady-state relation between the CO concentration, NOx concentration, and gas mixing temperature against the cooling air flow rate. This relation is shown in **Fig. 4**. Case (1) corresponds to Zone 1, and Case 2 corresponds to Zone 2. When the combustion state is in Zone 3 of **Fig. 4**, the CO concentration and the NOx concentration are simultaneously kept at a low level.

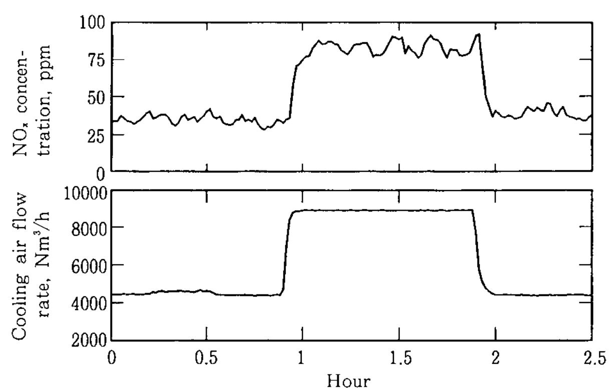

Fig. 3 Relation between NOx and cooling air

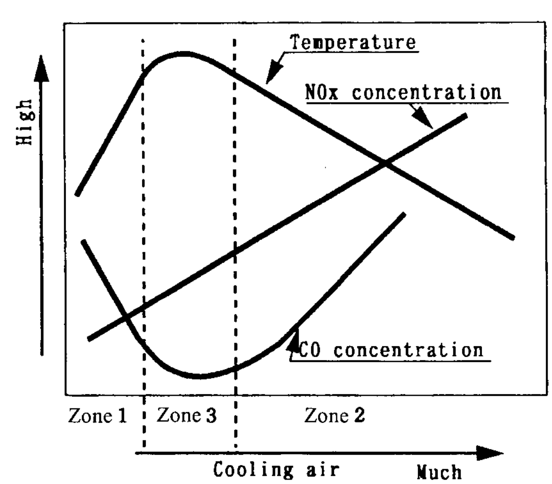

Fig. 4 Relation between CO, NOx and temperature

4. Introduction of hybrid control system

The findings derived in **Chapter 3** suggest that maintaining the combustion state within Zone 3 in **Fig. 4** is effective for simultaneously reducing the CO and NOx. To do this, stable combustion should first be achieved over a long time period. Stable combustion for a long period is achieved by controlling the refuse charge rate to correspond to the set rate of steam generation, maintaining a constant amount of refuse in the furnace, and optimizing the combustion air supply rate based on an intrafurnace combustion model.

Within the furnace, however, unexpected changes in the combustion state frequently occur from various causes. It is difficult to make a model of these changes, and a control system structured on a model would not accommodate them. We adopted a fuzzy control system[2] to accommodate such short term fluctuations. The combustion state in the furnace is stabilized for both the long term and short term by combining these two different control systems, as shown in **Fig. 5**.

5. Control system for long-term stabilization of combustion

5.1 Modeling of combustion process

The control system for long-term stabilization of combustion is based on analysis of the dynamic responses of various kinds of operating variables in the refuse incinerator and on analysis of time-based changes of effects caused by changes in the refuse composition and charging rate. Prior to constructing the control system, we created an intrafurnace combustion model to study the function of the control system and improve its effectiveness.

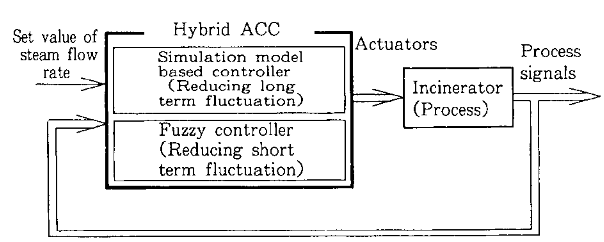

Fig. 5 Block diagram of Hybrid ACC

Basic assumptions used for modeling are listed below.

(1) Refuse on grates is divided into blocks for each under-grate hopper that supplies combustion air.

(2) Gas passage is divided into the combustion chamber, the bypass flue, the main flue, and the gas mixing chamber.

(3) The model in each block is a complete mixing model based on a heat and material balance of the refuse material and exhaust gas.

(4) Refuse consists of water, combustible components, and ash. The combustible components consist of C, H, and O.

(5) Reaction within the refuse layer and reaction in the gas stream are expressed by eqs.(1) through (5).

$$C + 1/2O_2 = CO + Q_1 \quad \text{.....(1)}$$

$$C + O_2 = CO_2 + Q_2 \quad \text{.....(2)}$$

$$CO + 1/2O_2 = CO_2 + Q_3 \quad \text{.....(3)}$$

$$CH_4 + 2O_2 = CO_2 + 2H_2O + Q_4 \quad \text{.....(4)}$$

$$H_2O(1) = H_2O(g) + Q_5 \quad \text{.....(5)}$$

where,

Q_i, $i = 1$ through 5 is the heat of reaction or vaporization.

Fig. 6 shows an outline of the model derived from these assumptions.

As shown in **Fig. 6**, the condition at each block for refuse on grates and gas in the gas passages is determined by the corresponding material and heat balances. For example, the material and heat balances for the refuse are given below.

$$dW_{ij}/dt = V_{i-1}W_{i-1j} - V_iW_{ij} + R_{ij} \quad \text{.....(6)}$$

$$d(\sum_j C_iW_{ij}T_i)/dt = V_{i-1}\sum_j C_jW_{i-1j}T_{i-1} - V_i\sum_j C_jW_{ij}T_i + Q_{ri} + Q_{gi} + Q_{fi} + \sum Q_R \quad \text{.....(7)}$$

where,

i : subscript denoting block number

j : subscript denoting refuse component

V_i : refuse moving rate

R_{ij} : reaction heat or vaporization rate of j-th component

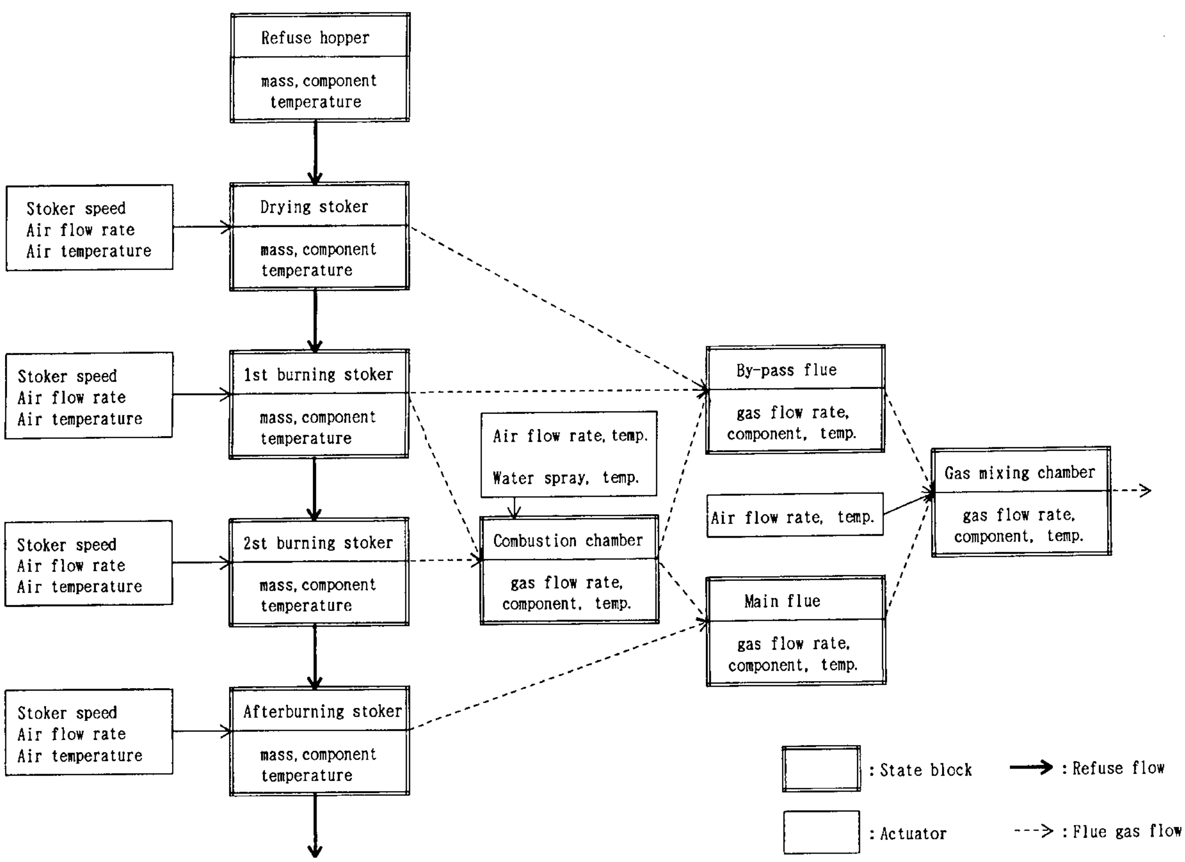

Fig. 6 Structure of mathematical model

Q_{ri} : heat transfer from combustion air to refuse
Q_{gi} : heat transfer from combusted gas to refuse
G_{fi} : heat transfer from flame to refuse
W_{ij}: weight of j-th component
C_j : specific heat of j-th component
T_i : refuse temperature

5.2 Simulation

To verify the validity of the derived intrafurnace combustion model, the model response characteristics were compared to data from a commercial incinerator under the condition where the net calorific value (Hu) for the refuse is temporarily reduced. The value Hu significantly affects the combustion state in the incinerator.

The solid line in **Fig.** 7 shows changes in the rate of steam generation during and after the occurrence of the temporary reduction in Hu. The broken line in **Fig.** 7 shows the results of the simulation model. The response patterns (e.g., the steam generation reduction rate) for the observed data and the simulated results are similar, indicating that the intrafurnace combustion model represents the commercial furnace state well.

5.3 Design of control system

After the intrafurnace combustion model was verified as described in **Section 5.2**, simulations and control parameter changes necessary for evaluating the control system design were conducted using the model.

The control system was designed on the basic concepts given below to provide control for the long term stabilization of combustion.

(1) The speed of the grates is controlled to assure stable charging of refuse to meet the target incineration rate, which is defined by the set steam generation rate and Hu, and to maintain a constant amount of refuse within the furnace.

(2) The total combustion air and the ratio of the air supplied from below the grates are adjusted in response to the combustion state.

5.4 Simulations of control system

To evaluate the control system performance, simulations were conducted by applying the new control system to the intrafurnace combustion model running under the same conditions as described in **Section 5.2**. As shown in **Fig. 8**, the control system demonstrated that fluctuations in the rate of steam generation are minimized even during temporary changes in Hu, and the validity of the control system was verified.

6. Control system for simultaneous reduction of CO and NOx generation using fuzzy control method

6.1 Introduction of fuzzy control system

As described in **Chapter 5**, a control system based on the intrafurnace combustion model provides stable combustion, even with variations in refuse quality, and assures operation within Zone 3 of **Fig. 4** on an average, long-term basis. In actual commercial furnace operations, however, short term changes that cannot be expressed by the intrafurnace combustion model occur. The sudden generation of CO shown in **Fig. 2** is one example of this type of phenomenon. Fuzzy control can be suitable for this phenomenon because of its characteristics, as shown below.

The characteristics of fuzzy control are:

(1) Control rules can be described by a linguistic expression.

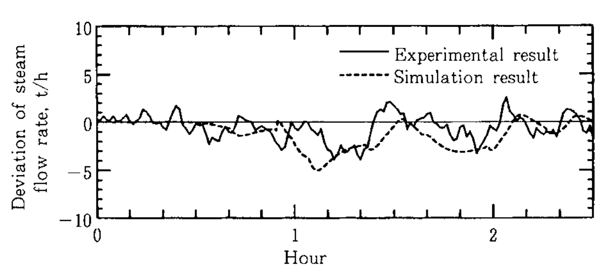

Fig. 7 Responses to change in Hu

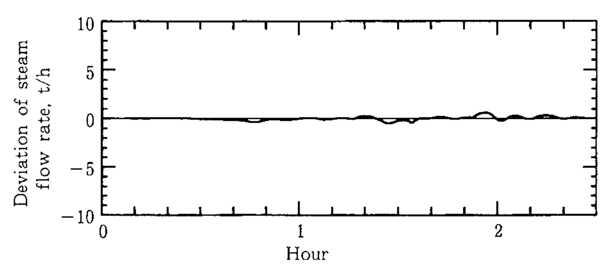

Fig. 8 Simulation results

(2) Control conditions can be readily optimized for each plant.
(3) Additions and changes of control targets can be performed flexibly.

The fuzzy control system has often been used for fluidized bed incineration plants manufactured by NKK.[3] Characteristic (1) is particularly effective for controlling a nonlinear oriented process and allows the CO and NOx generation to be stabilized within the levels in Zone 3 of **Fig. 4**, even with sudden changes in the combustion state.

6.2 Rules of fuzzy control

For the simultaneous reduction of CO and NOx, we established a set of control rules to determine the cooling air flow rate and the water spray rate based on the analysis of CO and NOx generation characteristics that were discussed in **Chapter 3**. The control rules are largely divided into the following groups.
(1) The rule group for maintaining the gas mixing chamber at a stable temperature.
(2) The rule group for maintaining the O_2 concentration above a specified level.
(3) The rule group for maintaining the CO concentration at a low level.
(4) The rule group for maintaining the NOx concentration at a low level.

7. Results of verification tests

A new Hybrid ACC was applied to a 150 ton/day capacity incineration plant in normal service. The hybrid ACC combines a control system developed on the basis of intrafurnace combustion model and simulations to assure long term, stable combustion, with a fuzzy control system to reduce short term changes in CO and NOx generation. The test results are shown in **Fig. 9** and **Table 1**. The concentration of CO and NOx in **Fig. 9** is an instantaneous value within a certain time range converted to a condition of 12% O_2.

The new ACC successfully stabilized the rate of steam generation and maintained a stable, low concentration of CO and NOx. No sudden spikes of CO occurred, such as is evident in **Fig. 2**. Since the intrafurnace temperature and the gas mixing chamber

Table 1 Experimental results (time averages and standard deviations)

Steam flow rate		NO_x concentration, ppm		CO concentration, ppm	
ave. t/h	s.d./ave. %	ave.	s.d.	ave.	s.d.
20.1	2.8	71	9.8	6.5	1.2

Temp. in combustion chamber, ℃		Temp. in gas mixing chamber, ℃	
ave.	s.d.	ave.	s.d.
927	21	929	17

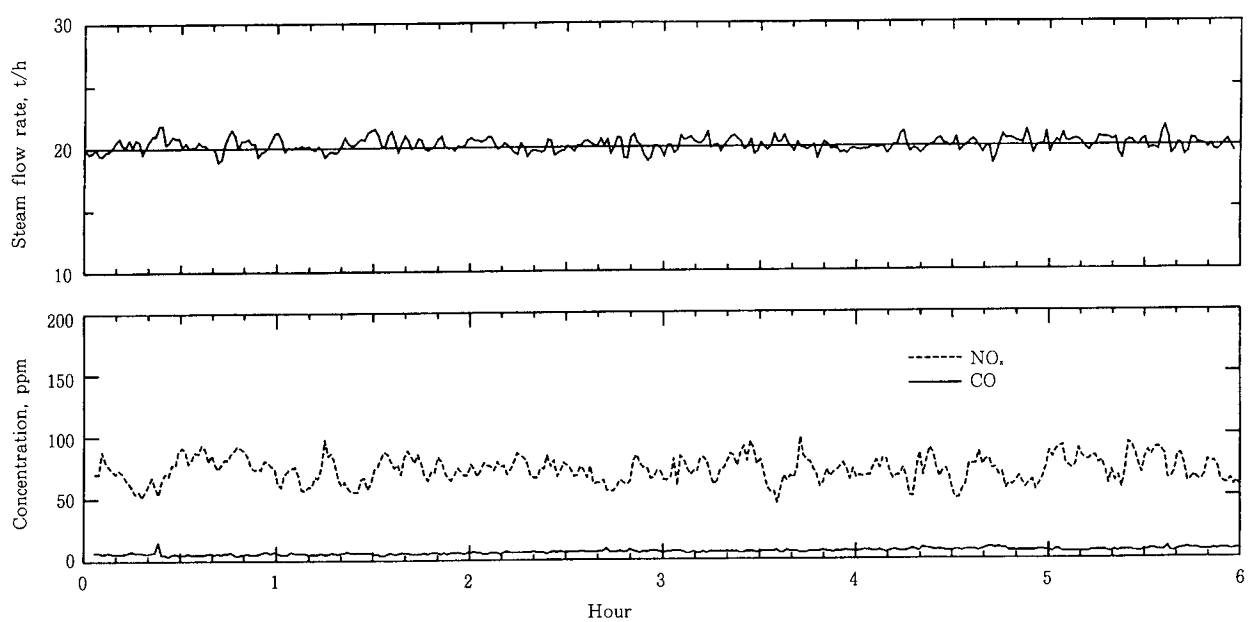

Fig. 9 Experimental results with Hybrid ACC

temperature were also stable, abrupt changes in the combustion state inside of the furnace were also suppressed.

8. Conclusion

The Hybrid ACC was developed to provide long-term, stable combustion and reduced short-term variations in the generation of CO and NOx for stoker-type refuse incinerators. Application of the Hybrid ACC to a commercial incineration plant revealed that the simultaneous reduction of CO and NOx generation was achieved. This simultaneous reduction is considered to be difficult in conventional combustion control systems. Moreover, both the average and peak values of the CO and NOx generation were stabilized at low levels. Furthermore, the Hybrid ACC stabilized the rate of steam generation more precisely than is possible with conventional ACC systems.

The control system is expected to fully satisfy future social needs for decreasing toxic substances in the flue gas and for increasing the energy recovery efficiency in refuse power generation plants.

References

1) Ohki, H. et al. "Automatic Combustion Control System of a Incinerator Plant Combined with PowerPlant". Nippon Kokan Technical Report. No. 90, p.85 - 95 (1981).
2) Nogami, Y. et al. "Fuzzy Combustion Control for Reducing both CO and NOx from Flue Gas of Refuse Incineration Furnace". '95 Symposium on Environmental Engineering, JSME. p.104 - 107 (1995).
3) Tanabe, M. et al. "Fuzzy Combustion Control for Fluidized Bed Incineration Plant". NKK Technical Report. No. 148, p.6 - 13 (1994).

Linear Tube Transportation System -Second Report-

Tomoji Fujisawa*, Takashi Misago**,
Osamu Araki*** and Toshiro Goriki****

NKK has developed three kinds of linear synchronous motor transportation systems (tube, vehicle and monorail) and has performed trial runs using test lines. The power source is a linear synchronous motor system that uses permanent magnets attached to the carrier and magnetizing coils on the fixed part. In particular, the linear tube transportation system has numerous useful characteristics. It can efficiently transport large quantities of materials to a designated destination using roller-supported capsules moving through a pipeline at high speeds. This report describes the configurations, mechanism, and capabilities of the systems and the performance results of trial runs including speed control and vertical climbs, focusing on the linear tube transportation system. Furthermore, the report introduces application concepts that utilize the features of linear motors, such as transportation of parcels and urban waste.

1. Introduction

Demand for the transportation of materials has increased constantly in recent years. However, most transportation relies on the use of trucks, creating environmental problems such as increased traffic congestion, noise and air pollution. In addition, lack of truck drivers has made it difficult to depend solely on this method of transportation. Accordingly, there are high expectations for a new distribution system that is automated and simple.

This report describes three kinds of linear motor transportation systems (tube, vehicle and monorail) that make automated, high speed transportation possible by utilizing the non-contact propulsion of a linear motor.

The tube type system[1], or trade name Linear Tube Transportation System (LTTS), uses a linear synchronous motor that consists of nonmagnetic tubes with magnetizing coils wound around them and permanent magnets (PM) attached to the capsule. The system can transport loaded capsules at high speeds inside the tube. Two tube sizes are available, with diameters of 300 mm and 500 mm. The system can be used for transportation between distribution terminals or between refuse incinerators using tubes installed through tunnels or below guardrails on highways.

The monorail and vehicle systems can be used for transportation and monitoring in factories, where their low noise and nonexplosive characteristics are advantageous. Another special application concept for these

* Logistics System Engineering Dept.
** Heavy Machinery and Parking System Engineering Dept.
*** Engineering Research Center
**** NK Plant Engineering Co.

types is in amusement park facilities such as roller coasters.

2. System configuration

2.1 Targets for system development

Targets for the development of transportation systems were set as follows:

(1) Capable of easy installation in a small space

(2) Efficient and capable of large load transportation (able to replace trucks)

(3) Able to perform long distance, high speed and automated transportation

2.2 Selection of linear motors

There are various types of linear motors. Three types of motors are primarily used for transportation[2)3)]: the on-ground primary member type linear induction motor (LIM) which consists of magnetizing coils attached to the fixed part as a primary member; the on-board primary member type LIM in which magnetizing coils are attached to a moving part as a primary member; and the on-ground primary member type linear synchronous motor (LSM).

High performance, rare-earth magnets have been developed that permit a larger clearance between the magnets and coils and that provide high thrust and low heat generating characteristics. Thus, the magnet type LSM was adopted for the LTTS, vehicle and monorail systems.

2.3 Principle of linear tube movement

The movement principle of the linear synchronous motor is as follows: a permanent magnet attached to a moving part generates magnetic flux. When the flux passes through the magnetizing coil, Fleming's left hand rule states that a current force *(Fe)* of attraction or repulsion is generated in proportion to the strength of the electric current and the number of turns in the coil, etc., as shown in the following equation.

$$Fe = NIlB$$

where,

N: number of turns in the coil

I: electric current

l: average coil length

B: flux density

In the linear motor system, synchronous sensors are used to control the direction of magnetizing coil current to obtain thrust in one direction. The principle of the movement is shown in **Figs. 1** and **2**. The vehicle and monorail systems use the propulsion system shown in **Fig. 1. Fig. 2** shows the propulsion principle of the LTTS.

Like the other two systems, the LTTS employs the on-ground primary member type linear synchronous motor (LSM), which consists of magnetizing coils wound around the nonmagnetic tube as a primary member and permanent magnets attached to the capsule as a secondary member. With the LTTS, the height of the cylindrical magnet that is magnetized in the axial direction is reduced as much as possible to increase the space available for loaded materials within the carrier body. Furthermore, cost saving is attained by extending the distance between the equally-spaced coils as much as possible. This, however, generates a high thrust ripple. Therefore, the two cylindrical magnets are installed at a distance to provide a half thrust cycle shift between them and thereby equalize the thrust.

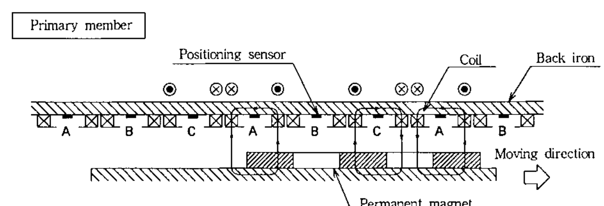

Fig. 1 Propulsion principle configuration of vehicle and monorail linear motor

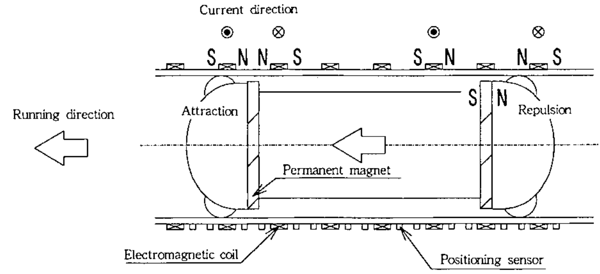

Fig. 2 Propulsion principle configuration of LTTS linear motor

3. Linear tube transportation system

NKK has developed two types of LTTS: type 300 (300 mm in diameter) and type 500 (500 mm in diameter). Type 300 consists of the linear tube, linear capsule and a 4 pole, 9 phase type power supply control device. This system was evaluated in full-scale tests using the test line. Type 500 was developed based on the type 300 to increase the capacity of the system. Their specifications are shown in **Table 1**.

3.1 Linear tube and capsule

The linear tube is a nonmagnetic, fiber-reinforced plastic (FRP) or stainless steel (SUS 304) pipe with magnetizing coils wound at equal intervals. Sensors are installed on the tube between coils in order to detect the position of the capsule. The number of turns on the coil is designed to provide the necessary thrust. Thin steel sheets are wrapped around the outside of the tube to improve the flow of magnetic flux through the coils and to prevent the influence of magnetic fields on the surroundings.

The type 300 linear capsule is supported by rollers and can be connected in multiple units. The set of five rollers that are supported by a suspension system is attached to each of the front and back sides of the capsule body. The carrier body is square and has a pendulum structure so that the door constantly faces upward. Two rare-earth cylindrical magnets are attached to each capsule, one near each end of the body. The type 500 linear capsule has one cylindrical magnet and a fixed position body (not a pendulum structure) and is fitted with a door for loading materials.

The capsule runs inside the linear tube. All electrical cables and signal lines are also attached around the tube. **Fig. 3** shows the configuration of the type 300 capsule. **Photo 1** is a general view of the type 500 LTTS.

Table 1 Specifications of the type 300 and 500 LTTS

Item	Specifications
Linear tube	FRP, ϕ300mm(300 type), ϕ500mm(500 type) Coil : Pitch 100~200mm, 100~150thrn Current density : 0~40A
Linear capsule	10 rollers supported type, many trains 300 type : 1700mm, 500 type : 1278mm
Kinds of linear motor	Linear synchronous motor Primary member : Electrical-magnetic coil on ground Secondary member : Permanent magnet on capsule
Speed	Max 600m/min

3.2 Test line

The type 300 test line is made of FRP in a loop configuration. The total length of the test line is 56 m, which includes a 45 degree sloped line, a vertical line and a branch line. This configuration permits both uphill and downhill operation. The capsule can be diverted from the loop line by using the branch line. (The traversing point switch is used connect or disconnect the branch line from the loop line.)

A terminal is situated at the end of each branch line section. The terminal uses saddle type magnetizing coils attached to half-cylinder tubes, and has a stopping device and a fork type, vertical transportation device.

The capsule with its pendulum body is stopped at the terminal, and its carrier body is then fixed on the terminal for automatically loading and unloading the containers. **Fig. 4** and **Photo 2** show the overall con-

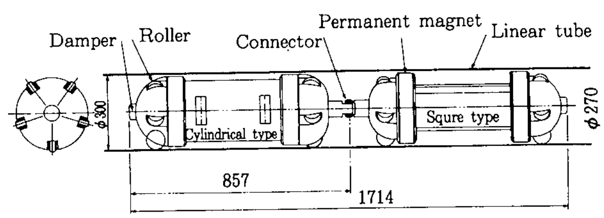

Fig. 3 Configuration of the type 300 linear capsule

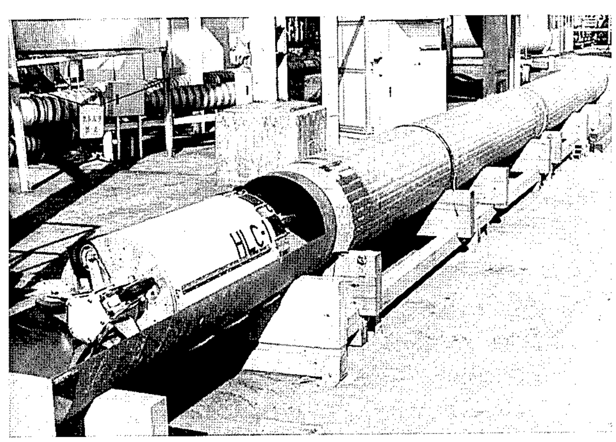

Photo 1 View of the type 500 LTTS

figuration and a general view of the loading and lifting system of the terminal, respectively.

The magnetizing coils are wound around the tubes at equal intervals, and the number of turns in the coils differs in the horizontal, sloped and vertical sections of the line. **Fig. 5** and **Photo 3** show the overall configuration and a general view of the test line, respectively. Specifications of the test line are given in **Table 2**.

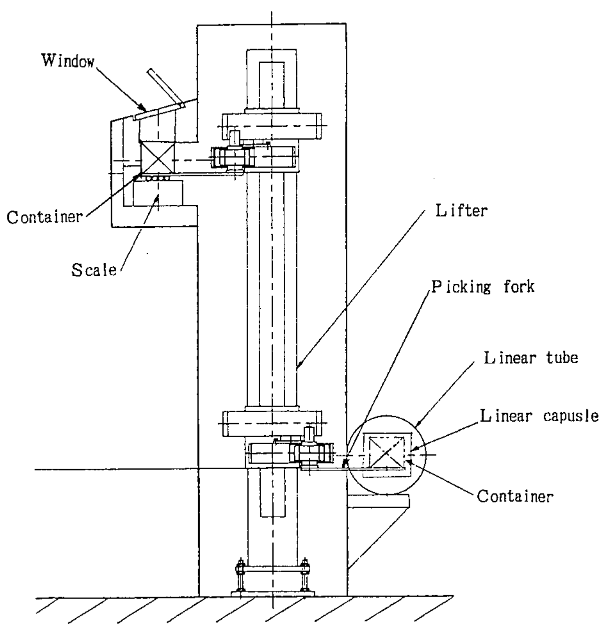

Fig. 4 Overall configuration of the LTTS terminal

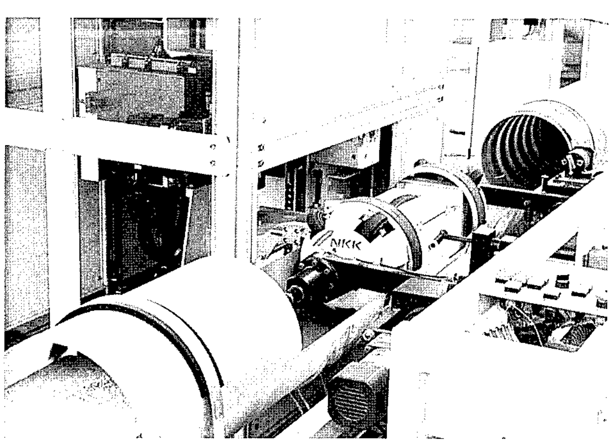

Photo 2 View of the type 300 linear capsule and loading and lifting system

3.3 Method of control

The type 300 LTTS employs a 4 pole, 9 phase power supply control, a speed control and a section control systems.

Two permanent cylindrical magnets are fixed to the capsule at a distance of one half of a thrust cycle, as mentioned earlier. The power source is controlled

Table 2 Specifications of the type 300 test line

Item	Specifications
Line profile	Roop shape, Lengh:56 m,
Bend	45～90°, Curve rate:7D(D:Diameter)
Branch line	Point switch of travers type
Slope angle	45～90°

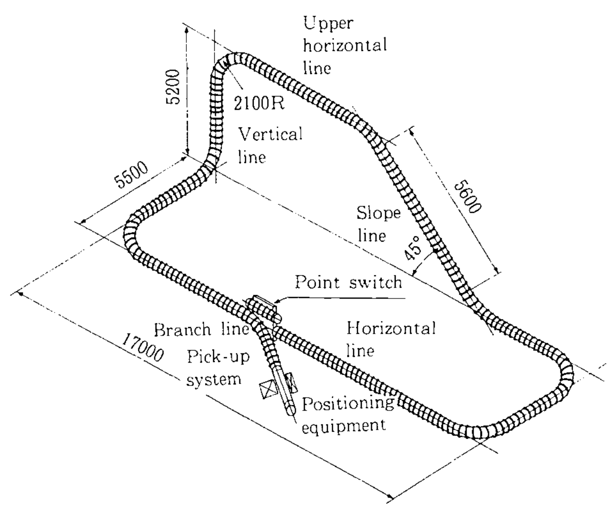

Fig. 5 Overall configuration of the type 300 test line

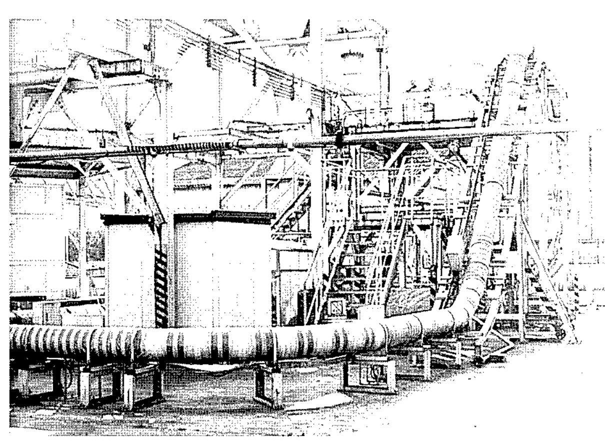

Photo 3 View of the test line

to generate attraction at the front and repulsion at the back of each magnet. The magnetizing coils are connected in series for each phase and are joined to the multiphase power source to provide high speed control. Sensors between the coils are linked to the magnetizing pattern control device. The magnetizing pattern is automatically set according to the position of the capsule detected by the sensors.

The speed is calculated based on the interval of the signal from the activated capsule position detecting sensors and is proportionally controlled using the pulse width modulation (PWM) method. A block-diagram for the capsule speed control is shown on **Fig. 6**. For stopping the capsule at the terminal, the speed is reduced from 2.0m/s down to 0.2 ~ 0.3m/s at a fixed rate, and the capsule is stopped when it reaches the designated position. The simulation results of the speed control for stopping the capsule are shown in **Fig. 7**.

Furthermore, the test line is divided into 18 sections, and electric power is supplied only to the section where the capsule is running. Solid state contactor (SSC) are used to change the section powered. Sensors installed between the coils detect the position of the capsule and send a signal for a section change for power supply. As such, section control is effective for saving power.

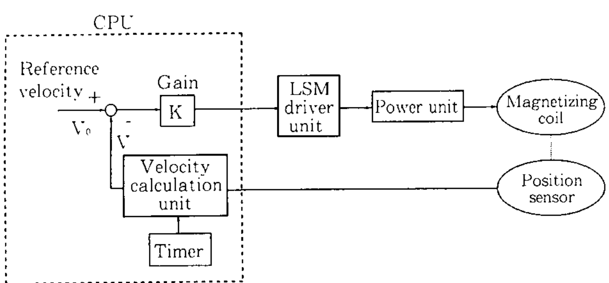

Fig. 6 The block-diagram for the capsule speed control

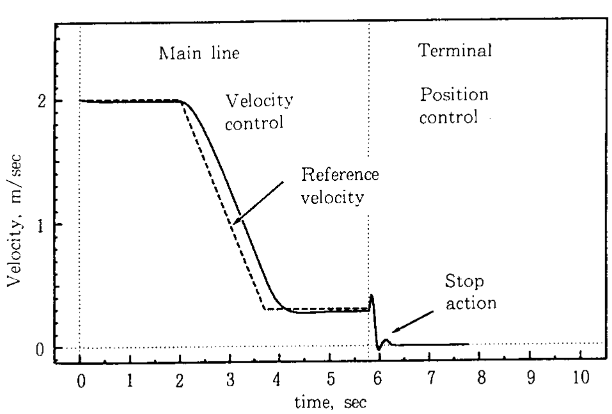

Fig. 7 Capsule stopping speed control simulation results

3.4 Results of the trial run

The trial run of the type 300 in the test line was performed with a load of 10 kg and a speed of 10 m/s. The results of the trial run are shown in **Fig. 8**. The abscissa represents the line position, while the ordinate represents the speed and electric power consumption. Thus, the chart shows the relation between the speed and power consumption. The speed was approximately 10 m/s in the horizontal line, and decreased to approximately 5 m/s when the capsule passed the bend and ran up the vertical line. The power consumption was approximately 5.5 kW in the horizontal line and approximately 18 kW in the upside vertical line. Braking is accomplished by reversing the direction of thrust, and the precision of the stopping position at the terminal was plus/minus 1 ~ 2 cm.

The trial run of the type 500 capsule reached a top speed of 4.7 m/s in the 10 m line. A trial run with a load of 110 kg was also performed, and the performance was verified.

4. Application concepts for linear motor

With the LTTS, the tube acts as the guide for linear capsule movement. The capsule is very safe and secure, and can be easily constructed by units. Furthermore, as the capsule does not have a propulsion

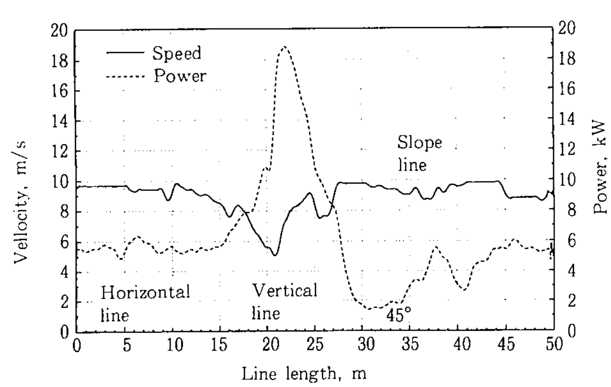

Fig. 8 Actual speed characteristics of capsule on the type 300 test line

device, maintenance, control and automation of the capsule are easy. Many suggestions can be made for applications of the LTTS that use these characteristics for each tube size, which are summarized in **Table 3**.

Small sized systems can primarily be used for indoor transportation of documents or patient's charts in hospitals, etc.. **Fig. 9** shows the indoor transportation concept. A medium sized system could supply parts from a warehouse to a factory via an underground tunnel or distribute goods from a store to an apartment. This size has a wide range of applications.

Large sized systems will be used for the high speed transportation of bulk materials. **Fig. 10** shows an example of the use of joint tunnels that may be used in the distribution of parcels, the transportation of goods to isolated islands, the removal of soil from construction works such as tunnels, or the delivery of earth and sand to a reclaimed land. The large sized system may also be used in the transportation of urban wastes between a primary waste collection plant and an incinerator or between incinerators for effective waste disposal.

A prototype monorail type monitoring system using the linear motor is shown in **Photo 4**. This monorail system may be used for transporting goods inside factories at low cost, for a short distance transportation system, for transportation in a gaseous environment that requires its nonexplosive nature, or for monitoring inside tunnels.

The vehicle system has permanent magnets attached on the bottom of the carrier and is capable of non-contact propulsion. Because of its low dust characteristics, this low profile vehicle system may be used in the transportation of food items or for transportation in refrigerated warehouses. Another application is for the propulsion of rides such as a roller coaster in an amusement park. **Photo 5** shows a prototype for a roller coaster that is 45 m long, has a slope of 45 degrees, provides a maximum speed of 10 m/s, and can produce 1200 N of propulsion.

Table 3 Application examples of LTTS for each tube size

Size	Pipe dia.	Applications	Conveyance weight
Small size	ϕ200～ 350mm	Conveyance in building or hospital	5～ 20kg
Middle size	ϕ400～ 700mm	Transportation in factory of baggage	100～500kg
Large size	ϕ750～1200mm	Transportation of baggage or trush	0.2～5.0ton

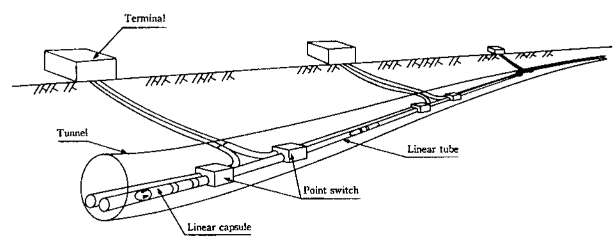

Fig. 10 Concept of transportation system through tunnels for the large sized LTTS

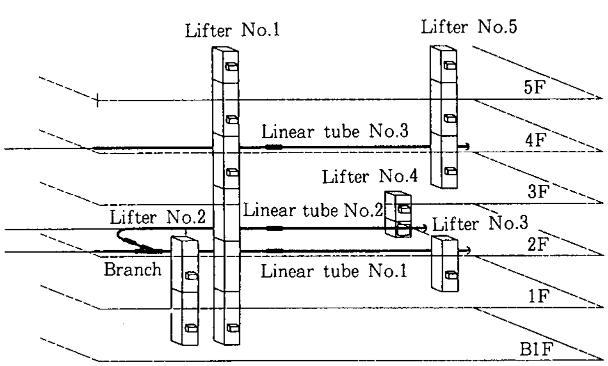

Fig. 9 Concept of transportation system in building for the middle sized LTTS

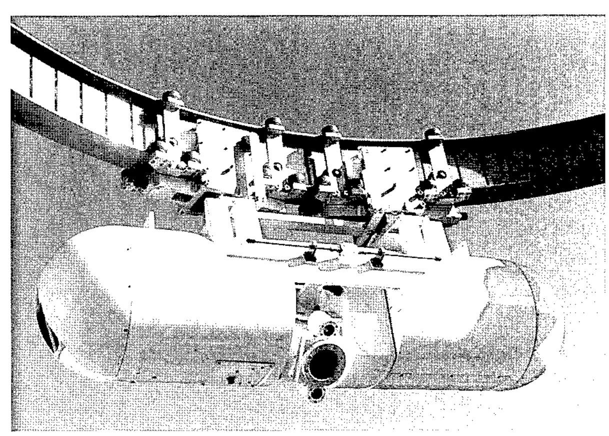

Photo 4 View of prototype monorail monitoring system with linear motor

5. Conclusion

Building more roads in urban areas is physically difficult due to lack of available land for road construction, increased noise and opposition from residents. The LTTS can solve such problems for material transport. The system may also be used as an innovative means of transportation inside buildings, taking advantage of its high speed and three dimensional capabilities.

Further applications of the LTTS toward the 21st century include a high speed transportation system in a very deep underground environment, a linear elevator system in high-rise buildings, a refrigerated warehouse materials handling system, a monitoring system and a capsule transportation network for distribution and waste disposal.

Further technical development is required to increase the speed and propulsion of the linear motors. The propulsion has improved along with the development of magnets. Taking advantage of the improved technology, we will make continuous efforts to develop transportation systems that utilize the features of linear motors to the full extent and put them to practical use.

References

1) Fujisawa, T . et al. "Development of Linear Tube Transportation System." NKK Technical Review. No.142, p.63-70(1993).
2) Yamada, H. "Industrial Linear Motor." The 2nd edition. Industrial Investigation Association. 1985.
3) "Linear Motors and Its Application." IEEJ, Magnetic Actuator Investigation Committee.

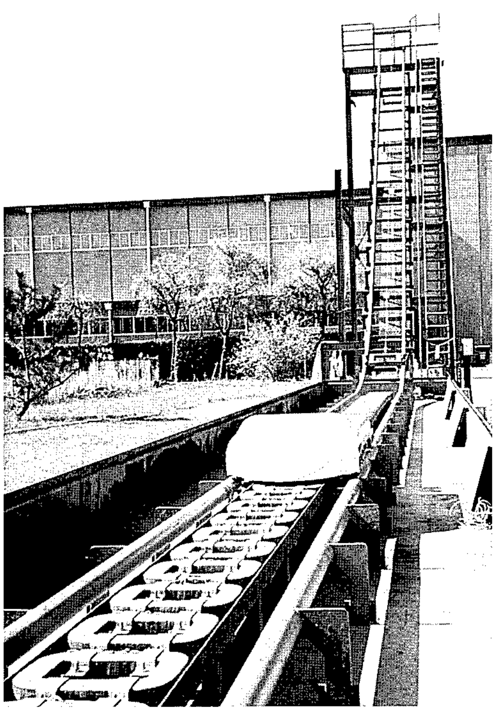

Photo 5 View of prototype amusement park roller coaster with linear motor

Port of Kawasaki Automated Container Terminal

Kiyotaka Hayakawa*, Tatsuya Nakajima**,
Hiroyuki Nagai**, Naomi Matsumoto***,
Sigekazu Takahashi****and Toshio Okawa*****

The first automated container terminal in Asia and the Pacific Ocean was completed at the Port of Kawasaki in March 1996. NKK developed and delivered the automated rail mounted gantry cranes for yard handling and the semiautomatic, dual trolley, quay container cranes for the Port of Kawasaki Phase-1 project. NKK also developed an advanced information processing system for terminal operation that links the container handling cranes. NKK's Automated Container Terminal system permits highly efficient, cost effective and reliable operation.

1. Introduction

The recent rapid movement toward the use of large container vessels and the heated competition among shipping companies has classified existing container terminals as either hub or feeder terminals. This tendency is likely to become more pronounced in the future. Thus, the terminal industry has become a fierce battleground. Terminals become more competitive by pursuing high productivity and high reliability of their container handling works. Along with this movement, there is a growing need for providing 24 hours a day, 365 days a year operation. In addition, the ability to provide information of container inventories for operating the facility based on the container vessel schedule has become important. The need is similar to that of hub airports. On the other hand, terminals have many labor problems that include poor motivation in the work environment, lack of manpower, and aging and unskilled workers. To ensure long term competitiveness under these circumstances, terminals must reduce their operating cost by introducing an automated terminal system where automated container handling and high level information processing are integrated.

NKK developed an automated container terminal system that consists of the automated container handling equipment and information processing system listed below. This system began operation as the Port of Kawasaki Container Terminal in March of 1996.

(1) Rail-mounted gantry crane (RMG)
(2) Dual-trolley type quay container crane
(3) Terminal operation system

This paper describes the various automated identification and control systems that are used in the automated container handling equipment, and outlines the control system for efficiently operating the container handling equipment that is included in the terminal operation system.

* Project Manager, Higashi-Ohgishima Project Team, Steel Structure & Machinery Engineering Dept.
** Manager, Higashi-Ohgishima Project Team, Steel Structure & Machinery Engineering Dept.
*** Manager, Heavy machinery engineering Sect., Steel Structure & Machinery Engineering Dept.
**** Manager, Logistics Sect., Steel Structure & Machinery Engineering Dept.
***** Senior Research Engineer, Control Engineering Research Dept., Applied Technology Research Center

2. Outline of the terminal

The Port of Kawasaki Container Terminal was constructed as a forerunner for ports that accept large vessels, incorporate labor-saving terminal operation, and provide highly efficient container handling. The following is an outline of the Terminal. In March 1996 when the Phase 1 construction was completed, the Port provided 14m of water depth with 350m of berth length, allowing 50000 DWT class container vessels to come alongside. The container yard is 700m long and 350m wide. By March 2001 when the Phase 2 construction will be completed, a 350m long berth will be added, and the water depth will be increased to 15m, which will allow 80000 DWT class container vessels to moor by the berth. **Photo 1** shows an overall view of the present Port of Kawasaki Container Terminal. **Table 1** lists the scale of the terminal at the completion of Phase 1 and Phase 2 construction.

Table 1 Major specifications of the terminal

Item	Upon completion of phase-1	Upon completion of phase-2 (incliuding phase-1)
Total quay length	350m	700m
Water depth	−14m	−15m
Maximum vessel	50,000 DWT	80,000 DWT
Quay crane	2 units	5 units
RMG	8 units	14 units
Internal movement vehicle	Tractor/chassis	AGV
Storage capacity (dry)	6,944 TEUs	12,152 TEUs
(reefer)	540 TEUs	945 TEUs
Annual handling capacity	240,000 TEUs	528,000 TEUs
Terminal area	24.5ha	

Remark RMG : Rail Mounted Gantry Granes
AGV : Automated Guided Vehicles

Photo 1 Port of Kawasaki Automated Container Terminal

2.1 Terminal layout

The terminal layout and level of automated container handling equipment were determined based on the terminal plan guideline.

<Container cranes>

All operations except part of the shipside and land side container handling are automated to reduce the manpower load.

<Container stacking yard>

An essentially unmanned system was established within the yard by introducing automated operation of the RMG and adding automated guided vehicles (AGV), which are unmanned vehicles exclusively for transporting containers, at the completion of Phase 2 and adopting a reefer container monitoring system.

The terminal layout has the following features.

(1) A shipside buffer system is used to significantly shorten the cycle time of yard side vessel working.

(2) A considerable increase in shipside container handling speed is achieved by allocating part of the stacking area exclusively as a buffer area for temporarily storing containers for loading and unloading vessels. The containers are stored in the buffer area to match the loading and unloading sequence before the vessel arrives.

(3) To ensure safety within the terminal, the path for the flow of external haulage vehicles in the terminal is separate from that of the RMG and internal movement vehicles (or AGV for Phase 2) within the terminal.

(4) The other end of the stacking area can be allocated as a container transferring zone, exclusively for trailers carrying containers in and out. This eliminates interference with the internal movement vehicles, including AGV. As a result, interaction between the AGV and external vehicles does not occur within the terminal, and the manned work zone is separated from the unmanned work zone, ensuring that safety measures can be readily implemented.

Fig. 1 shows the terminal layout at completion of the Phase 2 construction. Other terminal facilities include: the control tower where the terminal operation is controlled during integrated and centralized mode; the entrance and exit gates, which are arranged to minimize the path of external vehicles within the terminal; the maintenance shop, where equipment repair is conducted; the quarantine yard, where the animals and plants are inspected; and the hazardous container yard, where hazardous materials are temporarily stored.

3. Automated handling equipment

At the completion of Phase 1 construction, the stacking yard for storing containers was 650m long, accounting for 4 blocks. The container handling equipment include 2 dual-trolley quay container cranes and 8 RMGs (two units for each block, or 8 units). A manned tractor/trailer system is used for transporting containers between the quay and stacking yard.

When Phase 2 construction is completed, the number of blocks will be increased to seven, and 5 dual-trolley quay container cranes and 14 RMGs will be located there. For further improving the automation of container handling, an AGV will be introduced for transporting containers within the terminal, replacing the existing manned tractor/trailer system.

3.1 Quay container crane

3.1.1 Outline

All the quay container crane operations are automated except part of handling at shipside and berth side. A feature of the quay container crane is automated container handling owing to the use of the dual-trolley and to the configuration of shipside and landside trolleys with a traverser. Another feature is the use of AC motor vector-inverter control system for all the major

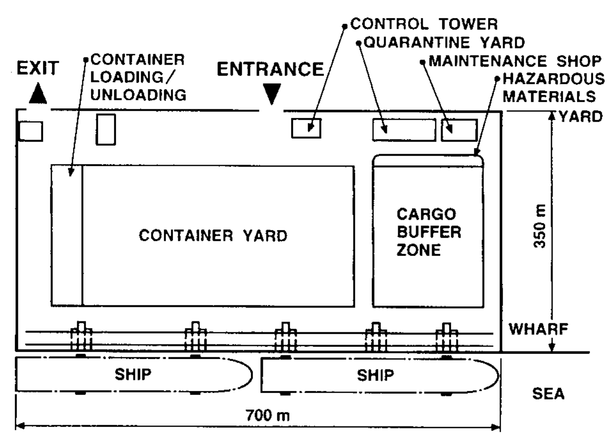

Fig. 1 Terminal layout plan (as completed in Phase 2)

motions including hoists. Although the system is rather expensive compared to a DC motor system, the inverter system has the following advantages.

(1) Excellent positioning precision

(2) Higher response rate than that of an electronic anti-sway control system, and capability for a wide range of anti-sway control in real time.

(3) Easy maintenance: no cleaning and replacing of brushes, which is required in DC motors.

A third feature is the adoption of a independent shipside operating cabin, which is typically attached to the shipside trolley. The operator does not need to move with the shipside trolley and can work exclusively with container handling on the vessel. This releases the operator from tiring work, allowing him to work longer. The separate shipside operating cabin has a mode that operates synchronously with the traverse of the shipside trolley, so the cabin also functions in a way that is similar to that of a conventional single trolley with an operating cabin. **Photo 2** shows an overall view of the container crane, and **Table 2** shows the major specifications of the quay container crane.

3.1.2 Automated operation system

Most conventional quay container cranes are manually operated. Even in automated systems, the automated part occupies a relatively small portion of a single container handling cycle. In contrast, the developed quay container crane achieves automated operation by using a dual-trolley system and an electronic anti-sway control system. These eliminate the landing and pickup areas both on the vessel and berth. **Fig. 2** shows details of the range of automated operation.

3.1.3 Computerized anti-sway control system

A major elemental technology of the automated operation is positioning control. In particular, the high speed traversing and high hoisting cranes require anti-sway control as a critical basic technology. For the cranes, we developed a computerized anti-sway con-

Table 2 Principal specifications of quay container cranes

PRINCIPAL PARTICULAR OF QUAY CRANE	
TYPE	: DUAL TROLLEY TYPE
TARGET VESSEL	: 50,000 DWT
RATED LOAD	: 40 LT
OUTREACH	: 45 m
RAIL SPAN	: 30.5 m
BACKREACH	: 15 m
LIFT(above the top of rail)	: 35 m
HOISTING SPEED (load/no load)	: 70/156 m/min
TROLLEY TRAVELING SPEED	: 210 m/min
HOISTING SPEED OF LANDSIDE TROLLEY	: 50/120 m/min
TRAVERSER TRAVELING SPEED	: 120 m/min
GANTRY TRAVELING SPEED	: 45 m/min
CONTROL SYSTEM	: FULL AC VECTOR INVERTER
OPERATOR'S CAB	: INDEPENDENT DRIVEN TYPE
OPERATING MODE	: AUTOMATIC(partly manual)

Photo 2 An overall view of quay container cranes

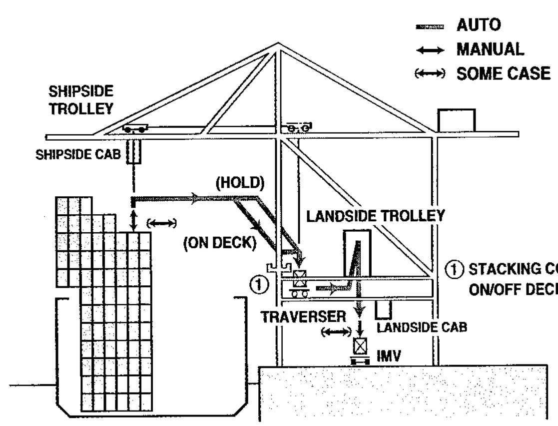

Fig. 2 Flow of automated operation of quay container cranes

trol system[1] that efficiently automates the operation with full scale utilization of the high speed traversing and hoisting performance. The combined traversing and hoisting motion and the container sway angle induced by disturbances such as wind force are detected on a real-time basis by using a CCD camera on the trolley to monitor a target attached to the head block, and then processing the image. The traversing motor is controlled to follow an ideal sway angle while tracking the generated sway angle signal. With this system, the sway range 5 sec. after stopping the trolley is controlled to a high accuracy of 100 mm or less.

Method: Image processing system with color CCD camera

Anti-sway control accuracy:
100 mm or less of sway range 5 sec. after stopping the trolley

Positioning accuracy: within ± 50 mm

Controllable motion: Simultaneous motion control for hoisting and traversing

Fig. 3 shows an example of anti-sway operation.

3.1.4 Automated identification system for stacked containers on the vessel

During container handling on the vessel, the high grade operation system generates information on the cross sectional area of containers stacked in each container bay and on the container handling sequence. Automated container handling is conducted on the basis of this information and sequence. For simultaneous hoisting and traversing motions to shorten the cycle time, additional information is also required on the actual stacking profile and the relative distance between the vessel and crane from the viewpoint of safety. The automated identification system uses laser distance sensors mounted on the trolley to determine the stacking profile in the vessel work bay throughout container handling.

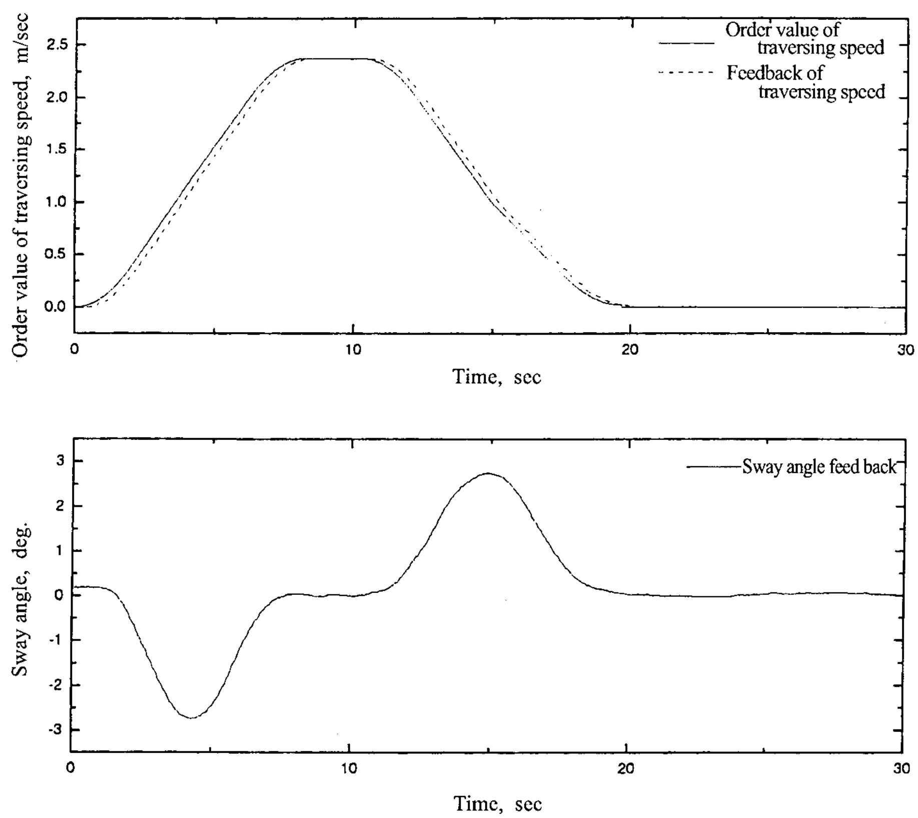

Fig.3 A result of anti-sway operation for hoisting and traversing

3.2 RMG

3.2.1 Outline

A high speed, rail-mounted gantry crane (RMG) system was adopted for stacking containers within the yard instead of a rubber-tired gantry crane (RTG), which is currently the most commonly used type in the world's container terminals. The reasons for using RMG are described below.

(1) RMG assures a higher positioning accuracy than RTG and allows traveling with a load.

(2) RMG allows higher traveling speeds than RTG.

(3) The small RMG has a lighter wheel weight and does not need a piled foundation, which minimizes the civil works cost.

As with the quay container crane, the RMG uses an AC motor vector-inverter control system. The basic reason for using the RMG is the same as that of the quay container crane. In addition, 24 hour, 365 day operation is a requirement, so that the high working ratio needed for the RMG is ensured by shortening the maintenance time compared to quay container cranes.

The RMG also uses the computerized anti-sway control system. The RMG has an additional mechanical auxiliary rope type anti-sway device as a precaution against container-swaying in the wind during unmanned operation. Thus the RMG has improved the container positioning accuracy. The synchronized-shift operation mode of 2 RMG units in each stacking block is available for import/export shifting of container between the shipside container buffer area and the stacking area. For the optimum shifting work planning system for the yard, a container handling sequence that minimizes interference of two RMG units was developed. The automated operation system simultaneously uses laser distance sensors mounted to the RMGs during container handling for interference avoidance control of the two units.

Photo 3 shows an overall view of RMGs, and **Table 3** shows the major specifications.

3.2.2 RMG automated operation system

The automated operation system allows either full automated or semi-automated operation for the four types of container handling operation shown in **Fig. 4**. The shipside buffer and reefer container handling, and part of shipside working are operated in automated mode except for placing and picking up containers on the yard trailers. Transfer between the shipside buffer and the stacking block is conducted in full automated mode, and the works are capable of unmanned handling at night. For external trailer carry in and take out work, only the setting of containers onto trailers is a manual operation. This work can be done from the RMG operator's cabin and also from the ground in remote operation mode.

3.2.3 Container position detection system

To achieve automated operation, a container hang-

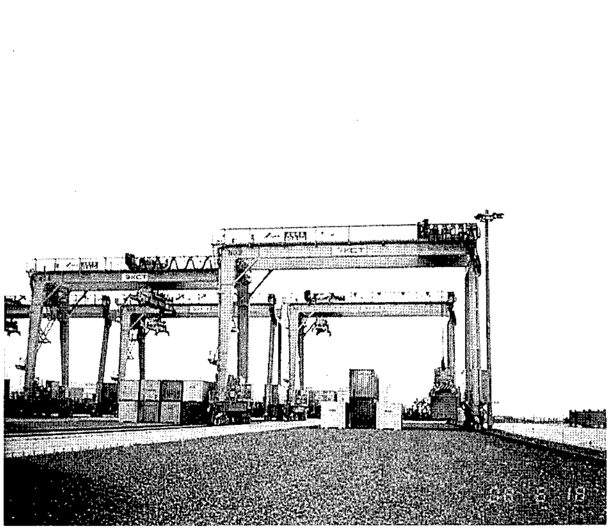

Photo 3 An overall view of RMGs

Table 3 Principal specifications of RMGs

PRINCIPAL PARTICULAR OF R M G	
RATED LOAD	: 40 LT
RAIL SPAN	: 25.5 m(covering 8 rows of containers)
LIFT (above the top of rail)	: 15 m(one over four)
HOISTING SPEED(load/no load)	: 35/75 m/min
CRAB TRAVELING SPEED	: 80 m/min
GANTRY TRAVELING SPEED	: 180 m/min
CONTROL SYSTEM	: FULL AC VECTOR INVERTER
OPERATOR'S CAB	: INDEPENDENT TYPE
OPERATING MODE	: AUTOMATIC (except for chassis landing and picking)
ANTI-SWAY SYSTEM	: HYBRID ANTI-SWAY (a combination of electric and mechanical)
MAJOR SENSORS	: SCAN THE PROFILE OF STACKED CONTAINERS DETECT CONTAINER'S POSITIONED DEVIATION

ing from an RMG is allowed to stack at a specified position only when it is within an allowable offset range. In particular, loaded containers are often under eccentric load conditions that cause an offset in the horizontal plane of containers hung by ropes.

The detection system uses a CCD camera mounted on the lower part of the crab and a target attached to the head block to determine the position of the head block. A skew adjusting device is used to automatically correct the position and allow the containers to be stacked.

Method: Image processing with color CCD camera

Accuracy of position detection: ± 10 mm

4. Terminal operation system

In an automated container terminal, automation is achieved not only by computerizing the conventional office work but also by computerizing the entire scope of operation, including planning, work instructions, and record control of the container handling equipment. In particular, when the container handling quantity and complexity increase, the role of the computer system is more important than ever to ensure the accuracy of work control. The computer system at the Port of Kawasaki Container Terminal has the following features to provide quick and correct service to ship and container owners with an improved terminal operation efficiency.

(1) A high speed network was developed using optical fibers to improve the reliability and high speed data transmission. This network includes information transmission to the container handling equipment

(2) A distributed computer system was adopted in anticipation of future expansion.

(3) Unified and integrated database management was adopted to improve the data reliability and to reduce the work load.

(4) With the duplex database system and uninterruptible power supply, data protection in an emergency is ensured, and automated container operation can be restarted within the shortest time.

(5) Increased efficiency and standardization of work were achieved by computerizing the work for allocating container storage areas and for preparing the container handling equipment operation plan. Previously, this work relied solely on skilled operators.

(6) Through integration of the system by connecting the automated operation system of container handling equipment, all the work from the office to the container

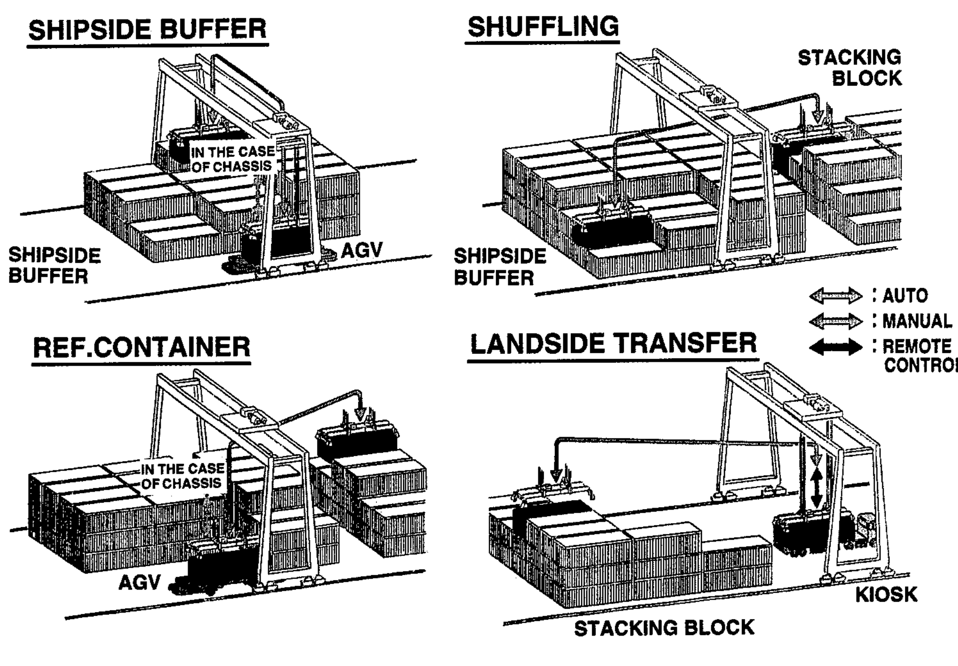

Fig. 4 Mode of automated operation for RMGs

handling operations are conducted under centralized control, thus improving reliability and accuracy.
(7) Reductions in labor and improvements in the efficiency of maintenance work were attained with the installation of various types of monitoring systems, such as the reefer container monitoring system.

Fig. 5 shows the scheme of the operation system.

4.1 Optimum export/import shifting scheduling system

A practical application example of the highly advanced scheduling technology that uses the terminal operation system is the scheduling system for shortening the container handling time through optimizing the shifting of export/import containers between the ship-side container buffer and the stacking block. The system minimizes interference between two RMGs and the waiting time due to interference between the two RMGs when picking and landing the containers. The system also minimizes the transfer time under no-load conditions between landing a container and picking up the next one. The system uses a mathematical optimizing method[2], and the operation plan is completed rapidly. **Fig. 6** shows the basic motion of the import/export shifting operation.

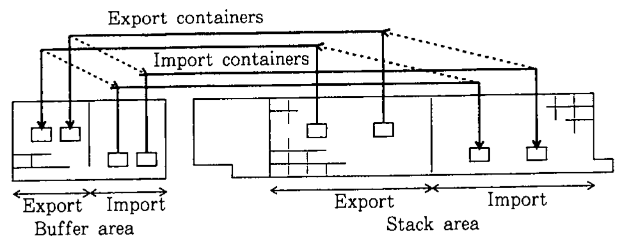

Fig. 6 Synchronized shuffling operation for two RMGs at the same lane

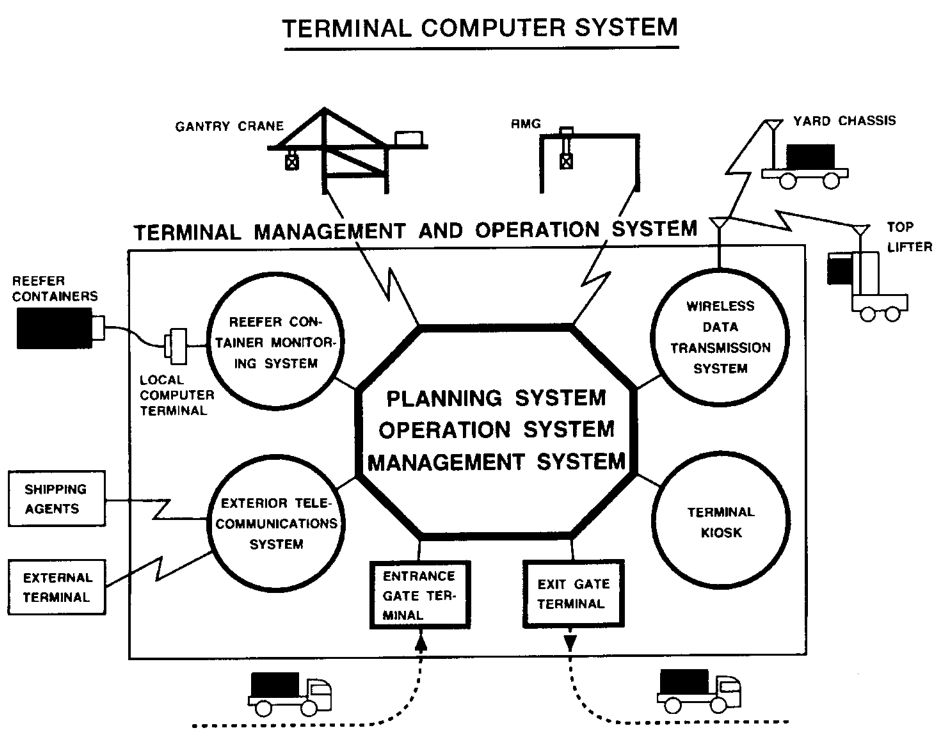

Fig. 5 Scheme of terminal information system

5. Conclusion

Terminal specifications depend not only on the container handling system, but also on the handling quantity and variety of containers, the landside transportation system, and the regional situation, including that of adjacent countries. Accordingly, a common method for automatization has not yet been established. Currently, only three automated container terminals are operating in the entire world including the Port of Kawasaki, which is our product. Nevertheless, terminals at the junctions of container distribution flow have been tending to operate 24 hours a day, 365 days a year. In addition, from the viewpoint of the on-line transmission of information on various types of containers among ship owners and agencies, container handling control on a real time basis and high reliability become essential. The number of automated terminals should increase toward the next century. In this respect, NKK will structure automated systems in response to individual terminal requirements.

We would like to express our appreciation to the Kawasaki Municipal Port Authority and Kawasaki Container Terminal, Inc. for their purchase of the container handling equipment and computer system, and also to NKK Plant Construction Co., Ltd. for their cooperation in the development work.

References

1) Date, T. et al. "Electronic anti-sway control for container handling cranes". NKK Technical Review. No.150, p.56-60(1995).
2) Kawai, N. et al. "Optimum Shuffling Plan of Container Yard." Production Scheduling Symposium. Kohen ronbun-shu, '95. p.169-174(1995).

Automated Warehouse System for Steel Pipe

Hirofumi Ishikawa*, Noriaki Shoda*,
Takashi Arai*, Yutaka Ishii*,
Yoshinori Kato**, Masaru Watanabe***
and Haruki Takeuchi****

NKK has proposed to reorganize and standardize the distribution process within the steel industry. The steel produced by the industry are extremely varied; steel with rolled, coiled, and H-beam shapes are examples of the variety of steel produced by NKK. Like other industries, the steel industry has had to reorganize its distribution process to improve quality and efficiency. NKK has done so by implementing a large-scale automated warehouse system for steel pipes. The automated system is guided by the concept of "Just in Time". This paper outlines the key features of the new automated warehouse system.

1. Introduction

The current industry-wide practice at steel pipe distribution centers focuses on the handling of bundles, which are steel pipes bundled with steel wire. The bundles are sent from the steel works by marine transportation. The current distribution process focuses on minimizing the amount of time that the ship must remain in port. Therefore, inspection, sorting, and storage of the bundles in steel frames are done only after all unloading is completed. To further reduce the time needed to load the bundles onto delivery cars, bundles are sorted according to their particular delivery sites before the shipping day and transferred again into steel frames for shipping. During this re-transfer work, bundles on the upper part of the steel frame stack must be transferred to other steel frames so that bundles on the lower part of the steel frame stack can be moved. This part of the distribution process requires a great deal of time and labor, as well as being dangerous; therefore, it was identified as a prime area of the process requiring improvement.

Adding to the necessity for process improvement, lead time requires minimizing because of the recent trend of small lot handling, which has increased the work load at steel distribution centers.

NKK was involved in the reorganization of the Osaka Distribution Center of NKK Marine & Logistics Corporation from the reorganization's inception. NKK designed and implemented the automated warehouse system using a centralized information system. The new warehouse system for steel pipes uses automated, palletless transfer, storage, and sorting equipment for bundles that is in continuous operation. **Photo 1** shows the automated warehouse.

* Manager, Logistics System Engineering Dept.
** Manager, NKK Plant Engineering Co., Civil Engineering Dept.
*** Manager, NKK Plant Engineering Co., Electric Instrument and Control Dept.
**** Manager, Logistics System Engineering Dept.

2. Overview of the automated warehouse system

2.1 Materials to be stored

Table 1 and **Fig. 1** show the dimensions and shapes of the bundles to be stored. The specifications for the bundles for special-grade pipes and gas pipes were based on survey and analysis of the inventory at Osaka Distribution Center. The bundles have the following features, which show that the materials to be stored do not have uniform shapes and require special care in automated handling:

(1) Pipes are tied together using steel wire or PVC string.
(2) Pipes may be loosely tied together.
(3) The number of pipes in a bundle is two or more.
(4) The edges of pipes in a bundle are not uniform.
(5) The pipes may have sockets.
(6) A bar-code tag is attached to one of the ends of every bundle.

2.2 Main specifications of the automated warehouse system

(1) Acceptance capacity: max. 200 bundles/h (200 t/h)
max. 740 bundles/d (740 t/d)
(2) Shipment capacity: max. 150 bundles/h (150 t/h)
max. 640 bundles/d (640 t/d)
(3) Inventory: about 11000 bundles (11000 t)

2.3 Specifications of the building

(1) Scale: 35 m wide x 180 m long x 35 m high
(2) Floor area: about 6000 m^2
(3) Structure: steel structure, one-story building

2.4 Outline of operation and facility structure

Fig. 2 shows the general arrangement of the automated warehouse system. The system is divided into four areas, although their structures are integrated(refer to **Fig. 3**): (1) the entry area, (2) the storage and removal area, (3) the sorting area, and (4) the shipping area. Following are descriptions of each area.

2.4.1 Entry area

The entry area handles the bundles unloaded from the vessel to promptly process them for acceptance. The distribution flow in the entry area is the following:

(1) A rope trolley crane unloads bundles to the transport car waiting on shore.

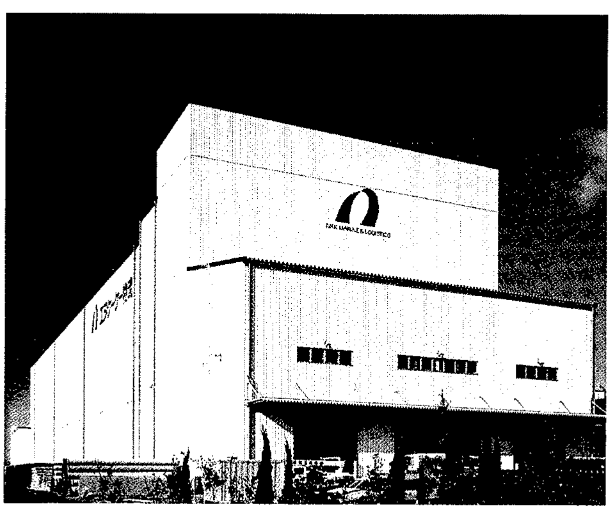

Photo 1 Overall view

Table 1 Dimension of bundles

Diameter (mm)	Weight(ton/bundle)		Width (mm)	Hight (mm)	Length (m)
	Average	Maxmum	Maxmum	Maxmum	
ϕ21.7 ϕ267.4	1.0	1.6	800	600	4.0 6.5

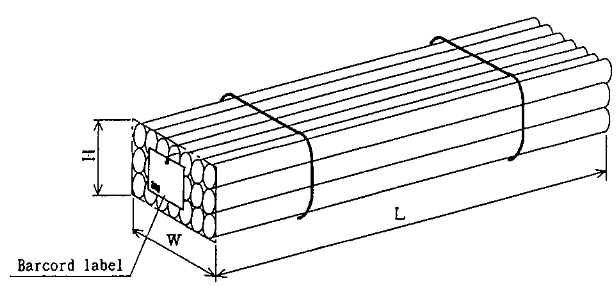

Fig. 1 Shape of bundle

(2) The transport car drives to the automated warehouse and transfers the bundles as a single entity onto an entry conveyer inside the automated warehouse (refer to **Photo 2**).

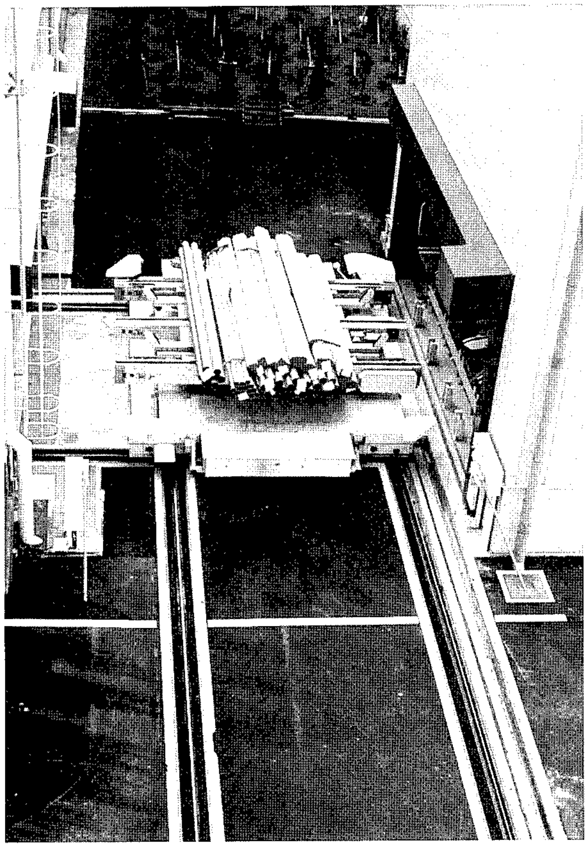

Photo 2 Transport car

(3) When the bundles are stacked on the entry conveyor, an operator manipulates an overhead crane to arrange the bundles so that they can be placed on the entry conveyer on a single level.

(4) A separating device automatically separates the bundles.

(5) An operator reads the bar-code on the tag on each bundle, using a manually-operated radio scanner linked to the central computer. This action performs all material acceptance inspection, and inventory confirmation. All succeeding steps before shipping are completely automated.

(6) Every bundle is sorted according to the computer command. The sorted bundle is transferred to a specified stacker crane via the sorting conveyer.

Entry area configuration:

- Transport car: 1 unit
- Entry conveyer: 1 unit
- Overhead crane (6 tons) with lifting magnet: 1 unit
- Separating device:1 unit
- Sorting conveyer: 1 unit

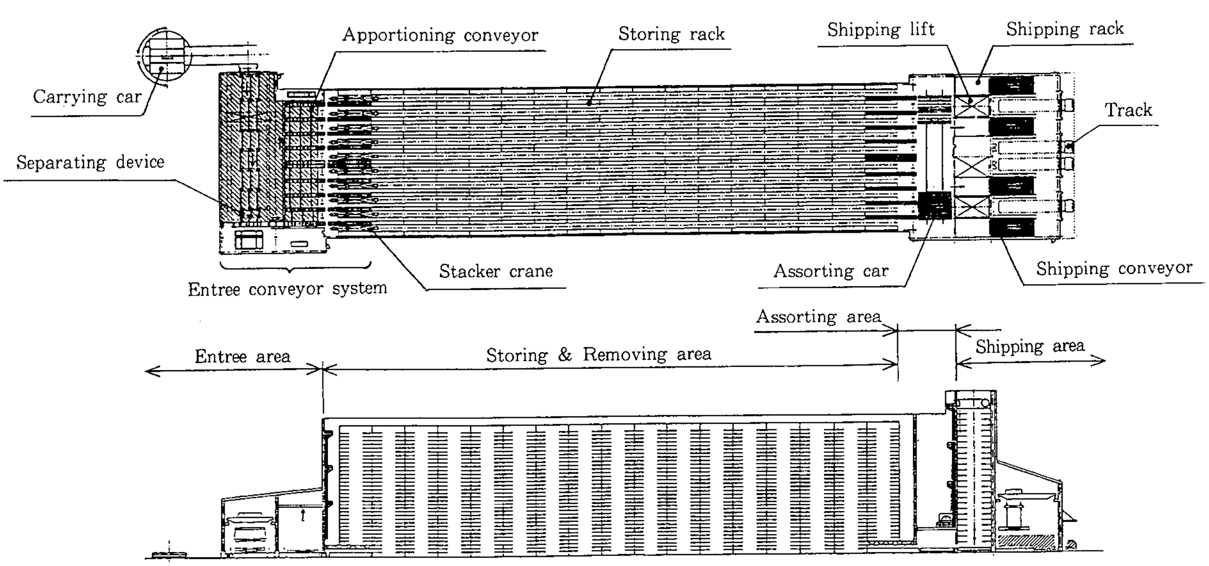

Fig. 2 General arrangement

2.4.2 Storage and removal area

In the storage and removal area, the bundles sent from the entry area are stored separately in one of four kinds of storage racks, depending on the bundle weight and size. During the night, bundles are automatically removed and sorted.

Storage and removal area configuration:

(1) Storage racks (one bundle per rack):

for 1.4 tons: 18 rows x 17 bays x 33 levels, equaling about 10000 racks

for 1.6 tons: 2 rows x 17 bays x 33 levels, equaling about 1,100 racks

(2) Stacker crane for 1.4 tons: 9 units

(3) Stacker crane for 1.6 tons: 1 unit

2.4.3 Sorting area

The sorting area is used to sort the bundles for each shipping delivery site. The bundles are placed one by one on the exit conveyors according to the request for sorting from the main computer. The sorting car transfers the bundles from the exit conveyor to a shipping rack for each delivery site, in a maximum quantity of five bundles at one time.

Sorting area configuration:

(1) Exit conveyer: 10 units

(2) Sorting car (max. 5 bundles at a time) : 1 unit

2.4.4 Shipping area

The shipping area stores the sorted bundles until shipping. Shipping is conducted automatically. Each individual rack stores a maximum of five bundles. The bundles are automatically removed from the racks and sent to the shipping platform using shipping lifts and shipping conveyors. The operator manipulates an overhead crane to load the transferred bundles to the trailer to complete shipping.

Shipping area configuration:

(1) Shipping racks (max. 5 bundles/rack) for 7 tons: 4 rows x 1 bay x 25 levels, equalling 96 racks

(2) Shipping lift (max. 5 bundles) for 7 tons: 2 units

(3) Shipping conveyer: 4 units

(4) Overhead crane for 10 tons: 2 units

2.5 System configuration

Fig. 4 shows the system configuration. A manual terminal with radio transmitting, bar-code reader is located in each entry and shipping area for convenience. The radio antenna is a multi-drop type, and a relay station connects it with the radio terminal. The computer for warehouse control is a client-server type connecting eleven clients and a single server over a high-speed network. The clients are largely grouped as follows:

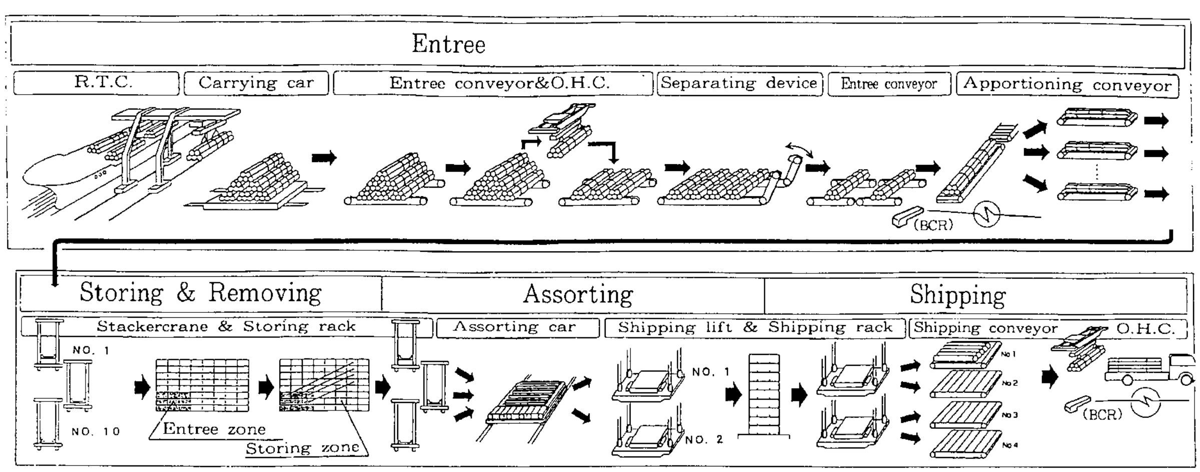

Fig. 3 Distribution flow

communication terminal; entry and shipping control terminal; radio terminal; entry and shipping terminal; and work terminal. Their functions are described below.

(1) The communication terminal connects to the main computer in the head office via a 3270 emulator. It sends and receives the warehouse and main computer data, functioning as the gateway.
(2) The entry and shipping control panels are connected to a single terminal by LAN. This terminal generates entry and shipping command information to the control panels.
(3) The radio terminal is connected to the manual terminal with radio bar-code reader. This terminal controls the radio information coming from the manual terminal.
(4) The entry and shipping terminal updates data based on the entry schedule and shipping schedule information coming from the main computer.
(5) The work terminal conducts inquiries and processes documents.

3. Features of the automated warehouse system

3.1 Palletless

The system handles bundles without putting them on pallets.

3.1.1 Necessity of a palletless system

The use of pallets requires work for preparing vacant pallets and returning used pallets. Automation of these tasks requires facility capacity. Storage area for vacant pallets is also necessary. To solve these issues, the palletless storage and transportation system was adopted.

3.1.2 Measures to achieve a palletless system

The main feature of the bundle is its non-uniform shape, as described in **section 2.1**. To cope with this feature, the automated system uses various types of

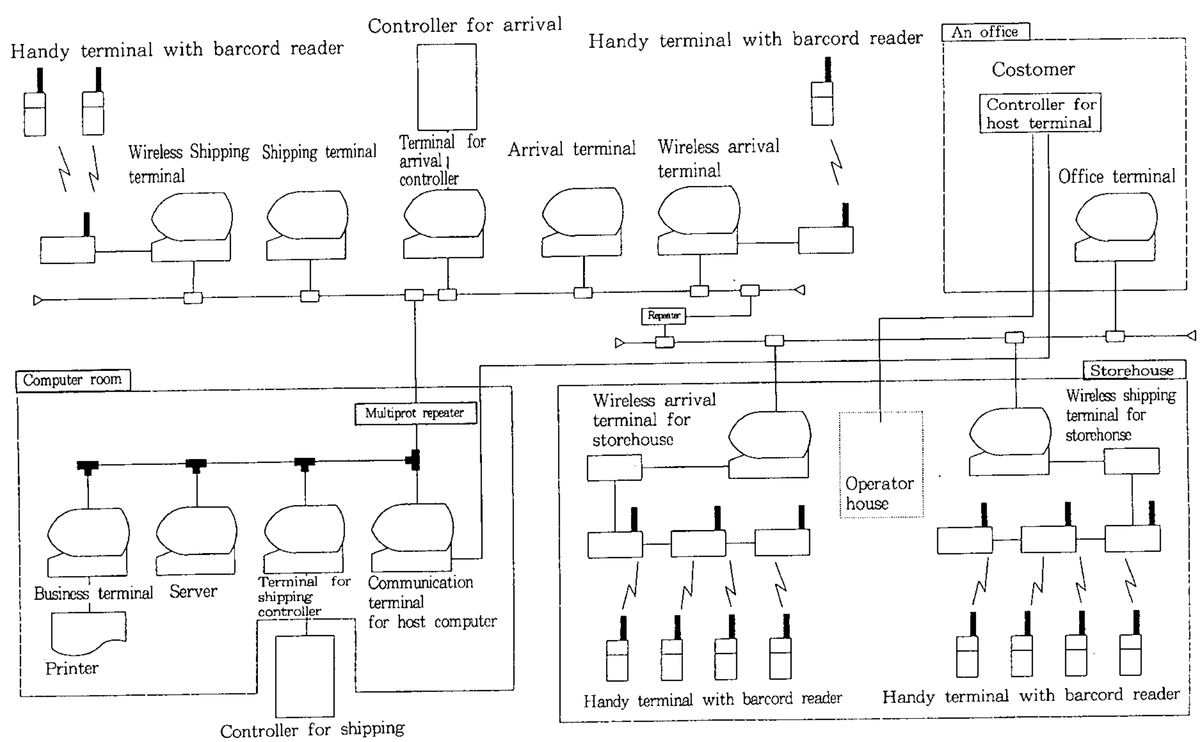

Fig. 4 Configuration of the computer system

sensors. The automated warehouse system has close to twice as many sensors as the pallet transfer system. For example, where the bundle in the longitudinal direction must be stopped in a way that is controlled accurately, a through-type photosensor with a wide detection area is used. An ordinary through-type photosensor without a wide detection area would not be sufficient, because the pipe edge position is not uniform within a bundle, and detection of only a specific point in the bundle edge plane may induce interference between a pipe edge beyond the photosensor scope and the bundle-handling facility.

3.2 Continuous operation of the warehouse system

The automated warehouse system is operated continuously. Daytime operation is for entry and shipping that requires operator interface. Night operation is for sorting and removal in preparation for entry and shipping. The basic operating schedule of the system is as follows.

(1)	8:00 - 11:45	Entry / Shipping
(2)	11:45 - 12:30	Sorting / Removal
(3)	12:30 - 20:00	Entry / Shipping
(4)	20:00 -	Daily processing
(5)	- 8:00	Sorting / Removal

Daily processing involves the updating of old data and scheduling of sorting, so that the work can begin at a predetermined time. Sorting is scheduled according to which bundles are being shipped on the next day. Sorting and removal ensure that storage racks are properly available, so as to minimize the entry process time, and help ensure that shipping racks are ready for shipping.

3.2.1 Daytime (entry)

Generally, an automated warehouse accepts material to fill lower racks, then upper racks. In the automated warehouse system, however, the cycle time of the stacker crane must be minimized to attain an entry capacity of 18 seconds/bundle. Therefore, the storage racks are grouped in three areas according to cycle time. Using preformulated logic, the system preferentially accepts bundles in the entry area to the shortest-cycle-time area; bundles are temporarily stored there until removal at night or margin time occurs.

3.2.2 Daytime (shipping)

In the automated warehouse system, the entry line and shipping line are physically separated, so shipping work can be performed without reducing daytime entry capacity. Because shipping can be done regardless of entry conditions, shipping is immediately activated on request; this is a key difference from previous automated warehouse systems. As described in **section 3.2.3**, shipping products are grouped in each delivery site zone during the nighttime removal work. This makes loading to the sorting car easier. If there is an emergency request to ship bundles that are not yet sorted, a flexible operation mode is available, in which shipping and sorting of bundles begin at the moment the request is received, and the bundles are delivered directly to the shipping platform without being placed on the shipping racks.

3.2.3 Night (sorting and removal)

According to the concept described in **section 3.2.1** for entry, bundles that are temporarily placed on the storage rack to minimize cycle-time are automatically removed during margin time or at night for transfer to an area designated for ready shipment by stacker cranes. In addition, the warehouse control computer prepares a sorting schedule based on the expected shipping information of the next day, which is received by 8:00 p.m. According to this schedule, the sorting car automatically sorts the bundles and transfers them from the storage rack, where they are stored separately, to the shipping rack, where they are stored in units of five bundles maximum, for each delivery site area.

3.3 Developed equipment

3.3.1 Separating device

The bundles loaded onto the transport car by a crane are in close contact, which prevents automated transportation of separate bundles. To cope with the situation, NKK developed a separating device, which increases the gaps between bundles (refer to **Photo 3**). A device that separates pipes was available, but not a device that separates bundles. The developed device detects the positions of bundles using a number of photosensors, then drives a stationary, ordinary slat conveyer and a slat conveyer that is enclosed by four units of swing arms moving in a synchronous mode. The device separates bundles of pipes, each ranging in diameter from 21.7 to 267.4 mm.

3.3.2 Sorting car

Photo 4 shows a sorting car in action. The sorting car has fully automatic functions for both transferring and sorting. The sorting car has its own driving function. It also has one set of slat conveyers and mini-vehicle for a single bundle and another set of conveyor for five bundles. The car sorts automatically using the process described below.

(1) The sorting car drives itself along the rails to load a single bundle, which is delivered from a storage rack onto the car using a single bundle slat conveyer.
(2) After the sorting car arrives at a specified position, the single bundle slat conveyer loads the target bundle. Then the mini-vehicle mounted on the sorting car transfers the bundle onto the five bundle slat conveyer.
(3) By repeating the action a maximum of five times, five bundles are gathered onto the five bundle slat conveyer.
(4) The sorting car drives to a specified shipping lift position, then transfers the five bundles as a single lot.

3.4 Data control

Bar-code data that were not effectively used in previous distribution practice are now used to gain centralized control of information, from entry to shipping. The bar-code data read from the tag on each bundle at entry and shipping are the control information. Inspection work at entry and shipping has become bar-code reading work.

The bar-code data read at entry are compared with scheduled entry information that was transmitted in advance from the main computer to the warehouse control computer. At the same time, a storage rack with adequate size for the bundle is allocated based on the weight and dimension data derived from the bar-code during transfer by the entry conveyor.

If the bar-code data are not included in the scheduled entry information, the manual radio terminal judges that the bundle is not the expected one and generates an alarm signal to notify the operator. Inspection and inventory confirmation work are thus completed.

On shipping of the bundles, the shipping order number and the shipping platform position are entered into the manual radio terminal, and the terminal generates the shipping command. Then, the sorted finished bundles are transferred to the shipping platform that is allotted by the shipping rack. The bar-code of the arrived bundle is read at the shipping platform, and inventory is updated.

These data are also transmitted to the main computer in the head office for data update.

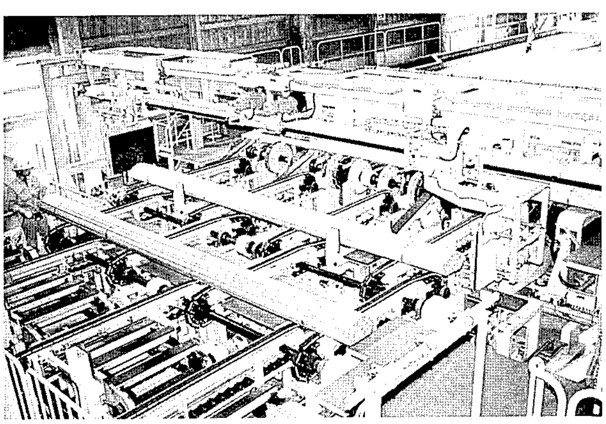

Photo 3 Separating device

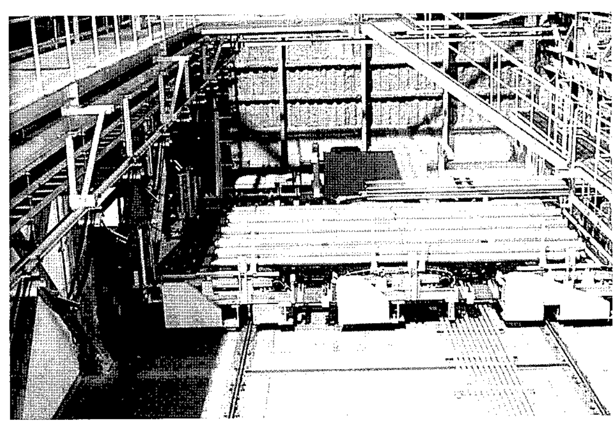

Photo 4 Sorting car in action

4. Conclusions

The introduction of the automated warehouse system has had the following results:

(1) Improvement of user service
• Reduction of lead time for shipping information and delivery
• Increase of shipping acceptance time by the adoption of removal at night
• Prompt response to small lot orders

(2) Efficiency
• Saving of manpower by as many as 30 persons compared with the manual handling warehouse system

(3) Improvement of work safety
• Elimination of crane work and work at height

(4) Effective use of site area
• Use rate of warehouse is reduced by half compared to manual handling warehouse system.

The automated warehouse system aims at automation according to the concept of "just-in-time" distribution flow. The full-scale, unmanned night operation is the most favorable for future distribution centers. Similar systems are expected to provide the same results for steel-handling firms and other steel material distribution centers. NKK will further study this system's applicability for other business systems.

References

1) Tanaka, T. et al. "Development and Commercialization of Automated Warehouse System for Small Size Pipes." Zairyo to Process (Materials and process). Vol. 3, No. 2, p. 535 (1990).
2) Ishikawa, H. et al. "Pipe Distribution Center." NKK Technical Report. No. 151, p. 77-81(1995).

Analysis of Imbalanced Fluid Force Inside a Cage-type, Low Noise, Control Valve

Yasuo Takagi* and Kazuo Kohda**

Relatively large, imbalanced fluid forces occur inside of a cage-type, low noise, control valve when used under severe conditions such as with large valve sizes and high direct or differential pressures. Analysis of the fluid force for such valve applications is therefore very important. The mechanism was analyzed, and a useful formula to calculate the imbalanced fluid force was derived.

1. Introduction

The imbalanced fluid force inside of a cage-type, low noise, control valve, including the piled disk type, is structurally small. Under some conditions, however, a large imbalanced force is generated that affects the function of the control valve. Thus, it is important to analyze the imbalanced force, especially when the valves are used for heavy duty processes such as high differential pressure applications. A practical method to analyze the imbalanced force acting on the plug of a cage-type valve is presented in this paper.

2. Mechanism of imbalanced fluid force generation

There are many varieties of cage-type, low noise, control valves, such as the multi-hole, multi-labyrinth and piled disk types. All of these types are considered to be a "cage type" in this paper. This type of control valve is used to suppress noise in severe conditions such as under high flow rates and high differential pressures.

When a large cage-type valve is used in high differential pressure conditions, a large imbalanced fluid force is generated inside the valve. This force may cause wear and other problems depending on the materials used.

Photo 1 shows a moderately worn plug of a cage-type control valve. Details of the valve and fluid con-

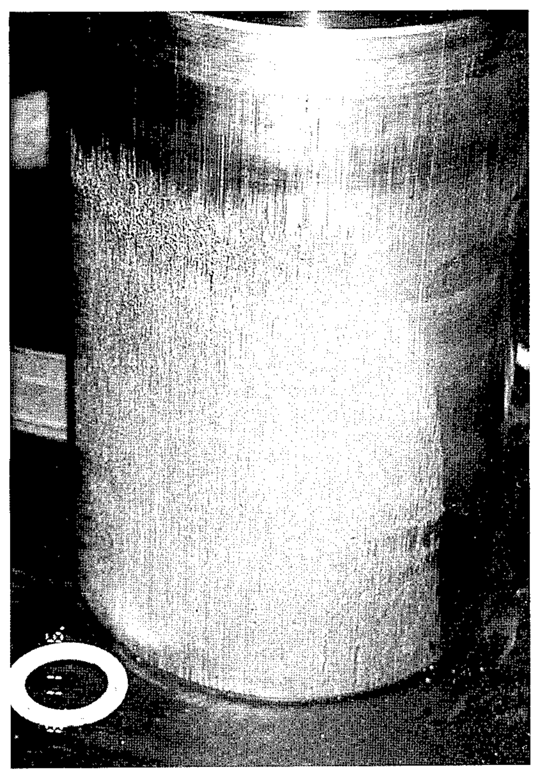

Photo 1 Worn plug surface

* Chief Engineer, Electrical & Control Engineering Dept.
** Chief Research Engineer, Dr., Engineering Research Center

dition for this case are listed as Case 2 in **Table 1**. The process from the generation of imbalanced fluid force to wearing out is as follows (see **Fig.1**).

a) When a valve opens, most of the gas flows out through the holes or labyrinths in the cage (indicated as "main flow" in **Fig.1(b)**). But, some of the gas flows into the narrow gap between the cage and plug, and then flows out through the cage (indicated as "leak flow" in **Fig.1(b)**).

b) The plug is slightly eccentric to the cage due to manufacturing tolerances, so the width of the gap, and therefore the amount of gas flowing into the gap, is not uniform but depends on circumferential position.

c) The pressure distribution around the plug becomes nonuniform, as shown in **Fig.2**. This imbalance of pressure generates the imbalanced force, which pushes the plug in the direction of the narrower gap side against the cage.

d) When the valve is operated in this condition, the plug and/or the cage suffer some wear depending on the materials used and the magnitude of the imbalanced force.

e) Once wear starts, the gap becomes wider, and the imbalanced force larger. The wider gap increases the amount of "leak flow." Moreover, the increased, imbalanced force, together with the increased friction coefficient due to wear, causes extremely large resistance to the valve motion. All of these effects reduce the ability to control the valve.

In order to avoid such undesirable conditions, quantitative analysis of the imbalanced force inside of a heavy duty control valve is very important.

3. Derivation of equations

3.1 Assumptions

A 3-dimensional analysis of compressible fluid flow in the narrow gap between the plug and the cage is necessary to accurately calculate the imbalanced force. Such analysis requires very complicated numerical methods, such as FEM or FDM, and is not practical.

A more practical and approximate method to calculate the force is presented in this section that is based on the following assumptions.

(a) The fluid is an ideal gas.

(b) The upstream pressure of the valve is much higher than that downstream.

(c) Gas is in stagnation conditions just before entering

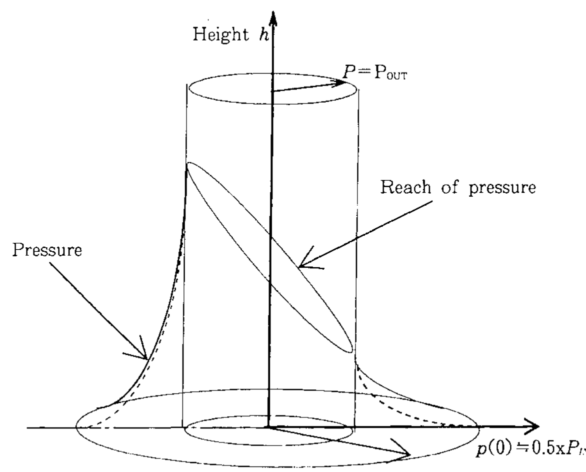

Fig. 2 Pressure around plug surface

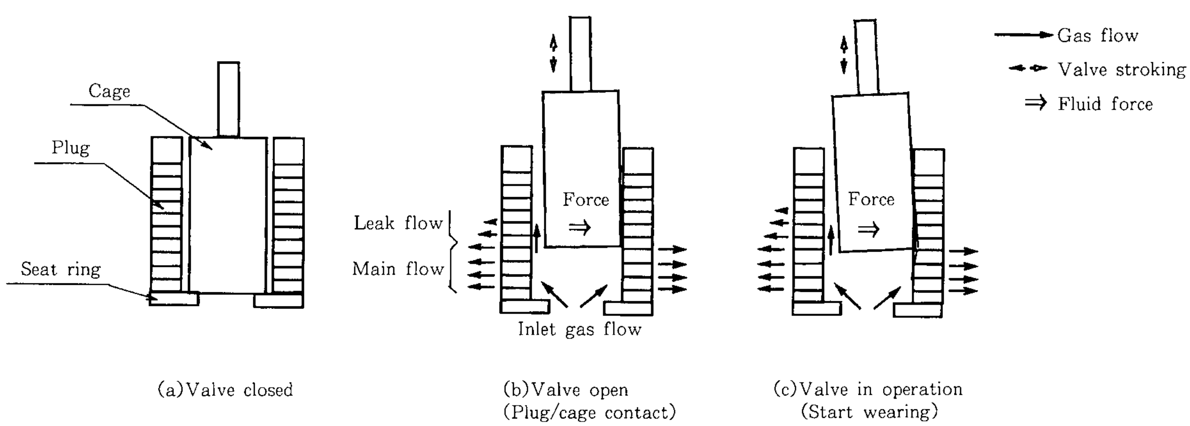

Fig. 1 Wearing process

the gap, and the sonic velocity is reached just after entering the gap. This change of condition is instantaneous and isentropic.

(d) Flow in the gap is isothermal and constant velocity.

(e) The flow in the gap is in the axial direction of the plug.

(f) The distribution of *Cv* values of the flow through the cage is continuous and uniform.

(g) The *FCI** equation for the case where the inlet pressure is more than twice that of the outlet is used incalculating the outflow of gas through the cage.

---

*: The *Cv* value is an indication of the valve capacity. When the flow rate of water is 1 gpm with a differential pressure of 1 psi, the *Cv* value of the valve is defined to be 1 (FCI-62-1). When applied to gas, the equation becomes (metric units):

$$Cv = \frac{q}{N_1}\sqrt{\frac{GT}{(P_{IN}^2 - P_{OUT}^2)}}$$

Where, $N_1 = 7.74\times10^{-2}$.

When, $P_{OUT} \leqq P_{IN}/2$, set $P_{OUT} = P_{IN}/2$

3.2 Derivation of equations

An infinitesimal volume of the gap between the plug and cage is considered, as shown in **Fig.3**. **Fig.3** also shows the coordinate system used in this study. Notations are as follows.

- α : Pressure ratio of critical flow condition to stagnation condition (-)
- δ_0 : Average width of the gap between the plug and the cage (m)
- δ : Plug displacement (m)
- θ :Angle measured from the position where the width of the gap is maximum (rad)
- κ : Specific heat ratio of the gas (-)
- a : Velocity of sound of the gas (m/s)
- a_N : Velocity of sound of the gas at 0°C, 1atm (m/s)
- Cvd : Cv value corresponding to unit valve stroke (= Cv value of the valve / stroke) (Cv value/m)
- F : Imbalanced force (bar • m^2)
- F_0 : Imbalanced force at $\delta = \delta_0$, i.e. when the plug touches the cage (bar • m^2)
- G : Specific gravity of the gas (-)
- h : Distance from the bottom of the plug (m)
- p : Pressure in the gap (bar)
- dp : Pressure drop (bar)
- $p(0)$: Pressure just after entering the gap (bar)
- P_{IN} : Pressure at the inlet of the valve (bar)
- P_{OUT}: Pressure at the outlet of the valve (bar)
- P_N : Pressure at the standard condition (=1.013 bar)
- q : Volumetric flow rate of gas in the gap (Nm^3/s)
- dq : Volumetric flow rate of the outflow gas through the cage (Nm^3/s)
- r : Radius of the plug (m)
- $T(0)$: Temperature of gas just after entering the gap (K)
- T_{IN} : Temperature at the inlet of the valve (K)
- T : Temperature of gas (K)
- T_N : Temperature at the standard condition (=273K)

3.2.1 Pressure at the bottom of the plug

The ratio of the pressure just after entering the gap (critical flow condition) to the pressure just before entering the gap (stagnation condition) is expressed as follows.

$$\alpha = p(0)/P_{IN} = \{1+(\kappa-1)/2\}^{\kappa/(\kappa-1)} \quad .....(1)$$

α is 0.546 for κ = 1.3 and 0.528 for 1.4. Thus, when gas enters the gap, the pressure suddenly drops to about half of the inlet pressure.

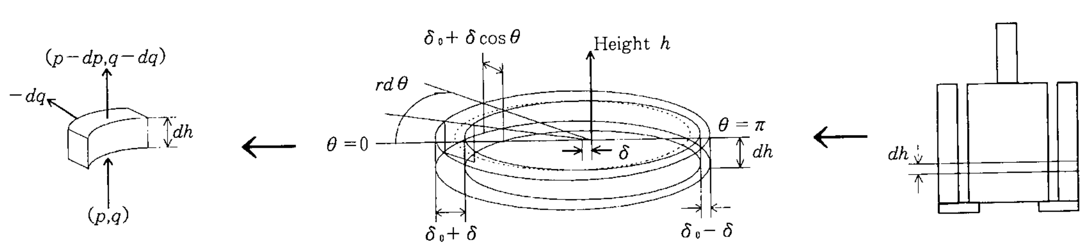

Fig. 3 Coordinates in gap space

3.2.2 Pressure distribution in the gap

The flow rate of gas through the holes or labyrinths of the cage, dq, is expressed as follows using the definition of Cv value.

$$-dq = \frac{N_1 Cvd\ p\sqrt{3}}{\sqrt{GT}\ 4\pi} dh\ d\theta \qquad .....(2)$$

The following relation is derived from the assumption that flow in the gap is isothermal and constant velocity.

$$q/p = (q-dq)/(p-dp) = Const. \qquad .....(3)$$

$$\therefore pdq = qdp \qquad .....(4)$$

Substituting eq.(4) into eq.(2), we obtain:

$$dh = -\frac{q\sqrt{GT}\ 4\pi\ dp}{N_1 Cvd\sqrt{3}\ p^2\ d\theta} \qquad .....(5)$$

The volumetric flow rate of gas in the gap is expressed by assuming that the velocity is sonic:

$$q = (\delta_0+\delta\ \cos\theta) r\, d\theta\, a \frac{pT_N}{P_N T}$$

$$= \frac{(\delta_0+\delta\ \cos\theta) r\, d\theta\, a_N p\sqrt{T_N}}{P_N\sqrt{T}} \qquad .....(6)$$

Combining eq.(5) with eq.(6), the following equation is derived

$$dh = -k_2\, dp/p \qquad .....(7)$$

where,

$$k_2 = \frac{4\pi(\delta_0+\delta\ \cos\theta) r a_N\sqrt{GT_N}}{\sqrt{3}\ N_1 Cvd\ P_N} \qquad .....(8)$$

After integrating eq.(7) under the boundary condition of $p = P(0) = \alpha P_{IN}$ at h=0, the following equation is obtained.

$$p = p(0)e^{-h/k_2} = \alpha P_{IN}\, e^{-h/k_2} \qquad .....(9)$$

This equation shows the pressure distribution in the gap.

Substituting $p = P_{OUT}$ into eq.(9), we obtain the height, h_l, at which the pressure in the gap equals the outlet pressure of the valve.

$$h_1 = k_2\ \ell n\frac{p(0)}{P_{OUT}} = k_2\, \ell n\frac{\alpha\ P_{IN}}{P_{OUT}} \qquad .....(10)$$

We call h_l "the reach of pressure," i.e., the maximum height at which the inlet pressure of the valve affects the pressure distribution in the gap.

3.2.3 Imbalanced force acting on the plug

(1) The case without wear

As is clear from **Fig.2**, the effective pressure that contributes to generating the imbalanced force is $p - P_{OUT}$. Thus, the component of the force generated by the effective pressure in the direction of the plug displacement is:

$$(p-P_{OUT})dh\ r\, d\theta\ \cos\theta \qquad .....(11)$$

The imbalanced force, F, is obtained by integrating eq.(11) for $0 \leqq h \leqq h_1$, and $0 \leqq \theta \leqq 2\pi$. That is,

$$F = 2\int_0^{\pi}\int_0^{h1}(p-P_{OUT})\ \cos\theta\, r\, d\theta\ dh \qquad .....(12)$$

Substituting eq.(8) and (9) into eq.(12), and using eq.(10), the following equation is obtained that can be used to calculate the imbalanced force.

$$F = \frac{4\pi^2 r^2\{\alpha P_{IN}-P_{OUT}\{1+\ell n(\alpha P_{IN}/P_{OUT})\}\}a_N\sqrt{GT_N}\,\delta}{\sqrt{3}\ N_1\ Cvd\,P_N}$$

$$.....(13)$$

Although the range of δ in the above equation is, $0 \leqq \delta \leqq \delta_0$ the physical condition corresponding to $0 \leqq \delta < \delta_0$ is unstable. In other words, the plug is forced against the cage (i.e., $\delta=\delta_0$) soon after the valve opens.

(2) The case of worn plug and cage

After the plug and the cage are worn, the gap on the touching side becomes narrower, and that on the opposite side becomes wider.

When the wear depth is greater than δ_0 (i.e., $\delta \leqq 2\delta_0$), the plug and cage are in contact for more than 1/3 of the circumference. So, we can assume there is no gap over the touching half of the circumference.

Using these assumptions, an approximate equation for calculating the imbalanced force was derived for the worn-out case. Only the result is shown below.

$$F = 8\pi r^2\{\delta_0+\delta\ \pi/4\}\ \{\alpha P_{IN}-P_{OUT}(1+\ell n(\alpha P_{IN}/P_{OUT}))\}$$
$$\times a_N\sqrt{GT_N}/\sqrt{3}\, N_1\ Cvd\, P_N \qquad ..... (14)$$

The relation between the displacement of the plug and the imbalanced force is shown in **Fig.4**. Note that the displacement and force are normalized by δ_0 and F_0, respectively.

4. Evaluation of derived equations

The imbalanced force was calculated using the equations derived above and evaluated for two cases, as described in this section.

4.1 Example of observed imbalanced force

The details of the valves and fluid conditions for the two cases considered here is presented in **Table 1**.

Case-1 is the experimental results of the imbalanced force. The fluid is compressed air. The test valve was specially designed to permit measurement of the force directly and has the following features.

(a) Wider gap between the plug and the cage than usual
(b) No seal ring at the top of the plug
(c) Modified ground part that has a special fulcrum to allow the plug to move around freely

Case-2 is the result from a large diameter, high differential pressure control valve that is installed at an actual plant. In this case, the imbalanced force could not be measured directly. The friction coefficient between the plug and cage was estimated from the increase in the required air pressure for the valve actuator after some wear appeared and was used for the evaluation.

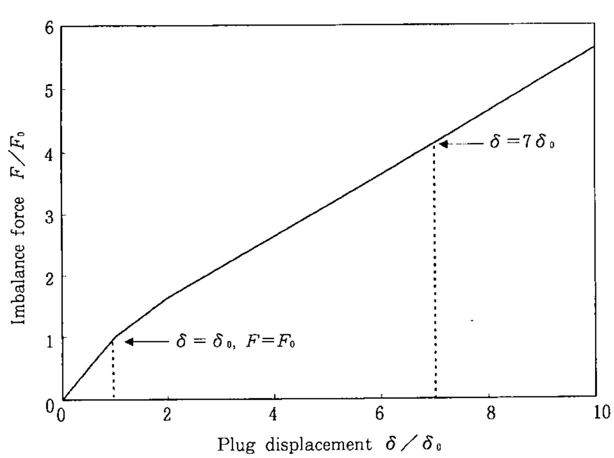

Fig. 4 Plug displacement vs. imbalanced force

4.2 Comparisons

(1) Case 1 (experimental results)

Fig.5 shows comparisons between the calculated imbalanced force and the measured value. The measurements were made in the condition where $\delta=\delta_0$ in **Fig.4**. As can be seen in this figure, good agreement was obtained.

(2) Case 2 (observed at an actual plant)

The valve was inspected when the thrust required to actuate the valve became 6000 N larger than that of the initial value due to wear. The total depth of wear was 1.7 mm, which corresponds to $\delta \approx 7\delta_0$ in **Fig.4**.

The relation between the imbalanced force and the increase of thrust is as follows.

(Imbalanced force)×(Friction coefficient) = (Increase of required thrust)

Using the calculated imbalanced force and the estimated increase in the required thrust based on the increased air pressure of the actuator, we obtain the friction coefficient as follows.

$$(6\times10^3)/(1.5\times10^4) = 0.4 \qquad \text{.....(15)}$$

This value, although larger than usual, is considered to be reasonable in the case of adhesive wear.

Thus, in both cases described above, the calculated results agree, or are consistent with the observa-

Table 1 Samples of fluid force

		Case 1 3"Test CV by air		Case 2 14"PCV for actual plant
Fluid		Compressed air		CH_4 Rich gas
P_{IN}	bar	6.96	5.96	60
P_{OUT}	bar	1.53	1.40	7.0
T_{IN}	K	300		300
G		1.0		0.55
r	m	$30*10^{-3}$		$100*10^{-3}$
δ_0	m	$0.45*10^{-3}$		$0.28*10^{-3}$
δ	m	$0.45*10^{-3}$		$2.0*10^{-3}$
Cvd	m^{-1}	$1.54*10^3$		$1.81*10^3$
F (*Calculated*) bar $* m^2 = 10^5 N$		34×10^{-5}	26×10^{-5}	0.15
F (*measured*) bar $* m^2 = 10^5 N$		32×10^{-5} average	26×10^{-5} average	$0.06/\mu^{(note)}=0.15$ at $\mu=0.4$

Note. μ: Coefficient of friction

tions. Therefore, these equations for calculating the imbalanced fluid force generated inside of a cage-type, low noise, control valve can be used for practical applications when the differential pressure is large.

4.3 The reach of pressure

The reach of pressure is 24 mm on the maximum gap side when the plug touches the cage. This value is calculated by using eq.(8) and (10) under the conditions of Case-2 shown in **Table 1**. Thus, the pressure in the gap falls to the outlet pressure within 1 inch from the bottom of the plug, even if the inlet pressure is as high as 60 bar.

This distance is very short compared to the plug diameter of 200 mm, indicating that the pressure gradient in the plug height direction is much larger than that in the circumferential direction. This suggests the validity of the assumption that the flow in the gap is in the axial direction of the plug.

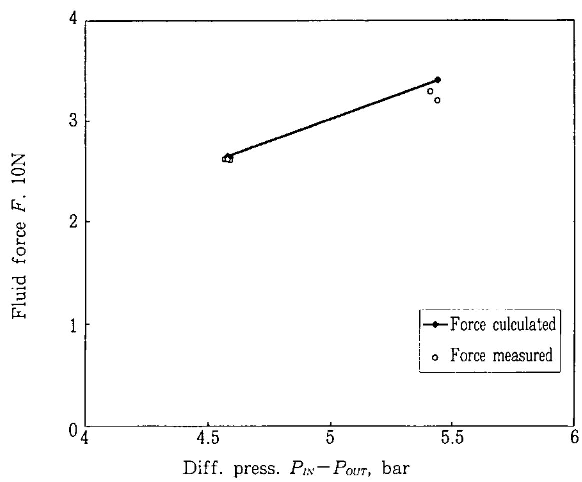

Fig. 5 Fluid force on plug

5. Conclusion

The calculated, imbalanced fluid force agrees with the measured value in experiments using a small valve and air as the test fluid. Moreover, the calculated result was consistent for a large valve installed in an actual plant, which is in a very different situation than that used in the experiments. These show that the equations to calculate the imbalanced fluid force presented in this paper are sufficiently reliable for practical use.

The equations can be used for cage-type, low noise, control valves, including piled disk types.

By using the equations, the imbalanced fluid force acting on the plug can be estimated. The results are very useful, for example, in selecting the optimum material and required surface processing for the valve.

Immersion-type, Optical Fiber Pyrometer for Continuous Caster

1. Introduction

Precise control of the molten steel temperature in iron making is extremely important for controlling product quality and reducing production cost. At present, immersion-type thermocouple probes are widely used for temperature measurement.

Because it is difficult to automate this measurement process, the insertion and removal of the probe is done manually, which is a hard, dirty, and risky job. It is also difficult to achieve continuous and frequent measurements. The measurement is costly because expensive thermocouples are replaced for each measurement.

To overcome these problems, NKK developed an "Immersion-type optical fiber pyrometer" to measure the temperature of molten metal. This method is being used for molten steel temperature measurement in the No. 3 continuous caster tundish at NKK Keihin Works.

A description is presented of the characteristics of the immersion-type, optical pyrometer, the configuration and operation of an automatic temperature measurement unit, and the application and results of the new system.

2. Characteristics of immersion-type optical pyrometer

Fig.1 shows the configuration and measurement principle using the immersion-type, optical fiber pyrometer. The new method is characterized by contact measurement in which one end of an optical fiber is immersed into the molten bath. The radiation given off at the submerged end is transmitted to a radiation thermometer at the other end, where the temperature is determined. Because the diameter of the optical fiber is very small (125 μm in diameter), inserting it into the molten bath produces a very small, hollow glass cylinder that has excellent black body properties. This is an excellent characteristic of the pyrometer that cannot be found in any other method and that enables highly accurate measurement without any influence of the radiation index. A metallic-encased optical fiber was developed under the trade name of FIMT (fiber in metallic tube) and used to improve the mechanical rigidity and heat resistance sufficiently to allow direct immersion of the fiber into molten metal. Rapid loss of the fiber in molten steel can be limited by wrapping the FIMT in a jacket of polyethylene.

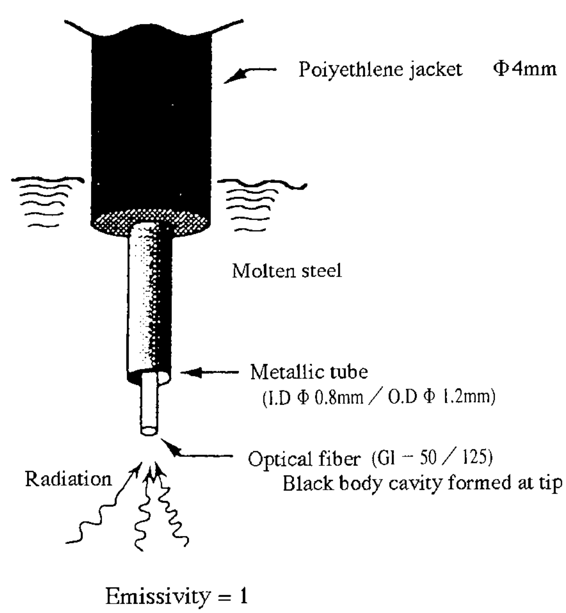

Fig. 1 Measurement principle and configuration of immersion-type optical fiber pyrometer

3. Measurement of molten steel temperature in a continuous caster tundish

3.1 Automatic temperature measurement unit

The configuration of the newly-designed, automatic, temperature measurement unit for a continuous caster tundish is shown in **Fig. 2**, and the technical specifications are given in **Table 1**. The appearance of the unit is shown in **Photo 1**.

The automatic temperature measurement unit consists of a bobbin wound with several hundred meters of the FIMT. A radiation thermometer is connected to the bobbin end of the FIMT. A sampling unit that handles the FIMT and a signal processing unit that performs sequential control of the whole unit and computes the temperature are also at this location. The sampling unit consists of a guide tube for the FIMT, a pulse motor to move the FIMT in and out of the molten steel, and a measuring roll that measures the length of the FIMT consumed.

The measuring process starts by moving a buggy with the sampling unit mounted on it forward to the measuring point above the tundish. The guide tube is placed directly above the surface of molten steel inside of the tundish. The FIMT is then inserted into the molten steel using the pulse motor and held for a specified time. After the temperature is recorded, the FIMT is removed from molten steel while injecting N_2 gas into the guide tube to extinguish fire at the FIMT, completing the measurement cycle. During insertion of the FIMT into the molten steel, the output data from the radiation pyrometer is sampled to determine the peak value. Error compensation is then computed to obtain the true temperature because the error increases with the length of FIMT consumed after calibration. Output data from the pyrometer provides enough of a plateau for sampling to ensure that stable measurement can be achieved.

After the measurement, no maintenance is necessary for the end of the FIMT that was melted and lost. Therefore, the measurement can be repeated continuously without any maintenance.

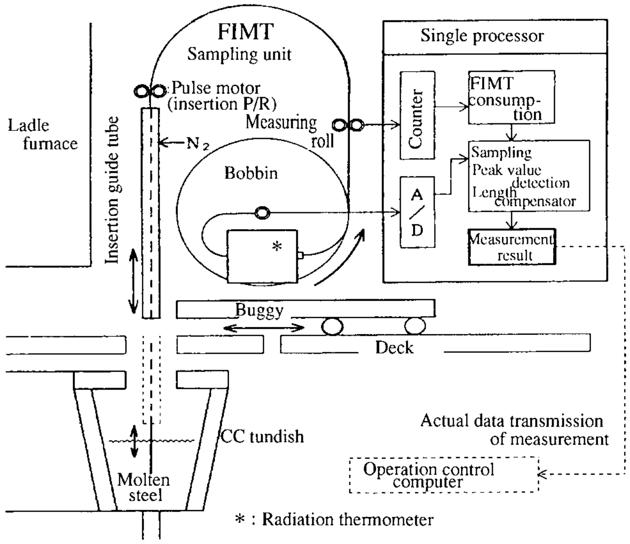

Fig. 2 Measurement system configuration

Table 1 Technical specification of unit

Items	Specification
Optical fiber	· Polyethylene jaket FIMT(ϕ 4mm×300m) · Optical fiber : GI 50/125 μ m · Bobbinn diameter ϕ 800mm
Radiation thermometer	· Detected element Si : 0.9 μ m · Measurement range 1050 - 1650 ℃ · Rensponse time 50ms
Sampling unit	· FIMT insertion depth 0 - 500 mm · FIMT insertion speed 0 - 10000 mm/sec · FIMT holding time 0 - 10 sec
Signal processing unit	· Sampling cycle 10ms · FIMT length compensator

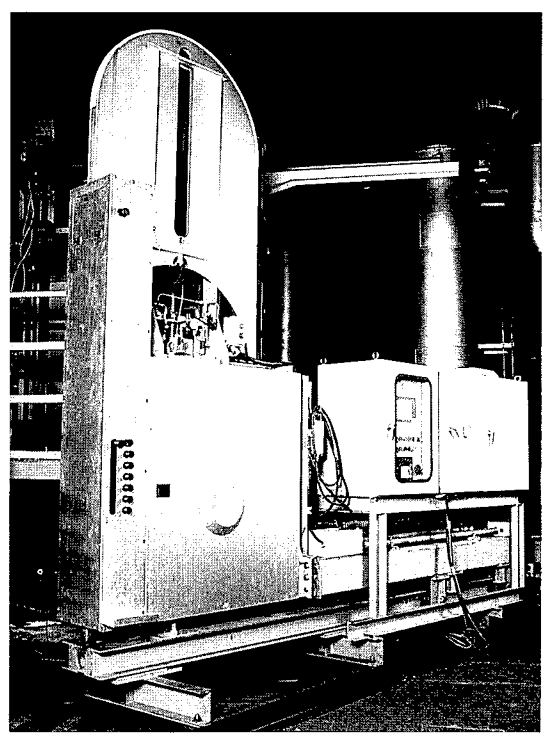

Photo 1 Appearance of automatic temperature measurement unit

3.2 Application of the new system

Fig. 3 shows a comparison between the automatic temperature measurement and measurement using immersion-type thermocouples. The immersion-type, optical fiber pyrometer has a measurement accuracy of ±3%, which is equivalent to that of current, immersion-type thermocouple measurements, while demonstrated excellent stability. The new method clearly has enough benefits to justify replacement of the immersion-type thermocouples.

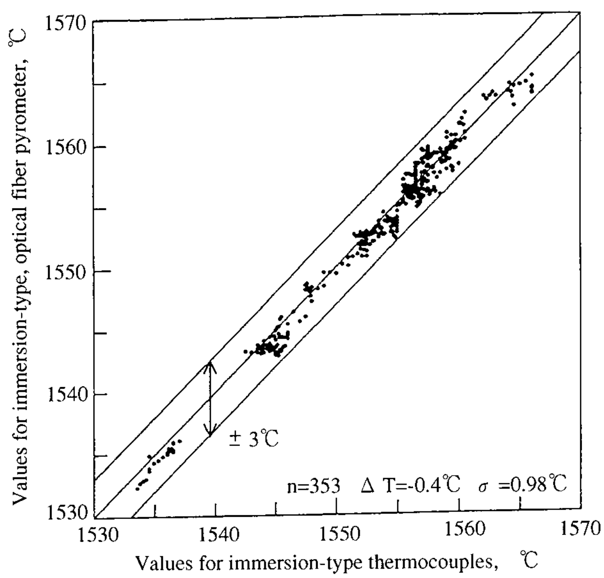

Fig. 3 Measurement result comparison (Correlation diagram)

By introducing the automatic temperature measurement unit, it is possible to improve the working environment over current measurement work, which is considered to be dirty, hard, and risky. In addition, the new system reduces the cost to approximately 1/3 of that for current, immersion-type thermocouples.

4. Conclusion

NKK developed and used a new, immersion-type, optical fiber pyrometer for measuring the temperature of molten steel in a continuous caster tundish. The basic design and engineering technology for automatic temperature measurement unit using this pyrometer was established.

The automatic temperature measurement unit can be used for processes other than iron and steel making, as well as for the continuous caster tundish, because it meets a wide range of other industrial needs that deal with molten metal other than iron and steel.

NKK currently plans to improve the system and widen its use to other applications.

Please refer to ;
Technology Sec, Process Control Dept.,
Keihinn Works
Hiroaki Miyahara
Akira Ohsumi

On-line Grain Size Measurement System for Stainless Steel Strip Annealing and Pickling Line

1. Introduction

Grain size is known as one of the most critical factors for characterizing austenitic stainless steel. The conventional method for measuring the grain size of a stainless steel strip is to evaluate the photomicrograph of a sample cut from the end of the coil. This method has problems because it takes a long time to get the results and it does not permit control of the grain size over the entire coil. We therefore developed an on-line, grain size measurement system for a stainless steel strip annealing and pickling line.

2. Principle of grain size measurement

It is known that ultrasonic waves transmitted through stainless steel are scattered by its grain boundaries and that the amplitude of the attenuation by ultrasonic scattering is approximately proportional to the grain size. The ultrasonic attenuation by scattering and the average grain size have the relationship shown by eq. 1.

$$D = S \cdot (f^4 / \alpha s)^{-1/3} \quad .....(1)$$

where S is a constant, D is the average grain size, f is the ultrasonic frequency and αs is the ultrasonic scattering attenuation constant.

Moreover, αs is shown by eq.2:

$$\alpha s = a_s / 2t \quad .....(2)$$

where a_s is the amount of attenuation by ultrasonic scattering during transmission through the strip, and t is the thickness of the strip.

3. Outline of measurement system

A schematic diagram of this system is shown in **Fig.1**. The system consists of a measuring head and a signal processing unit. The measuring head can roll freely on the strip to maintain horizontal alignment between the transducer and strip surface. The transducer transmits the ultrasonic pulse and receives the multiple back reflection echoes from the strip. The term as is calculated from the first and second back reflection echoes. The signal processing unit consists of a pulser and gain controlled amplifier, digital signal memory storage for the reflected echo signal, a calculator for determining grain size from the reflected echo, and an amplifier gain controller. The amplifier gain is controlled to maintain a constant first back echo amplitude and to produce a high signal-to-noise ratio. The measured grain size is continuously displayed on the monitor and recorded as a chart. The specifications for this system are shown in **Table 1**. The system is shown in **Photos 1** and **2**.

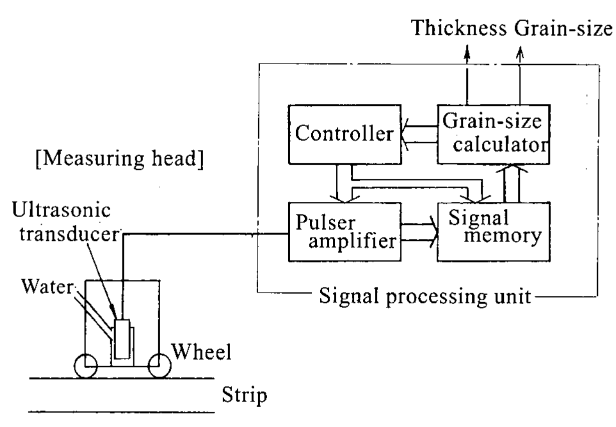

Fig. 1 Schematic diagram of the system

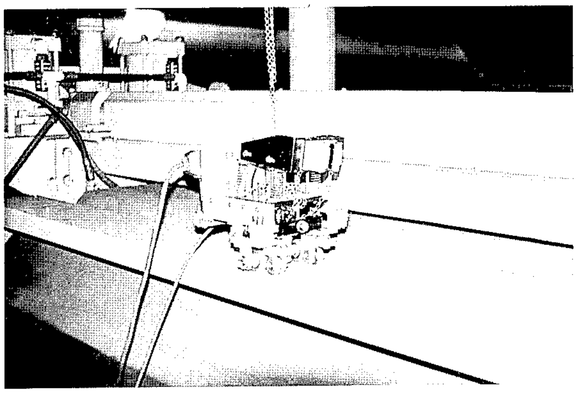

Photo 1 Measuring head

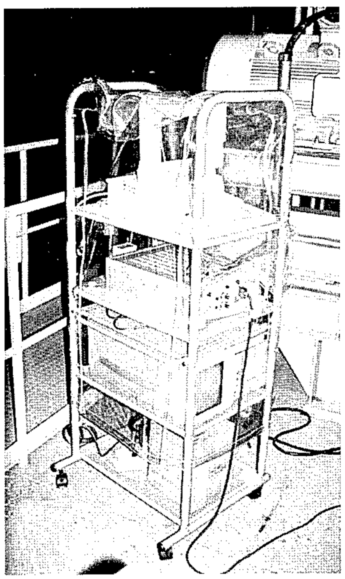

Photo 2 Signal processing unit

4. Application in stainless steel strip annealing and pickling line

To confirm the performance of the system, the system was used experimentally on an annealing and pickling line for stainless steel strip in the Fukuyama works. To estimate the reliability of the grain size measured by the system, the measured grain size of the sample cut from the end of coil and that made using the linear intercept technique on a photomicrograph were compared. **Fig.2** shows the result. It is clear that the sensitivity of the grain size measured by this system is within ± 5.0 μm over the entire range

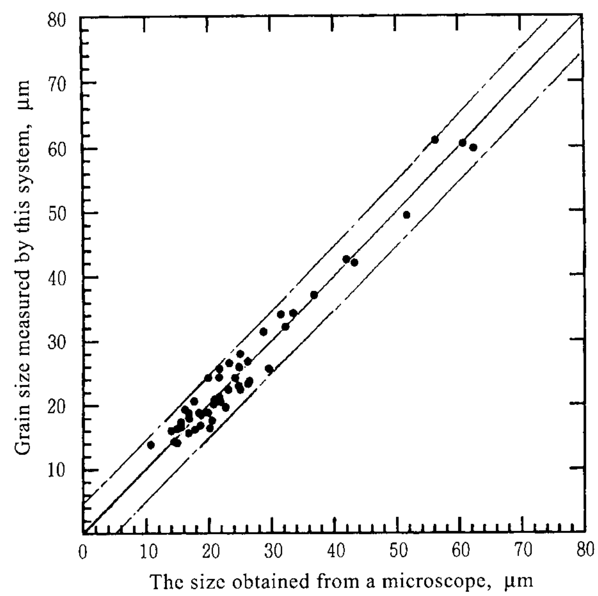

Fig.2 Static evaluation of the system

Table. 1 Specifications for the system

Item		Specification	
Measuring head unit	Ultrasonic transducer	• Center frequency • Frequency band • Nominal-size	20 MHz 12.5 - 27.5 MHz/-6dB Ø6.0 mm
	Measuring head	• Coupling • Adulate mechanism	Water coupling (water distance 10mm) Wheel type rolling on the strip
Signal processing unit	Pulser reciever	• Amplifier range	60 dB
	Signal memory	• Sampling frequency • Sampling point • Resolution	100 MHz 512 Point 8 bit
	Grain-size calculator Controller	• Type • Output • Control parameter	PC98 personal computer Thichness, Grain-size Amplifier in pulser reciever

of grain size. **Fig.3** shows the variations in grain size when the system is applied on-line. A dummy coil is used as a buffer when the annealing condition or strip thickness is changed. The grain size of the dummy coil is generally larger and more widely scattered than the product coil because of repeated use. **Fig.3** shows this condition clearly.

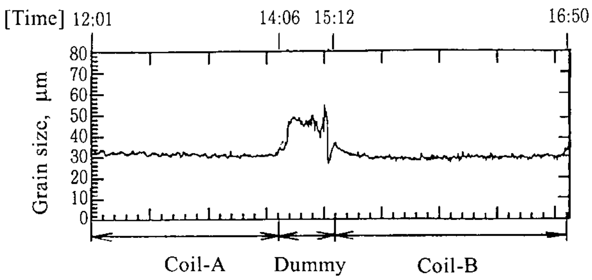

Fig. 3 Dynamic grain size monitoring chart

5. Conclusion

We developed a grain size measurement system based on the correlation between the attenuation by ultrasonic scattering, ultrasonic wavelength and the grain size. The system can measure the grain size of the stainless steel over the entire coil in real-time. At present, the system is being used experimentally for quality control in our annealing and pickling line.

Please refer to:

Control Engineering Research Dept., Applied Technology Research Center

Ryuichi Okuno

Iizuka Yukinori

NKK CORPORATION

HEAD OFFICE

1-1-2 Marunouchi, Chiyoda-ku, Tokyo 100, Japan
Tel: 03 (3212) 7111
Cable: KOKANNK TOKYO, KOKAN JUKOO TOKYO, KOKANSHIP TOKYO
Telex: 222-2811 (NKK J), 222-2816 (NKSHIP J)

Organizations

Research and Development Division, Steel Division, Engineering Division, LSI Division, Urban Development Division, New Business Center

Research Centers

Applied Technology Research Center, Materials & Processing Research Center, Engineering Research Center

Works

Iron and Steel Works: Keihin (Kawasaki), Fukuyama
Works: Tsurumi, Tsu, Shimizu, Toyama

Overseas Offices & Affiliates

New York
NKK America Inc. New York Office
450 Park Avenue, New York, N.Y. 10022 U.S.A.
Tel: (212) 826-6250 Fax: (212) 826-6358 Telex: 233495 (NKK UR)

Houston
NKK America Inc. Houston Office
333 Clay Street, Suite 3000, Houston, Texas 77002 U.S.A.
Tel: (713) 658-0611 Fax: (713) 658-0006

Santa Clara
NKK America Inc. Santa Clara Office
2350 Mission College Boulevard, Suite 380, Santa Clara, California 95054 U.S.A.
Tel: (408) 982-8277 Fax: (408) 982-9809

Washington
NKK America Inc. Washington D.C. Branch Office
1215 17th street, N.W. Washington D.C 20036 U.S.A.
Tel:(202)467-8010 Fax:(202)452-8075

Vancouver
NKK CORPORATION Vancouver Office
P.O. Box 49168, Four Bentall Centre, Suite 3394-1055 Dunsmuir Street, Vancouver, B.C. V7X 1J1 Canada
Tel: (604) 687-0091 Fax: (604) 688-7020

London
NKK Europe Ltd. London Office
4th Floor, West Block, 11 Moorfields High Walk, London EC2Y 9DE U.K.
Tel: (071) 628-2161 Fax: (71) 638-1374 Telex: 886310 (NKK LN G) 887602 (NKK LN G)

Düsseldorf
NKK Europe Ltd.
Immermannstrasse 43, 40210 Düsseldorf, Germany
Tel: (0211) 353481 Fax: (211) 361-3589 Telex: 8587839 (NKK D)

Rotterdam
NKK Netherlands B.V.
9th Floor, Room No. 913, Calandstraat 66, 3016 CD Rotterdam, The Netherlands
Tel: (31) 10-436-13-44 Fax: (31) 10-436-14-57

Singapore
NKK CORPORATION Singapore Office
78 Shenton Way, #15-03, S-0207 Republic of Singapore
Tel: 2217277 Fax: 2244568 Telex: 21308 (NKK SP RS)

Jakarta
Jakarta Representative of NKK CORPORATION
Midplaza, 19th Floor, JL. Jend, Sudirman Kav. 10-11, Jakarta 10220, Indonesia
Tel: 5707572 / 3 Fax: (21) 5703294 Telex: 65637 (PMK IA)

Beijing
NKK CORPORATION Beijing Office
1720, Beijing Fortune Building, Chaoyang District, Beijing, People's Republic of China
Tel: 500-4375, 501-4385 Fax: 1-500-3844 Telex:210556 (NKK CN)

Hong Kong
NKK CORPORATION Hong Kong Office
402 Fairmont House, 8 Cotton Tree Drive, Central, Hong Kong
Tel: 810-0604 / 0595 / 4218 Fax: 810-4262 Telex:802-83003 (KOKAN HX)

Bangkok
NKK CORPORATION Bangkok
11th Floor, Ramaland Building 952 Rama IV Road, Bangrak. Bangkok 10500, Thailand
Tel:(2)632-9270 Fax:(2)632972

NKK

NKK CORPORATION